NTNU

Norwegian University of
Science and Technology

Numerical Modeling of Wave Hydrodynamics and Wave Interaction with Porous Structures with REEF3D

Athul Sasikumar

Coastal and Marine Engineering and Management
Submission date: July 2016
Supervisor: Hans Sebastian Bihs, BAT

Norwegian University of Science and Technology
Department of Civil and Transport Engineering

ERASMUS +: ERASMUS MUNDUS MOBILITY PROGRAMME

Master of Science in

COASTAL AND MARINE ENGINEERING AND MANAGEMENT

CoMEM

NUMERICAL MODELING OF WAVE HYDRODYNAMICS AND WAVE INTERACTION WITH POROUS STRUCTURES WITH REEF3D

Norwegian University of Science and Technology
8 July 2016

Athul Sasikumar

The Erasmus+: Erasmus Mundus MSc in Coastal and Marine Engineering and Management is an integrated programme including mobility organized by five European partner institutions, coordinated by Norwegian University of Science and Technology (NTNU).

The joint study programme of 120 ECTS credits (two years full-time) has been obtained at two or three of the five CoMEM partner institutions:

- Norges Teknisk- Naturvitenskapelige Universitet (NTNU) Trondheim, Norway
- Technische Universiteit (TU) Delft, The Netherlands
- Universitat Politècnica de Catalunya (UPC). BarcelonaTech. Barcelona, Spain
- University of Southampton, Southampton, Great Britain
- City University London, London, Great Britain

During the first three semesters of the programme, students study at two or three different universities depending on their track of study. In the fourth and final semester an MSc project and thesis has to be completed. The two-year CoMEM programme leads to a multiple set of officially recognized MSc diploma certificates. These will be issued by the universities that have been attended by the student. The transcripts issued with the MSc Diploma Certificate of each university include grades/marks and credits for each subject.

Information regarding the CoMEM programme can be obtained from the programme coordinator:

Øivind A. Arntsen, Dr.ing.
Associate professor in Marine Civil Engineering
Department of Civil and Transport Engineering
NTNU Norway
Telephone: +4773594625 Cell: +4792650455 Fax: + 4773597021
Email: oivind.arntsen@ntnu.no

CoMEM URL: https://www.ntnu.edu/studies/mscomem

CoMEM Thesis

This thesis was completed by:
Athul Sasikumar

Under supervision of:
Hans Bihs , Asscociate professor, NTNU
Arun Kamath, Postdoc, NTNU

As a requirement to attend the degree of
Erasmus+: Erasmus Mundus Master in Coastal and Marine Engineering and Management (CoMEM)

Taught at the following educational institutions:

Norges Teknisk- Naturvitenskapelige Universitet (NTNU)
Trondheim, Norway

Technische Universiteit (TU) Delft
Delft, The Netherlands

At which the student has studied from August 2014 to July 2016.

NORWEGIAN UNIVERSITY OF SCIENCE AND TECHNOLOGY
DEPARTMENT OF CIVIL AND TRANSPORT ENGINEERING

Report Title:	Date:08/07/2016			
Numerical Modeling of Wave Hydrodynamics and Wave Interaction with Porous Structures with REEF3D	Number of pages (incl. appendices): 98			
	Master Thesis	X	Project Work	
Name: Athul Sasikumar				
Professor in charge/supervisor: Prof. Hans Bihs				
Other external professional contacts/supervisors: Arun Kamath, Nadeem Ahmad				

Abstract:
This thesis presents validation of newly implemented VARANS method in the CFD model REEF3D for simulating porous media flow that occurs in coastal and offshore engineering problems. The VARANS method is based on adding the effect of the porous media via the Darcy-Forchheimer equation to the momentum equation. The applied type of porosity models relies on empirical resistance coefficients which often needs to be measured or calibrated.

The first part of thesis deals with the validation of the CFD model REEF3D. This was done by conducting experiments in the wave flume tank at NTNU. Three different tests were performed, wave tank with no obstacles, with the presence of a step structure and with an abutment structure. These tests were validated in REEF3D with the aim to study about the wave generation, changes in wave kinematics due to structures, water particle velocities and absorption capabilities. Different grid sizes were used in the study to know about the accuracy variation in results. Also wave generation methods like Relaxation methods and Dirichlet method based on shallow water theory and intermediate water theory was tested. Similarly wave absorption methods like relaxation method and active wave absorption methods were also tested since the absorption capabilities of the wave flume was uncertain. The best agreement between the experimental and numerical results were found by using Dirichlet method for wave generation and active absorption method for wave absorption with a grid size of 0.005 m. The Dirichlet method for wave generation provides the best match only because the wavemaker in the wave flume does not have active absorption. Due to this the wave reflected from the structure travel between the wavemaker and the structure, undergoing multiple reflections and affecting wave generation.Through these validation cases, it showed that REEF3D has the capability of correctly modeling the regular wave propagation both in generation and absorption of the waves as well as simulating the wave behavior interacting with structures.

In the second phase of the thesis, flow inside a porous medium introduced. The numerical model is first validated for simple experiments for flow passing through a porous dam with different porous materials. Excellent agreements are obtained for the case using crushed rock with diameter of 15 mm for the porous dam. Reasonably good agreements are also obtained when small uniform glass beads with diameters of 3 mm are used. The seconds validation case is done for a porous abutment in a three dimensional wave tank. The VARANS method implemented in REEF3D is proven to reproduce the relevant hydraulic process in wave-structure interaction in a three-dimensional domain. In the final part of this study, porous breakwaters are tested in the numerical model. This tests was done as a starting point for further improvements in the CFD model REEF3D for dealing with complicated porous flows. The model already showed good promise in case of breakwaters with a single porous layer.

Keywords:

1. CoMEM
2. REEF3D
3. Wave-Porous structure Interaction
4. VARANS

MASTER THESIS

(TBA4920 Marine Civil Engineering, master thesis)

Spring 2016
for
ATHUL SASIKUMAR

Numerical Modeling of Wave Hydrodynamics and Wave Interaction with Porous Structure with REEF3D

Numerisk modellering av bølgehydrodynamikk og bølge interaksjon med porøse strukturer med REEF3D

BACKGROUND

Computational Fluid Dynamics (CFD) based numerical wave tanks find numerous applications in the field of coastal and marine engineering. The validation of such models for the wave kinematics should be carried out in a detailed manner through comparisons to experimental observations to establish confidence in the model and carry out further research. There are many porous structures used for coastal and harbour protection. CFD modelling of wave-porous structure interaction can provide further details on the hydrodynamics involved. The porous nature of the porous structures makes it a challenging task to numerically model wave- porous structure interaction.

TASK DESCRIPTION

Description of task

In order to validate the wave hydrodynamics calculated in REEF3D, experiments will be carried out at the wave flume. The experiments will involve studying wave propagation and wave kinematics through the measurement of free surface elevations and fluid velocity in the wave flume for an empty wave tank, wave propagation around an abutment and wave propagation over a submerged rectangular shoal. The experimental observations will be compared with the numerical results from REEF3D to validate the model. Further research will be carried out to study the influence of the different wave generation and absorption methods in the numerical wave tank. The numerical work will be extended to study the wave interaction with a porous structure including the effect of the porosity of the structure.

Aims and purpose

The Masters' thesis work will be carried out with the following objectives:

- Carry out experiments to measure the wave kinematics in an empty wave tank, with an abutment and with a submerged rectangular obstacle.
- Validate the wave hydrodynamics in REEF3D by comparing numerical results to experimental data.
- Simulate wave interaction with a porous structure.

Subtasks and research questions

As an introduction, the candidate must show that she/he has the advanced knowledge of the field of numerical modelling of wave hydrodynamics using CFD based numerical wave tanks with respect to theory and methods with in general. The candidate should conduct the experiments, replicate the setup numerically and compare the numerical and experimental results. He should demonstrate the ability to validate a numerical model with careful execution of the experiments and the numerical model and to extend upon the study through further re-search using the CFD model. After the hydrodynamics have been validated, the wave interaction with a porous structures is studied and the representation of the porosity is investigated.

The thesis work will address the issues of validation of a CFD model for wave hydrodynamics and the modelling of wave interaction with porous structures using REEF3D.

General about content, work and presentation
The text for the master thesis is meant as a framework for the work of the candidate. Adjustments might be done as the work progresses. Tentative changes must be done in cooperation and agreement with the professor in charge at the Department.

In the evaluation thoroughness in the work will be emphasized, as will be documentation of independence in assessments and conclusions. Furthermore the presentation (report) should be well organized and edited; providing clear, precise and orderly descriptions without being unnecessary voluminous.

The report shall include:

- Standard report front page (from DAIM, http://daim.idi.ntnu.no/)
- Title page with abstract and keywords.(template on: http://www.ntnu.no/bat/skjemabank) CoMEM students must include CoMEM as one of the keywords.
- CoMEM page (Only CoMEM students)
- Preface
- Summary and acknowledgement. The summary shall include the objectives of the work, explain how the work has been conducted, present the main results achieved and give the main conclusions of the work.
- Table of content including list of figures, tables, enclosures and appendices.
- A list explaining important terms and abbreviations should be included.
- List of symbols should be included
- The main text.
- Clear and complete references to material used, both in text and figures/tables. This also applies for personal and/or oral communication and information.
- Thesis task description (these pages) signed by professor in charge as Attachment 1.
- The report musts have a complete page numbering.

The thesis can as an alternative be made as a scientific article for international publication, when this is agreed upon by the Professor in charge. Such a report will include the main points as given above, but where the main text includes both the scientific article and a process report.

Submission procedure
Procedures relating to the submission of the thesis are described in IVT faculty webpage:
http://www.ntnu.edu/ivt/master-s-thesis-regulations

On submission of the thesis the candidate shall submit to the professor in charge a CD/DVD('s) or a link to a net-cloud including the report in digital form as pdf and Word (or other editable form) versions and the underlying material (such as data collection, time series etc.).

Documentation collected during the work, with support from the Department, shall be handed in to the Department together with the report.

According to the current laws and regulations at NTNU, the report is the property of NTNU. The report and associated results can only be used following approval from NTNU (and external cooperation partner if applicable). The Department has the right to make use of the results from the work as if conducted by a Department employee, as long as other arrangements are not agreed upon beforehand.

Start and submission deadlines
The work on the Master Thesis starts on (date) 12/02/2016

The thesis report as described above shall be submitted digitally in DAIM at the latest (date:) 07/08/2016 at 11.59 pm.

Professor in charge: **Hans Bihs**

Other supervisors: **Arun Kamath, Nadeem Ahmad**

Trondheim, Date _____

_____
Professor in charge (sign)

Numerical Modeling of Wave Hydrodynamics and Wave Interaction with Porous Structures with REEF3D

A Masters' Thesis
submitted to the Faculty of Civil & Transport Engineering
at the Norwegian University of Science and Technology

by

Athul Sasikumar

Abstract

This thesis presents validation of newly implemented VARANS method in the CFD model REEF3D for simulating porous media flow that occurs in coastal and offshore engineering problems. The VARANS method is based on adding the effect of the porous media via the Darcy-Forchheimer equation to the momentum equation. The applied type of porosity models relies on empirical resistance coefficients which often needs to be measured or calibrated.

The first part of thesis deals with the validation of the CFD model REEF3D. This was done by conducting experiments in the wave flume tank at NTNU. Three different tests were performed, wave tank with no obstacles, with the presence of a step structure and with an abutment structure. These tests were validated in REEF3D with the aim to study about the wave generation, changes in wave kinematics due to structures, water particle velocities and absorption capabilities. Different grid sizes were used in the study to know about the accuracy variation in results. Also wave generation methods like Relaxation methods and Dirichlet method based on shallow water theory and intermediate water theory was tested. Similarly wave absorption methods like relaxation method and active wave absorption methods were also tested since the absorption capabilities of the wave flume was uncertain. The best agreement between the experimental and numerical results were found by using Dirichlet method for wave generation and active absorption method for wave absorption with a grid size of 0.005 m. The Dirichlet method for wave generation provides the best match only because the wavemaker in the wave flume does not have active absorption. Due to this the wave reflected from the structure travel between the wavemaker and the structure, undergoing multiple reflections and affecting wave generation.Through these validation cases, it showed that REEF3D has the capability of correctly modeling the regular wave propagation both in generation and absorption of the waves as well as simulating the wave behavior interacting with structures.

In the second phase of the thesis, flow inside a porous medium introduced. The numerical model is first validated for simple experiments for flow passing through a porous dam with different porous materials. Excellent agreements are obtained for the case using crushed rock with diameter of 15 mm for the porous dam. Reasonably good agreements are also obtained when small uniform glass beads with diameters of 3 mm are used. The seconds validation case is done for a porous abutment in

a three dimensional wave tank. The VARANS method implemented in REEF3D is proven to reproduce the relevant hydraulic process in wave-structure interaction in a three-dimensional domain. In the final part of this study, porous breakwaters are tested in the numerical model. This tests was done as a starting point for further improvements in the CFD model REEF3D for dealing with complicated porous flows. The model already showed good promise in case of breakwaters with a single porous layer.

Acknowledgments

This thesis work is done as per the requirement for a graduate student in the two year mobility, Erasmus Mundus Masters Course: Coastal and Marine Engineering and Management (CoMEM).

First and foremost I sincerely thank my family for their support, who have made me the person I am. I thank them deeply for their unconditional love and constant motivation. I thank my main supervisor Hans Bihs for his guidance during the course of my work. It is he who encouraged me to pursue this topic and ensured that I get the right help and direction each time. I would like to thank my co-supervisor Arun Kamath for all the assistance he provided for the execution of this thesis. His patience in dealing with my questions and his availability for discussions at all times is deeply appreciated.

I would also take this opportunity to extend my gratitude to all the professors who have educated me during my two-year CoMEM programme. I especially thank Prof. Oivind Arnsten and Sonja Hammer, who particularly took care of the CoMEM cohort at NTNU. Finally I would like to thank my CoMEM classmates for their support and most importantly, friendship throughout the past two years.

Contents

List of Figures

List of Tables

List of Symbols

λ	Wavelength
D	Diameter
ρ	Density
t	Time
∇	Divergence operator
U	Velocity
$i,\ j,\ k$	Vectors along the x, y and z-axes
μ	Fluid viscosity (dynamic)
P	Pressure
g	Acceleration due to gravity
ϕ	Level set function
i (*in numerical schemes*)	Time step of iteration
$\omega_1,\ \omega_2,\ \omega_3$	WENO stencil weights
$\alpha_1,\ \alpha_2,\ \alpha_3$	WENO stencil weight determiner
$IS_1,\ IS_2,\ IS_3$	WENO stencil smoothness indicators
L	Spatial discretization of the function
C	Courant Number
ν	Fluid viscosity(kinematic)
ν_t	Eddy viscosity
V	Maximum viscosity
S_{max}	Source term contribution from surface and volume forces
U^*	Intermediate velocity
k	Turbulent kinetic energy
ω	Specific turbulent dissipation
$c_\mu,\ c_{\omega 1},\ c_{\omega 2},\ \sigma_k,\ \sigma_\omega$	Closure coefficients
S_{ij}	Strain tensor
ω_s	Specific turbulent dissipation at free surface
U^+	Dimensionless wall velocity
y^*	Distance from the nearest wall
κ	constant = 0.4
Δy_p	Distance from the wall to cell centre
ϵ_{wall}	Mean wall thickness
2ϵ	Transition zone thickness
$S(\phi)$	Smooth signed distance function

Φ	Velocity potential
$\Psi(x)$	Relaxation function
$_p$	Steepness exponent
η	Free surface elevation
ω_f	Wave angular frequency
k_f	Wave number
a	Wave amplitude
H	Wave height
z	Height to the free surface from bed
dx	Grid cell width
KC	Keulegan-Carpenter number
Re	Reynolds number
Re_p	Pore Reynolds number
x, y, z	Position of structure in the flume
Δt	Numerical time step
d	Water depth
I	Hydraulic gradient
K	Hydraulic conductivity
u_f	Filter velocity
V_P	Pore Volume
V_T	Total Volume
u^p	Pore velocity
D_p	Pore size
U	Characteristic velocity
D	Characteristic length scale
a, b, c	Dimensionless coefficient
$D_5 0$	Median grain size
$D_n 50$	Nominal diameter
n	Porosity
$D_n 50$	Nominal diameter
γ_f	Virtual mass coefficient
$\alpha,\ \beta$	Resistance coefficient

Chapter 1

Introduction

1.1 General

Coastal zones normally accommodate large population densities and a number of facilities, such as ports, harbors, areas for environmental and recreational use, comprising of large economic and ecological value. In places where a natural defence against the action of the sea is absent, coastal modification schemes are implemented in order to preserve the shoreline or to create an expansion of land.

The design of coastal structures in modern times has become increasingly complex with a multitude of functions competing for vital space in coastal areas worldwide. In addition, the sea level rise due to climate change requires improving the design to ensure the safety of existing coastal structures. Optimum solutions are required for these complex matters, and the role of the coastal engineer here is to make the correct assessment based on the physical processes in the coastal region and the management of the coastal region.

One of the important hydrodynamic processes in coastal regions is the interaction of water waves with permeable coastal structures such as a rubble-mound breakwater. Rubble mound breakwaters have armour layers that are built of concrete pieces or crushed rocks. Even vertical breakwaters, which may be seen as an impervious structure, have a porous foundation which affects the stability of the caisson due to the uplift pressure. Research on these structures has been historically based on physical scale model testing. The study of three-dimensional fluid-structure interaction problems in the field of coastal engineering requires the use of complex models able to reproduce very different processes.

The progress achieved in the last decade in numerical modeling of wave structure interaction (mainly based on models using the Navier-Stokes equations) suggest these models will become increasingly important for the coastal engineer. One of the determining factors to generalize the use of numerical models for coastal engineering is

that the most advanced ones can handle flow through porous media, thus being able to simulate any structural typology.

1.2 Wave Hydrodynamics

Waves undergo deformations due to varying bottom topography and interaction with submerged and emerged obstacles. For past many years, many numerical models have been used to predict the behavior of these waves. It is essential to ascertain that the numerical model represents the fluid physics involved in these interactions in a realistic manner. The nearshore hydrodynamics include the transformation of wind-generated deep water waves into shallow water waves and then, due to breaking, into motions of different types and scales. The shallow water waves transform into small-scale turbulence, larger-scale coherent vortical motions, low-frequency waves and steady flows. The hydrodynamics only include the fluid motions and not the processes of sediment transport and morphological evolution. For short-term fluid computations, it is acceptable to ignore these processes because the transported sediment only has a weak influence on the hydrodynamics. Once a wave with a certain frequency and amplitude is generated it will propagate with a certain speed and direction. These properties will remain the same over a very long distance as long as the properties of the medium in which the wave travels will remain the same. However, if the wave with a certain wavelength encounters a sloping seabed with decreasing depth, and the wavelength is of the same order as the depth, the amplitude and direction will be affected by the limited water depth. The propagation of a wave is thereby affected and the wave will start to deform.

These effects can be described by the linear wave theory. The equations derived from the linear theory are applicable for waves with relatively low amplitude. When waves grow and steepen, they become nonlinear and the linear theory is not applicable anymore. However, in case the linear theory no longer holds, nonlinear theories are available such as the higher order Stokes wave theory, cnoidal wave theory, and the stream-function theory. The phenomenon of waves changing in the longitudinal direction (i.e. in the direction of propagation) due to variation in the group velocity in that direction is called shoaling, and the result is either an increase or decrease in wave amplitude. If the phase speed is changed along the wave crest because of a variable depth along the wave front, the wave will turn towards the shallower water. This process is called refraction. Another phenomenon is diffraction, which is caused by sudden change of amplitude along a wave front. This variation in amplitude is usually caused by a structure and causes the wave to turn towards the region with lower amplitude.

1.3 Computational fluid dynamics in Coastal Engineering

Coastal and marine civil engineering is the study of waves and the resulting loads, interaction and effects on the coast and related marine structures. Understanding the flow and wave phenomenons plays a vital role in making good qualitative and quantitative assessments.

Fluid flows are governed by partial differential equations which represent different conservation laws for the mass, momentum and energy. These conservation laws are represented by the Navier-Stokes equation which cannot be solved analytically. Earlier investigations were completely limited to experimental techniques to gain insight into such complex flow situations which are expensive, difficult and time consuming process. As an alternative, since these flow problems are represented by partial differential equations, numerical methods came into use to solve these equations. The basic approach of this method is to approximate such PDE systems by a large system of algebraic equations which can be solved by means of computers. Then, the flow problem is solved by the calculation of basic parameters such as the velocities, the pressure and the turbulence.

The accuracy of the experimental results which largely depend on the tools used, accuracy of numerical solutions depends on the quality of discretization used (Ferziger Peric, 1996) [33]. So fluid mechanics in conjunction with numerical analysis, computer science and engineering has led to the origin of new scientific discipline: Computational Fluid Dynamics (Zijlema, 1996) [45], or in a general way, Computational Fluid Dynamics (CFD) is a term that includes all techniques that involve numerical techniques to approximate and predict the motion of fluids using the Navier-Stokes equation. One of the disadvantages of such CFD methods are that they are computationally expensive and time consuming, but the recent advancements in computational power and efficient algorithms, large scale and 3D simulations can be carried out on fine grids to obtain a detailed solution of the flow field.

The CFD models are very useful in assessing complicated flow problems associated with waves and wave propagation such as wave breaking, wave interaction with structures and also computing the wave forces on different marine structures. Computational Fluid Dynamics (CFD) based numerical wave tanks require numerical recipes that ensure accuracy in generation, propagation and dissipation of waves. Use of numerical modeling as a research tool for the coastal engineer is gaining importance. A growing number of numerical models for wave-structure interaction have been developed in the past decades, with increasing complexity and accuracy. In particular the advent of CFD models based on the Reynolds-Averaged Navier-Stokes (RANS) equations has enabled the computation of flow fields with a sufficient level of detail and accuracy. In light of the previous concerns, the possibility of computing pressures

and flow velocities inside a permeable coastal structure is regarded as a significant added value to the design process.

Few articles in recent literature have presented numerical wave tanks using CFD methods based on the open-source CFD code OpenFOAM such as Jacobsen et al. (2011) [22] and Higuera et al. (2013) [18]. These numerical wave tanks use the Volume-of-Fluid (VoF) method to obtain the free surface with second-order accurate finite volume discretization schemes on an unstructured collocated grid. Wave generation and absorption is carried out using the relaxation method (Jacobsen et al., 2012) [22] or the active wave generation and absorption method (Higuera et al., 2013) [18]. The models have been applied to several problems in the field of coastal and ocean engineering such as wave interaction with porous coastal structures (Higuera et al., 2014) [18], slamming forces on bridge decks (Seiffert et al., 2014), wave forces on a cylinder due to non-linear waves, focussed irregular waves and multi-directional irregular waves (Paulsen et al., 2014); showing detailed flow features and accurately evaluating wave forces. These studies show that simulations in a CFD-based numerical wave tank can be used to investigate detailed wave hydrodynamics related to near-field wave-structure interaction which are not offered by other modeling approaches.
In the numerical model used in the current study, REEF3D, the level set method (Osher and Sethian, 1988) [32] is used for free surface capturing, the fifth-order Weighted Essentially Non Oscillatory (WENO) (Jiang and Shu, 1996) scheme for convection discretization scheme and a third-order Runge-Kutta scheme (Shu and Osher, 1988) [35] for time discretization on a staggered grid for tight velocity-pressure coupling. This provides numerically stable and accurate solutions to the RANS equations along with a sharp representation of the free surface and avoiding numerical damping of the waves propagating in the numerical wave tank.

1.4 Objectives of the study

- Carry out experiments to measure the wave kinematics in an wave tank with no obstacles, with an abutment and with a submerged rectangular obstacle.
- Validate the wave hydrodynamics in REEF3D by comparing numerical results with experimental data.
- Literature review on flow through porous media and implementation of VARANS in REEF3D
- Simulate fluid interaction with a porous structure using REEF3D.

Chapter 2

Numerical Model

This chapter briefly deals with the basic concepts of CFD and the computational methods employed in REEF3D, the CFD model used in this study.

2.1 Introduction to REEF3D

In this study, the open source CFD model REEF3D is used to fluid-porous structure interaction and other studies related to it. REEF3D is an open-source CFD program developed at the Department of Civil and Transport Engineering with special focus on solving problems in the field of marine, coastal and ocean engineering. The accurate modeling of waves requires higher order discretization schemes and a sharp representation of the free surface. REEF3D accomplishes this with the fifth-order WENO scheme for convection discretization and the level set method for obtaining a sharp representation of the free surface. The model describes the flow using incompressible RANS equations [4]. Turbulence is modeled with the two-equation $k - \omega$ model. These methods mentioned above is be explained in later chapters. Following are the few applications of REEF3D.

- Numerical Wave Tank
- Wave Forces
- Breaking Waves
- Floating body
- Open Channel flow
- Marine CFD

2.2 Governing Equations

2.2.1 Reynolds-Averaged Navier-Stokes Equations (RANS)

The RANS equations are the governing equations of Computational Fluid Dynamics (CFD). The RANS equations describe fluid flow and consist of a continuity equation and a momentum equation. An earth-bound Cartesian axis system (x,y,z) is used with the origin in the still water level with the z axis positive upwards.

The RANS equations are defined with the assumption of an incompressible fluid. The momentum conservation together with the continuity equation leads to the Navier-Stokes equations which provides a description of the flow:

$$\frac{\partial u_i}{\partial t} + u_j \frac{\partial u_i}{\partial x_j} = -\frac{1}{\rho}\frac{\partial p}{\partial x_i} + \frac{\partial}{\partial x_j}\left[\nu\left(\frac{\partial u_i}{\partial x_j} + \frac{\partial u_j}{\partial x_i}\right)\right] + g_i \tag{2.1}$$

where, u is the velocity averaged over time t, ρ is the fluid density, p is the pressure, ν is the kinematic viscosity and g is the acceleration due to gravity.
Eq. 2.1 has the following terms:

- The left hand side of the equation has a transient term given by a time derivative.
- The left hand side of the equation has a set of convection terms involving first order derivatives of the velocity components in the three coordinate directions.
- The right hand side of the equation has a diffusive term that involves a second derivative in all space dimensions of the per-unit-mass quantity in the balance equation. It is associated with the processes that tends to smooth out gradients in the flow.
- The right hand side of the equation contains terms, such as source and sink terms.

2.3 Numerical Methodology

2.3.1 Discretization Methods

To solve partial differential equations which contain different non-linear coefficients, time-dependence of the coefficients or the higher-order of the equations, three numerical methods can be categorized. These methods are used in such a way that most of the global/continuous information of the original problem and more importantly, the inherent structure, is retained. The 3 methods are as follows

- Finite difference methods

- Finite volume methods
- Finite element methods

The finite difference method is the most common method to solve partial differential equations and is the method used in this study. Finite volume methods calculate the values of conserved quantities, mass and momentum, averaged over a control volume. The values of the conserved quantities are considered within the control volume. Finite element methods approximate continuous quantities as a set of discrete quantities at discrete points. They can be applied to problems with great complexity.

For modeling fluid flows a second categorization can be made. Lagrangian models follow a fluid particle as it moves while Eulerian models have a fixed grid. Eulerian models are better capable to model topological changes. The RANS equations are solved with an Eulerian finite volume method. In this method the domain is subdivided using a mesh (grid). Each mesh cell is a control area (two dimensional domain) or control volume (three dimensional domain). For each of the cells the Navier Stokes equations are solved. A staggered grid is a grid on which the unknown variables are not located at the same grid points.Where as the collocated grid arrangement, all the variables are defined at the cell edges. Collocated finite volume methods for the incompressible Navier-Stokes equations suffer from pressure-velocity decoupling which gives rise to spurious pressure modes.

The following properties of the numerical solution should be satisfied for applicability to a particular problem:

- Consistency: Consistency defines a relation between the numerical scheme and the differential equation. A numerical scheme is consistent if the converges towards the continuous operator (with derivatives) of the PDE for $\Delta t, \Delta x \to 0$ (vanishing truncation error).
- Stability: Stability of a numerical solution ensures that the error caused by a small perturbation in the numerical solution remains bounded. A stable method should not diverge with the time.
- Convergence: The solution of the numerical scheme converges towards the real solution of the PDE for $\Delta t, \Delta x \to 0$.
- Accuracy: The scheme should not introduce too much numerical damping. In particular strongly varying, nonlinear flow problems ask for the implementation of higher-order schemes. Higher-order methods are generally less stable and an appropriate balance between robustness and accuracy needs to be found.
- Time step restrictions: Many numerical schemes are only stable under certain stability restrictions resulting in an upper bound on the time integration step. One can think of various scenarios in which these restrictions needlessly increase

the amount of computational time. It is better to avoid as much as possible artificial mathematical constraints like the CFL condition.

- Boundary conditions: When designing a numerical scheme it is relevant to consider the implementation of boundary conditions, both from the perspective of accuracy and stability and from the perspective of ease of implementation.

- Computational efficiency: A numerical scheme needs to be computationally efficient. Parallel computation for example can highly increase the efficiency of the scheme. Conditional statements and complex problems (e.g. limiters and Riemann solvers) can severly increase the computational load. Many modern compilers provide the possibility of program optimization, for example by means of vectorization of iterations.

2.3.2 Convection Discretization

The RANS equation mentioned in section 2.1 consist of convective, diffusive and source terms. These terms need to be discretized first in order to numerically solve the equation. Few of the schemes using finite difference are mentioned below.

- First-Order Upwind (FOU) Scheme:

  First-order upwind scheme uses the values upstream to evaluate the property on the boundaries of the cell and then use them to compute the value at the center of the cell. As it is a upstream value, it takes into account the flow direction. First-order upwind schemes are easy to converge and but are less accurate.

$$\frac{\partial u}{\partial x_j} = \frac{(u_i - u_{i-1})}{\Delta x_j}$$

- Central Difference Scheme (CDS): This method uses the points downstream and upstream of the point at which the values are calculated. It can be written as:

$$\frac{\partial U}{\partial x} = \frac{u_{i+1} - u_{i-1}}{2\Delta x}$$

  For damped situations this scheme is unconditionally unstable. As a result, in a case of large gradients, the performance of CDS would be in question. It is however more convenient compared to other high order discretization schemes and is independent of the flow direction.

- Weighted Essentially Non- Oscillatory (WENO) Scheme:

  WENO is a non-oscillatory scheme therefore, it can be applied especially for a stable calculation with minimum risk and this methods allow robust solutions and permit higher-order solutions at discontinuities. This methods relax the requirement of no overshoots or oscillations near a discontinuity. The first ENO scheme is given by Harten (1983) [16]. The third and fifth-order finite difference WENO schemes in a multi space dimension were constructed by Jiang (2000)[24], with a general framework for the design of the smoothness indicators and the nonlinear weights. An example of the implementation of this scheme in the Hamilton-Jacobi form to the level set function, ϕ_x in x-direction is presented as:

$$\phi_x = \begin{cases} \phi_x^- & if\ U_1 > 0 \\ \phi_x^+ & if\ U_1 < 0 \\ 0 & if\ U_1 = 0 \end{cases} \tag{2.2}$$

  The WENO approximation for a given level set function might be a combination of three possible approximations:

$$\phi_x^{\pm} = \omega_1^{\pm}\phi_x^{1\pm} + \omega_2^{\pm}\phi_x^{2\pm} + \omega_3^{\pm}\phi_x^{3\pm} \tag{2.3}$$

  The three ENO stencils defined for ϕ are

$$\begin{aligned} \phi_x^{1\pm} &= \frac{q_1^{\pm}}{3} - \frac{7q_2^{\pm}}{6} + \frac{11q_3^{\pm}}{6} \\ \phi_x^{2\pm} &= -\frac{q_2^{\pm}}{6} + \frac{5q_3^{\pm}}{6} + \frac{q_4^{\pm}}{3} \\ \phi_x^{3\pm} &= \frac{q_3^{\pm}}{3} + \frac{5q_4^{\pm}}{6} - \frac{q_5^{\pm}}{6} \end{aligned} \tag{2.4}$$

  with,

$$\begin{aligned} q_1^- &= \frac{\phi_{i-2} - \phi_{i-3}}{\Delta x},\ q_2^- = \frac{\phi_{i-1} - \phi_{i-2}}{\Delta x},\ q_3^- = \frac{\phi_i - \phi_{i-1}}{\Delta x}, \\ q_4^- &= \frac{\phi_{i+1} - \phi_i}{\Delta x},\ q_5^- = \frac{\phi_{i+2} - \phi_{i+1}}{\Delta x} \end{aligned} \tag{2.5}$$

  and

$$\begin{aligned} q_1^+ &= \frac{\phi_{i+3} - \phi_{i+2}}{\Delta x},\ q_2^+ = \frac{\phi_{i+2} - \phi_{i+1}}{\Delta x},\ q_3^+ = \frac{\phi_{i+1} - \phi_i}{\Delta x}, \\ q_4^+ &= \frac{\phi_i - \phi_{i-1}}{\Delta x},\ q_5^+ = \frac{\phi_{i-1} - \phi_{i-2}}{\Delta x} \end{aligned} \tag{2.6}$$

  the weights are written as:

$$\omega_1^{\pm} = \frac{\alpha_1^{\pm}}{\alpha_1^{\pm} + \alpha_2^{\pm} + \alpha_3^{\pm}},\quad \omega_2^{\pm} = \frac{\alpha_2^{\pm}}{\alpha_1^{\pm} + \alpha_2^{\pm} + \alpha_3^{\pm}},\quad \omega_3^{\pm} = \frac{\alpha_3^{\pm}}{\alpha_1^{\pm} + \alpha_2^{\pm} + \alpha_3^{\pm}}, \tag{2.7}$$

and

$$\alpha_1^{\pm} = \frac{1}{10}\frac{1}{\left(\widetilde{\epsilon} + IS_1^{\pm}\right)^2}, \quad \alpha_2^{\pm} = \frac{6}{10}\frac{1}{\left(\widetilde{\epsilon} + IS_2^{\pm}\right)^2}, \quad \alpha_3^{\pm} = \frac{3}{10}\frac{1}{\left(\widetilde{\epsilon} + IS_3^{\pm}\right)^2} \tag{2.8}$$

with the regularization parameter $\widetilde{\epsilon} = 10^{-6}$ in order to avoid division by zero and the following smoothness indicators:

$$\begin{aligned} IS_1^{\pm} &= \frac{13}{12}\left(q_1 - 2q_2 + q_3\right)^2 + \frac{1}{4}\left(q_1 - 4q_2 + 3q_3\right)^2, \\ IS_2^{\pm} &= \frac{13}{12}\left(q_2 - 2q_3 + q_4\right)^2 + \frac{1}{4}\left(q_2 - q_4\right)^2, \\ IS_3^{\pm} &= \frac{13}{12}\left(q_3 - 2q_4 + q_5\right)^2 + \frac{1}{4}\left(3q_3 - 4q_4 + q_5\right)^2 \end{aligned} \tag{2.9}$$

2.4 Time Discretization

REEF3D has the 2nd order Adam-Bashforth, the third order TVD and the fourth order Runge-Kutta schemes included in the code for the purpose of higher accuracy, as flow characteristics change rapidly over the time. This study uses the third-order TVD Runge-Kutta scheme.

- Adam-Bashforth Scheme: It is an explicit 2nd order scheme given by Hairer (1983) [14] that employs the values from the previous time steps for evaluating the value for the next time step for temporal integration. An application of the scheme to the level set function is :

$$\phi^{n+1} = \phi^n + \frac{\Delta t_n}{2}\left(\frac{\Delta t_n + 2\Delta t_{n-1}}{\Delta t_{n-1}} L\left(\phi^n\right) - \frac{\Delta t_n}{\Delta t_{n-1}} L\left(\phi^n\right)\right) \tag{2.10}$$

  The term 'L' represents the spatial discretization.

- Third Order-Total Variance Diminishing (TVD) Runge Kutta Scheme: This is an explicit 3rd order scheme which rules out the spurious oscillations by suppressing the local extrema [17]. An example of a such implementation is the third order TVD Runge Kutta scheme [35]:

$$\begin{aligned} \phi^{(1)} &= \phi^n + \Delta t L\left(\phi^n\right) \\ \phi^{(2)} &= \frac{3}{4}\phi^n + \frac{1}{4}\phi^{(1)} + \frac{1}{4}\Delta t L\left(\phi^{(1)}\right) \\ \phi^{n+1} &= \frac{1}{3}\phi^n + \frac{2}{3}\phi^{(2)} + \frac{2}{3}\Delta t L\left(\phi^{(2)}\right) \end{aligned} \tag{2.11}$$

2.5 Turbulence Modeling

The RANS equations are solved for the domain in an iterative process. For turbulent flows, this requires a very fine numerical grid when full computation of the turbulent fluctuations is done, which would result in an unrealistic high computational cost. Instead the turbulence is approximated with a turbulence model. In table 2.1, few elaboration of the possibilities is shown in which it becomes clear that a higher accuracy also results in higher computational costs. One of the often used models is the k-ω model which is most widely used and validated.

Table 2.1: Advantages and disadvantages of several turbulence models, [1]

Turbulence model	**Advantages**	**Disadvantages**
Direct numerical modeling (DNS)	- For low Re numbers	- Huge costs - Huge amount of data
Large-eddy simulation (LES)	- For complex flows and structures in flows -Gives a lot of information	- High costs - Difficult to identify time convergence - Requires additional treatment at no-slip walls
Standard k-ϵ model	-Most widely used and validated	- Round jets - Flows involving significant curvature
k-ω model	-For low Re regions -No wall functions required -Adverse pressure gradients	- Fine mesh needed close to the wall

The present study uses the Wilcox's $k-\omega$ model [44] along with RANS equation. REEF3D also has provision for $k-\epsilon$ model [27], EARSM [43], SST [29] and LES model.

- $k-\omega$ Model

  The $k-\omega$ model is a two-equation model based on the energy transport equations. One of the variables transported is the turbulent kinetic energy, k and the other is the turbulent dissipation, ω. Then the eddy viscosity, ν_t is calculated using k and the ω (Eq. 2.16). The transport equations for k and ω are given as :

$$\frac{\partial k}{\partial t} + u_j \frac{\partial k}{\partial x_j} = \frac{\partial}{\partial x_j}\left[\left(\nu + \frac{\nu_t}{\sigma_k}\right)\frac{\partial k}{\partial x_j}\right] + P_k - \beta_k k\omega \tag{2.12}$$

$$\frac{\partial \omega}{\partial t} + u_j \frac{\partial \omega}{\partial x_j} = \frac{\partial}{\partial x_j}\left[\left(\nu + \frac{\nu_t}{\sigma_\omega}\right)\frac{\partial \omega}{\partial x_j}\right] + \frac{\omega}{k}\alpha P_k - \beta\omega^2 \tag{2.13}$$

$$\nu_t = min(\frac{k}{\omega}, \sqrt{\frac{2}{3}}\frac{k}{|S|}) \tag{2.14}$$

where, P_k is the production rate and the closure coefficients $\sigma_k = 2$, $\sigma_\omega = 2$, $\alpha = 5/9$, $\beta_k = 9/100$, $\beta = 3/40$. $|S|$ is the mean strain rate, which can be large in the case of oscillatory flow motion. The eddy viscosity ν_t is limited using Eq. (2.34) to avoid overproduction of turbulence in strained flow outside the boundary layer. Increased turbulent dissipation takes place in the vicinity of the free surface due to reduced turbulent length scales. Damping of the turbulent fluctuations also occurs normal to the surface leading to redistribution of intensity parallel to the interface. Due to a high value of $|S|$ near the air-water interface, a standard RANS turbulence closure will give inaccurate results. Thus, additional turbulence damping is required. The specific turbulent dissipation at the free surface is given by:

$$\omega_s = \frac{c_\mu^{-\frac{1}{4}}}{\kappa} k^{\frac{1}{2}} \cdot \left(\frac{1}{y'} + \frac{1}{y^*}\right) \tag{2.15}$$

where, $c_\mu = 0.07$ and $\kappa = 0.4$. y' is the virtual origin of the turbulent length scale and has a value 0.07 times the water depth found empirically by [20]. y^* is the distance from the nearest wall for a smooth transition to wall boundary value of ω. The specific turbulent dissipation is activated around the interface by multiplying it with the Dirac delta function $\delta(\phi)$:

$$\delta(\phi) = \begin{cases} \frac{1}{2\epsilon}\left(1 + \cos\left(\frac{\pi\phi}{\epsilon}\right)\right) & if \ \ |\phi| < \epsilon \\ 0 & else \end{cases} \tag{2.16}$$

2.6 Modeling of the Free Surface

A large collection of fluid problems involve moving interfaces such as air-water dynamics, breaking surface waves. In many such applications, the interplay between the interface dynamics and the surrounding fluid motion is subtle, with factors such as density ratios, temperature jumps across the interface, surface tension effects and boundary conditions playing significant roles in the dynamics. The free surface of water is modeled using a two-phase flow approach. The different methods available for this is given below:

- Volume of Fluids (VOF) Method: Volume of Fluid (VOF) technique, which was first reported by Nichols and Hirt [19]. The VOF method consists of three ingredients: a scheme to locate the surface, an algorithm to track the surface as a sharp interface moving through a computational grid, and a means of applying boundary conditions at the surface. VOF method is an Eulerian fixed-grid technique with an interface tracking scheme.

- Level Set Method (LSM):

  Level set methods are computational techniques for tracking moving interfaces; they rely on an implicit representation of the interface whose equation of motion is numerically approximated using schemes built from those for hyperbolic conservation laws. The resulting techniques are able to handle problems in which the speed of the evolving interface may sensitively depend on local properties such as curvature and normal direction, as well as complex physics off the front and internal jump and boundary conditions determined by the interface location. Level set methods are particularly designed for problems in multiple space dimensions in which the topology of the evolving interface changes during the course of events.

- Particle Level Set Method:

  The Particle Level set (PLS) method [9] is an interface capturing method that uses the advantages of both Eulerian and Lagrangian methods. The main representation is a signed distance function evolved using Level set methods and it uses auxiliary marker particles to accurately track the surface and correct the signed distance function. The method has been very popular and successfully used in both research and in visual effects

2.7 Solution to Navier-Stokes equation

In order to obtain a complete solution of the RANS equation present in Eq. (2.1), the pressure contribution represented in the momentum conservation needs to be solved. Direct solution for this is not possible due to the involvement of non-linear terms which makes it computationally expensive. The numerical model REEF3D offers many algorithms for the treatment of the pressure term such as:

- Projection Method (PJM)
- Semi Implicit Method for Pressure Linked Equation (SIMPLE)
- SIMPLEC (SIMPLE-Consistent)
- SIMPLER (SIMPLE-Revised)

- PISO (Pressure Implicit with Split Operator)

The most common and the implemented scheme for solving the incompressible RANS equations is the so-called projection method. Here, the starting point is the consideration of the time-discrete RANS equations using a forward Euler scheme; i.e., it will compute the solution u^{n+1} at time t^{n+1} from the solution of the previous time step u^n [5]. One of the advantages of using this method is that it decouples the velocity and pressure field. First, we compute an intermediate velocity field U_i^* by ignoring pressure gradients using the transient equation.

$$\frac{\partial(u^* - u_i^n)}{\partial t} + u_j^n \frac{\partial u_i^n}{\partial x_j} = \frac{\partial}{\partial x_j}\left[\nu(\phi^n)\left(\frac{\partial u U_i^n}{\partial x_j} + \frac{\partial u_j^n}{\partial x_i}\right)\right] + g_i \tag{2.17}$$

In the second step, the projection step, the pressure is used to determine the velocity at time step $n+1$.

$$\frac{\partial(u_i^{n+1} - u_i^*)}{\partial t} + \frac{1}{\rho(\phi^n)}\frac{\partial p^{n+1}}{\partial x_i} = 0 \tag{2.18}$$

Since the pressure term in the above equation is unknown, it is calculated using a divergence operator such that divergence of U_i^{n+1} equals zero is applied. The equation obtained then is called Poisson pressure equation.

$$\frac{\partial}{\partial x_i}\left(\frac{1}{\rho(\phi^n)}\frac{\partial P}{\partial x_i}\right) = -\frac{1}{\Delta t}\frac{\partial U_i^*}{\partial x_i} \tag{2.19}$$

2.8 Iterative Solver

For solving Eq. 2.19, two type of methods are available; namely direct methods and iterative methods. Since direct methods are computationally expensive, iterative solvers are the preferred option for the solution of Poisson equation. There are various iterative techniques available like the Jacobi method, the Gauss-Seidel method, the Successive Over-Relaxation method, the Conjugate Gradients method, the Bi-Conjugate Gradient method, and the Multigrid method.

For this present study the HYPRE solver library is employed. HYPRE is a software library of high performance preconditioners for solutions of large and sparse linear systems on massively parallel computers [11]. In the HYPRE library, Bi Conjugate Gradient Stabilized (BiCGstab) method is used to solve the Poisson equations and

it is preconditioned with PFMG. The Bi Conjugated Gradient (BiCG) is used for non-symmetric equations. This method first converts non-symmetric systems into symmetric systems. This method is given by der Vorst (1992) [39], and it converges faster and produces more stable solutions.

2.9 Immersed Boundary

Simulation of the flow around immersed boundary is carried out on a grid (usually Cartesian) which does not conform to the boundary shape. This is not a viable option when dealing with a flow around a complex geometry. The Numerical model used in this study REEF3D allows to deal with such problems using ghost cell immersed boundary method [2]. The cut cells and complex geometries can be accounted for using this method. This method detects the boundary and determine the adjacent ghost cells and then extrapolate to find the ghost cell value required to impose the boundary condition implicitly. Fig 2.1 shows the extrapolation along the orthogonal lines across the solid boundary using the ghost cell immersed boundary condition.

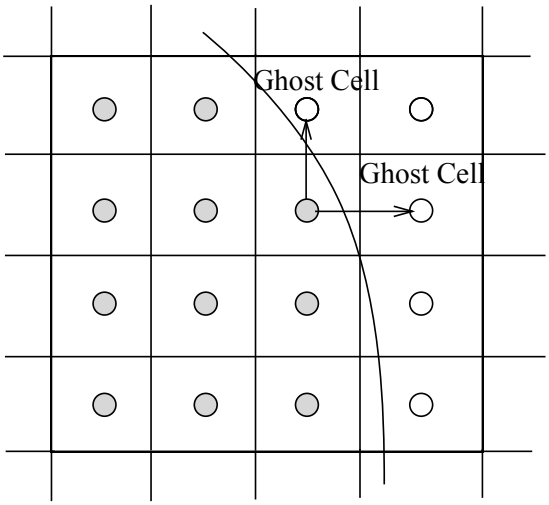

Figure 2.1: Ghost Cell Immersed Boundary

2.10 Numerical Wave Tank

The accurate prediction and modeling of the behavior of ocean waves is an important aspect in the field of coastal and ocean engineering. In the last few years the computational power has increased and numerical models and numerical wave tanks (NWT) have become an increasingly viable option for the modeling of waves. A numerical wave tank is an alternative to the physical modeling because studying different wave

conditions and implementing the modifications are more conveniently performed using numerical models. There are different methods on which Numerical wave tanks are based on. Some of them are:

- RANS equations with free surface description by VOF method
- RANS equations with free surface description by Level Set Method
- Combination of Potential theory and RANS equations

In order to replicate the behavior of a physical wave tank the boundary conditions of the numerical wave tank need to be chosen to recreate physical behavior. The numerical wave tank consists of 6 boundaries: inlet, outlet, atmosphere, bottom and front and back.

2.10.1 Wave Generation and Absorption

Typical inlet boundaries for free surface flows are of Dirichlet type. This fixed value boundary condition is the simplest and the first to be implemented in most wave generating models, since theories give analytical expressions for free surface and the velocity distribution throughout the water column. To generate waves using this method, two variables for each time step are required. The first one is the free surface level at the generation boundary and the other one is velocity (horizontal and vertical components). This kind of boundary condition can be used to replicate the behavior of any laboratory wave maker (at a resolution equal to cell size).

Relaxation method can be used to generate waves at the beginning and to absorb waves at the end and thereby prevent reflected waves from effecting the wave generation as shown in Fig. 2.2. Wave generations are in Zone 1 and wave absorption in zone 3.

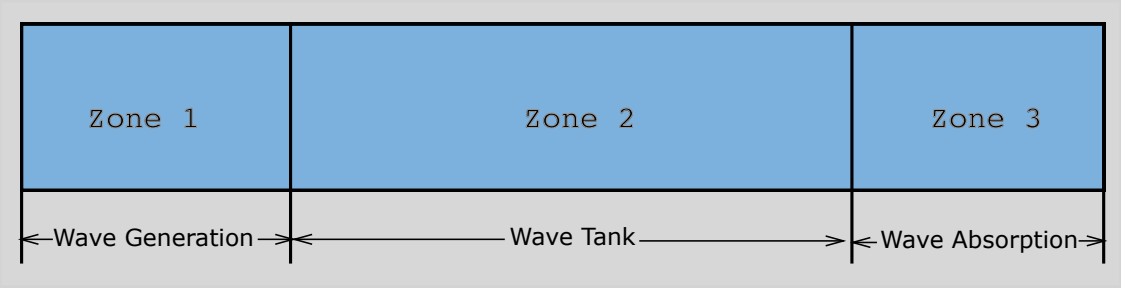

Figure 2.2: Sections of a Numerical Wave Tank

In this Relaxation method generated waves are moderated after every time step with an analytical solution [26]. The relaxation zones 1 and 3 is obtained using following rules on pressure and velocity.

$$
\begin{aligned}
u_{relaxed} &= \varphi(x) u_{analytical} + (1 - \varphi(x) u_{computational} \\
p_{relaxed} &= \varphi(x) p_{analytical} + (1 - \varphi(x) p_{computational}
\end{aligned}
\tag{2.20}
$$

$$
\begin{aligned}
u_{relaxed} &= \varphi(x) u_{computational} + (1 - \varphi(x) u_{analytical} \\
p_{relaxed} &= \varphi(x) p_{computational} + (1 - \varphi(x) p_{analytical}
\end{aligned}
\tag{2.21}
$$

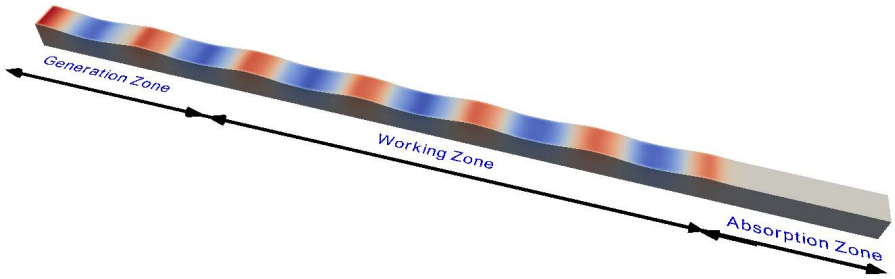

Figure 2.3: Different zones in the numerical wave tank

Chapter 3

Validation and Discussion

3.1 Lab setup and Experiments

The aim of this section is to validate the numerical model by comparing the results between experimental data and numerical data. Several laboratory tests were conducted in the wave flume tank at NTNU. This section describes all the laboratory equipment used for the experiments, methodology followed for conducting the tests and data acquisition. Then, the experiments are simulated using REEF3D and the results are compared and discussed.

3.1.1 Flume Setup

All laboratory experiments were carried out in the wave flume at the hydrodynamic laboratory at NTNU. The flume is 20m long, 0.85m wide and 0.6m deep (Fig. 3.1). It has a hydraulically driven piston-type wave maker as shown in Fig. 3.2a. Normally the input parameters of the wave generators are the wave period (or frequency) and the wave height. There are wave absorbers placed at the opposite end of the flume and are made out of perforated steel plates. These wave absorbers are used to prevent the reflecting of the waves.

3.1.2 Equipment

- **Wave Gauges**: The wave gauge system is a simple and reliable device for measuring changing water levels in physical models and is used with data acquisition and analysis software to measure wave height in a flume or a 3D basin. The wave gauges are made out of steel tubes and it measures the water level as the immersed depth proportional to the output voltage of the wave gauges. The wave probes operate by measuring the electric current that flows between two stainless steel wires that are immersed in water(Fig. 3.2b).

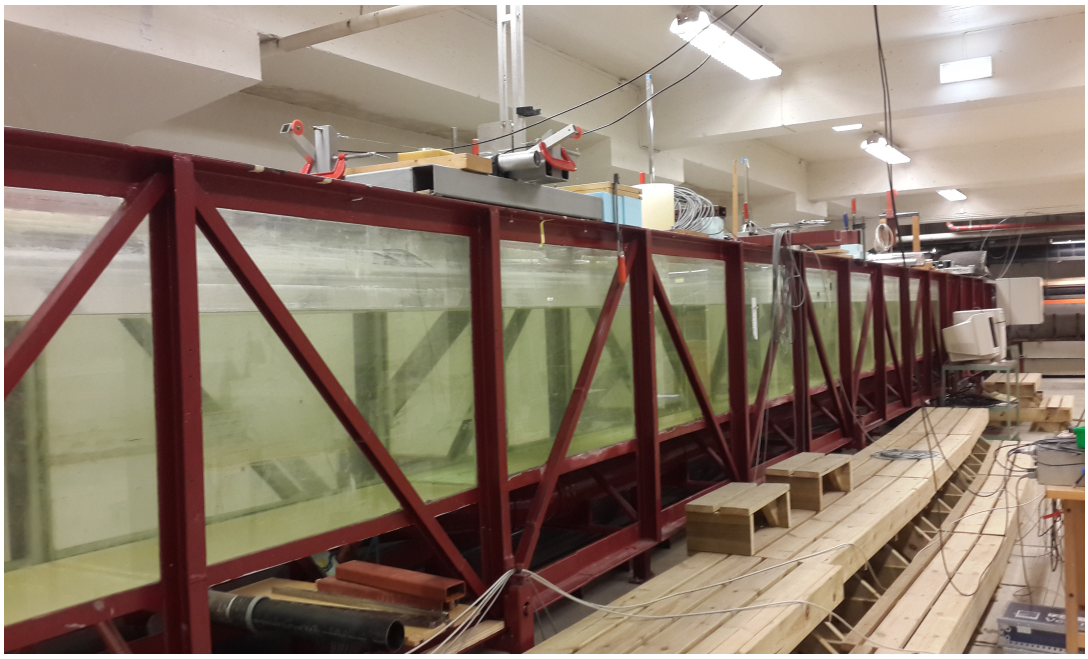

Figure 3.1: Wave flume at hydrodynamics laboratory, NTNU

(a) DHI wave maker

(b) Wave gauge used in the experiment

Figure 3.2: Wave gauge and Wave maker used in experiments

Eight wave gauges are used throughout the experiments and their positions are changed according to the area of interest. Normally these wave gauges have to

be calibrated before running the waves, if the water level is changed or if the wave flume is refilled.

The calibration of the wave gauges is done by lifting or lowering the wave gauges and adjusting the voltages based on the heights. For example, adjust the wave gauges so that 20cm of water level height corresponds to 10V (20cm = 10V). So lowering of the wave gauge by 5 cm should be set to a corresponding voltage of 2 volts (or 2.5 volts). Similarly if we lift the wave gauge by 10 cm (i.e. back to 0 and the lift 5 cm), the corresponding voltage should be -2 volts. This is called as the Gain factor,which depends on water quality (conductivity in water). A filter of 10Hz (Low pass filtering) is used to remove random noises in the measurements (ripples). These waves give analogue signals to relevant wave gauges are converted to digital signal in order to get required data. So, an amplifier system and an analogue-digital convertor is employed. This amplifier system shown in figure 3.3 is not just for converting signals but also it plays an important role on data acquisition. For all the tests, the sampling rate was 40 Hz with a warm up time of 10 s. Warm up time indicates how long the wave maker run before making samples to make sure that waves have propagated across the gauges.

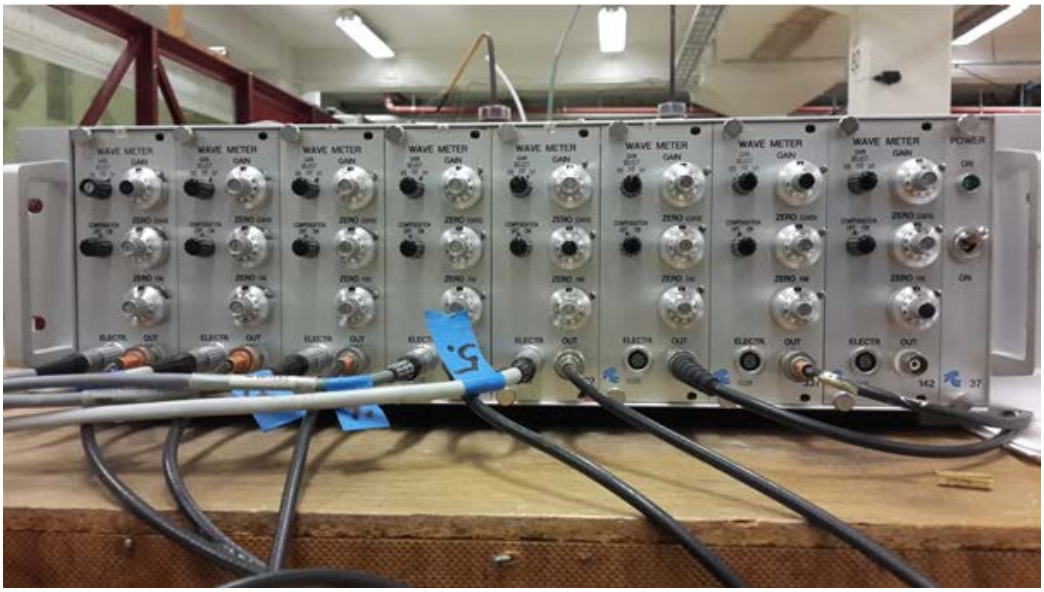

Figure 3.3: Amplifier

- **Acoustic Doppler Velocimeter**

  Two Vectrino velocitimeters are used in the experiments to measure the water particle velocity in the flume. [31].In these velocitimeter a pulse is transmitted from the centre transducer, and the Doppler shift introduced by the reflections from particles suspended in the water, is picked up by the four receivers. The echo is then processed to find the Doppler shift, the scaling is adjusted with the

measured speed of sound in the liquid , and the velocity vector is recorded or transmitted to a PC at a rapid rate. In the lab, water is usually quite clean and requires artificial introduction of particles. This is called seeding. To check if water is properly seeded, the Vectrino ADV software interface provides readout of signal-to-noise ratio (SNR). This is an indicator of how well the flow is seeded; the higher the SNR, the better the seeding and the more reliable the velocity measurements. In the laboratory, the minimum SNR at which the ADV should be operated is about 15. Four acoustic probe tips (one transmitter and three receivers), all send and receive acoustic information in a fluid volume below the ADV, referred to as the sampling volume. Because the ADV is inserted into the flow, the sampling volume must be far enough away from the probe tip so as not to disturb the flow and the velocity measurements. Sampling rate is kept at 200 Hz with a transmit length of 1.8 mm and sampling volume of 5.50 mm.

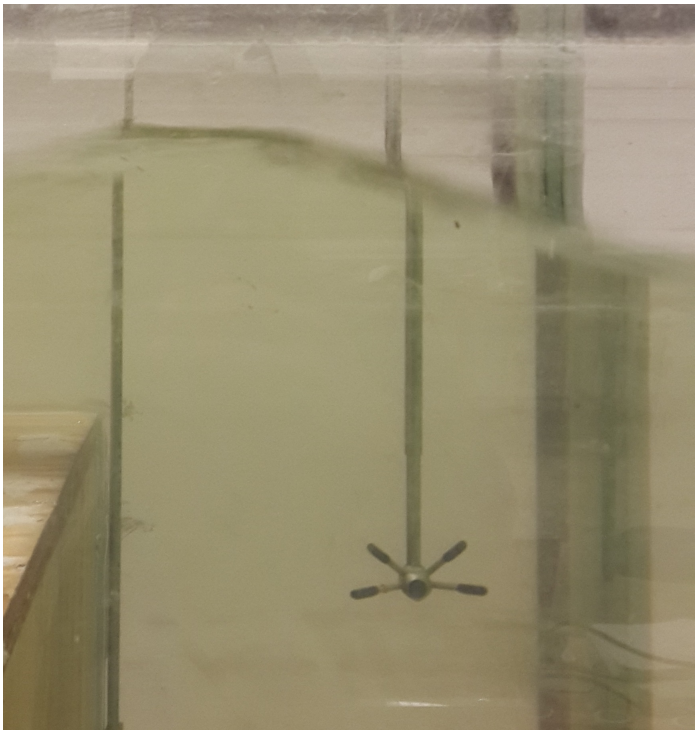

Figure 3.4: ADV used in the experiment

3.1.3 Test Methodology

The methodology implemented for conducting the lab experiments for validating the numerical model will be discussed here. 3 set of experiments were done in the flume,

- **Wave flume without obstacles**
- **Step structure in wave flume**
- **Abutment Structure in wave flume**

3.1.3.1 Wave flume without obstacles

There is no active absorption at the wave generation and also only a artificial beach is present at the other end of the flume. First set of tests were conducted in an empty flume with an aim to see whether there are reflections in the flume. These tests were important to analyze the wave propagation and possible reflections in the flume and is critical for the remaining tests which have structures present in the flume. A plan view of the flume with the locations of wave gauges and ADVs are shown in Fig. 3.6 and a propagation of regular wave in flume is shown in Fig. 3.5 . Accurate distances of wave gauges and ADVs were measured which is important while simulating the same cases in the numerical model for accurate results. These distances are shown in Table 3.1. For wave gauges both the distance from wave maker (x) and from the front wall of flume (z) is important. In case of ADVs the distance from wave maker (x), distance from the bottom of the tank (y) and from the front wall of flume (z).

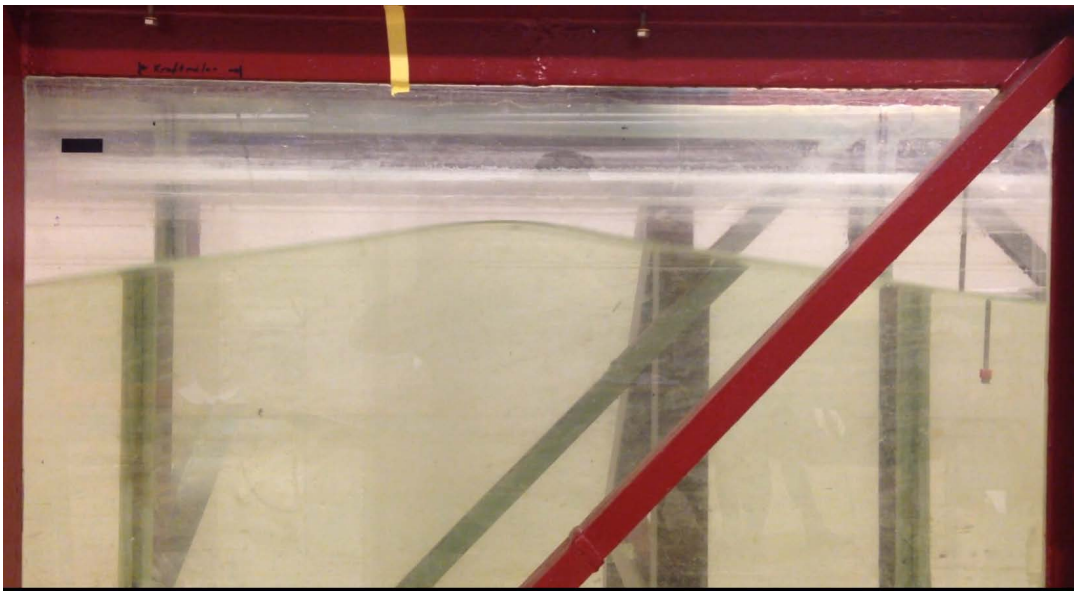

Figure 3.5: Empty flume with Regular waves

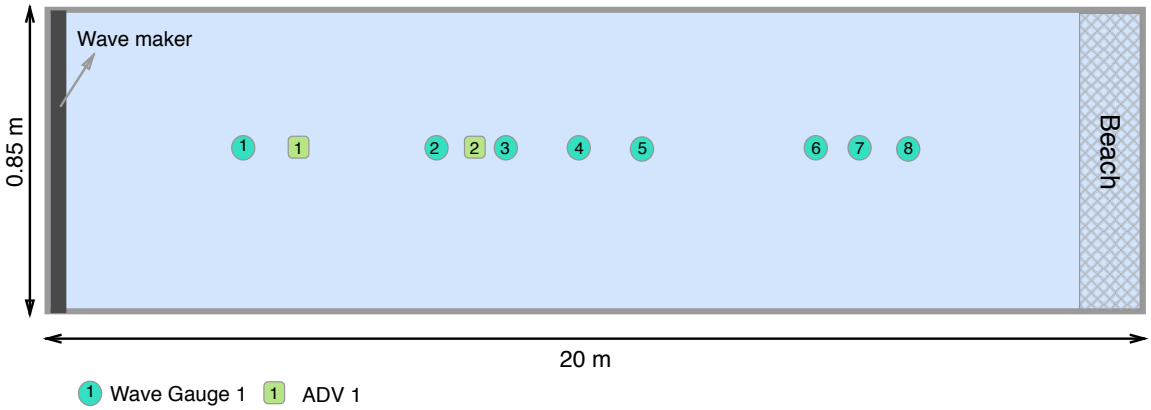

Figure 3.6: Set up for Empty wave tank test

Table 3.1: WG and ADV locations for EWT (WM - Wave Maker, FW - Front Wall, WL - Water Level

WG	x (m) From WM	z (m) From FW	ADV	x (m) From WM	y (m) From WL	z (m) From FW
WG1	5	0.3	**ADV 1**	5.775	0.365	0.3
WG2	9.25	0.3	**ADV 2**	9.535	0.365	0.3
WG3	9.85	0.3				
WG4	10.15	0.3				
WG5	10.50	0.3				
WG6	15	0.3				
WG7	15.5	0.3				
WG8	16	0.3				

A total of 8 wave gauges and 2 ADVs were used as shown in figure 3.6. The location of wave gauges for the empty wave tank tests were chosen in order to study the wave propagation and reflection. The artificial beach at the end of the flume is a sloping faced system with multiple perforated sheets and these sheets extended further into the tank to absorb longer wave lengths. Through these test the absorption capacity of this artificial beach can be analyzed. This will be concluded after simulating these cases in the numerical model and then comparing it with the experimental data which will be discussed in the upcoming sections.

There were 12 set of tests conducted in the flume for different combinations of wave height and wave period (Table 3.2).For all the test water depth was kept at 0.5m in the flume and tests were done for regular waves. The reasons behind selecting these combinations of wave heights and periods were,

- To validate for cases with small and high waves
- The highest wave height should not go over the wave gauges, so the amplitude of the waves should not be larger than the rods of wave gauges above water level
- Too high and too long waves can cause reflections at the end of the flume and also in front of the structure (if present)

These combinations mentioned in Table 3.2 are similar to those used for the tests with structures. During the tests, it was made sure that the water level came to complete rest before the start of the next test. As mentioned in section 3.1, these wave gauges are really sensitive and it was important to check if the zero level of wave gauges corresponds to 0 volt in the system. Some of these wave gauges was subjected to calibration after the tests as they were inaccurate.

Table 3.2: Test sequence for Empty wave tank

Test Number	**Wave Height, H (m)**	**Wave Period, T (s)**
T1	0.01	0.75
T2	0.05	0.75
T3	0.08	0.75
T4	0.10	0.75
T5	0.01	1.0
T6	0.05	1.0
T7	0.08	1.0
T8	0.10	1.0
T9	0.01	1.25
T10	0.05	1.25
T11	0.08	1.25
T12	0.10	1.25

3.1.3.2 Step structure

The step structure was 2 m long, 0.6 m wide and 0.4 m high (Fig. 3.7). Similar to wave tank tests with no obstacles, water depth for test with step structure was also kept at 0.5 m. Four Wave gauges are kept on top of the step structure since that's where a lot of wave transformations are expected to happen. Also 2 ADV'S were placed, one 5.75 m from wave maker and other one 9.9 m from wave maker (In front of the step). The arrangement of step structure, wave gauges and ADVs is shown in Fig. 3.8. The distances of wave gauges and ADVs are shown in Table 3.3.

During the experiments, it was observed that for higher waves there were good amount of reflection in front of step. This was expected since the water level was set at 0.5 m and the height of the step structure was 0.4m high. The reason for such a high step is to make sure that the data obtained via wave gauges will contain complex changes in free surface and will be ideal for validating with the numerical model. For wave heights upto 0.04 m there were only a small amount of transformation (close to shoaling). For wave height of 0.05 m shoaling was clearly visible, and for wave height higher than 0.05 m, it started breaking as soon as it started propagating over the step structure (depth induced breaking). After the step, these waves were transformed into low frequency waves and also the reflection from the front of the step structure clearly effected the wave generation.

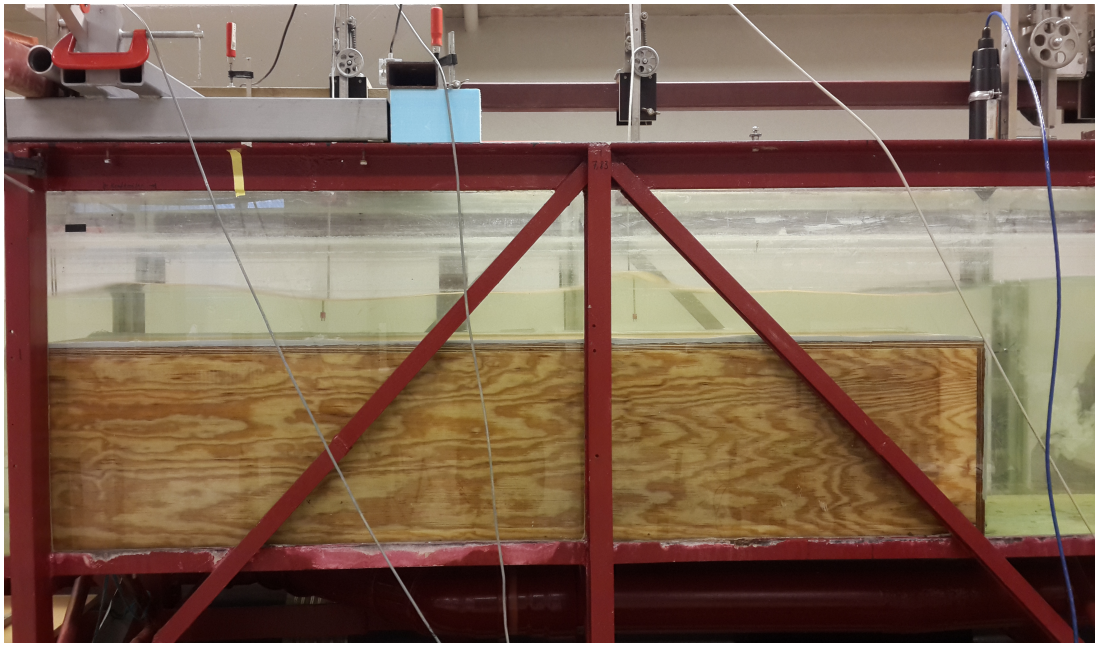

Figure 3.7: Step structure in Flume

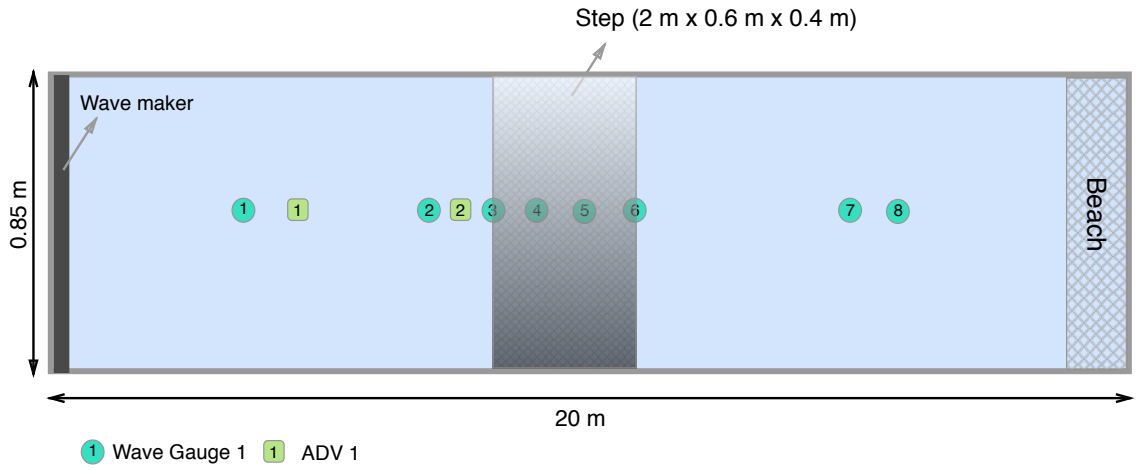

Figure 3.8: Set up for Step structure test

Table 3.3: WG and ADV locations for Step structure (WM - Wave Maker, FW - Front Wall, WL - Water Level

WG	x (m) From WM	z (m) From FW	ADV	x (m) From WM	y (m) From WL	z (m) From FW
WG1	5	0.3	**ADV 1**	5.775	0.35	0.3
WG2	9.625	0.3	**ADV 2**	9.905	0.35	0.3
WG3	10.038	0.3				
WG4	10.763	0.3				
WG5	11.468	0.3				
WG6	12.098	0.3				
WG7	14.5	0.3				
WG8	15.50	0.3				

The list of tests done for the step structure is shown in table 3.4. The reason for these combinations are exactly the same as those mentioned for the tests in wave tank with no obstacles. For wave heights higher than 0.05 m, which resulted in breaking, the data acquired by ADV-2 were not ideal since they was close to the step. Also wave gauges close to wave breaking didn't provide much valuable data. Some of these acquired data will be shown in validation section where the accuracy of the numerical model will be analyzed. Wave heights used for the tests ranged from 0.034 to 0.1 and wave periods of 0.75 s, 1.0 s and 1.25 s.

Table 3.4: Test sequence for Step structure

Test Number	**Wave Height, H (m)**	**Wave Period, T (s)**
T1	0.034	0.75
T2	0.04	0.75
T3	0.05	0.75
T4	0.08	0.75
T5	0.1	0.75
T6	0.034	1.0
T7	0.04	1.0
T8	0.05	1.0
T9	0.06	1.0
T10	0.08	1.0
T11	0.1	1.0
T12	0.034	1.25
T13	0.04	1.25
T14	0.05	1.25
T15	0.06	1.25
T16	0.08	1.25
T17	0.1	1.25

3.1.3.3 Abutment Structure

The next set of experiments was done using an abutment structure in the flume. The flume was drained after the tests with the step structure and then the abutment was attached to the back wall of the flume. The abutment had to stick strongly to the wall in-order to resist any kind of movement during waves. The abutment structure was 0.8 m high, 0.3 m wide and 0.5 m long, with a distance of 0.3 m remaining between the structure and the glass walls for the wave to propagate (Fig. 3.9). The flow through these gap was expected to undergo transformation and 3 wave gauges was kept in this confined space. One gauge at the beginning of the abutment, one in the middle and one at end of the abutment. Apart from this, 2 Wave gauges were kept between the abutment and the wave maker to capture the incoming flow and the remaining wave gauges were placed after the structure. It would have been ideal to keep more wave gauges in that confined space between Abutment and glass walls, but attaching more than 3 wave gauges in a space of 0.5 m was not possible. The arrangement of wave gauges and ADVs are shown in Fig. 3.10. The exact distances for these wave gauges and ADVs are shown in Table 3.5. 2 ADVs was kept between the start of the Abutment and wave maker; 1 to capture the particle velocity of the incoming wave and other one to capture the changes in velocity due to narrowing of the flume. During the experiments it was important to keep the SNR (Signal to Noise Ratio) above 15. This was made sure by adding dye near the probe points of ADV's which increased the SNR.

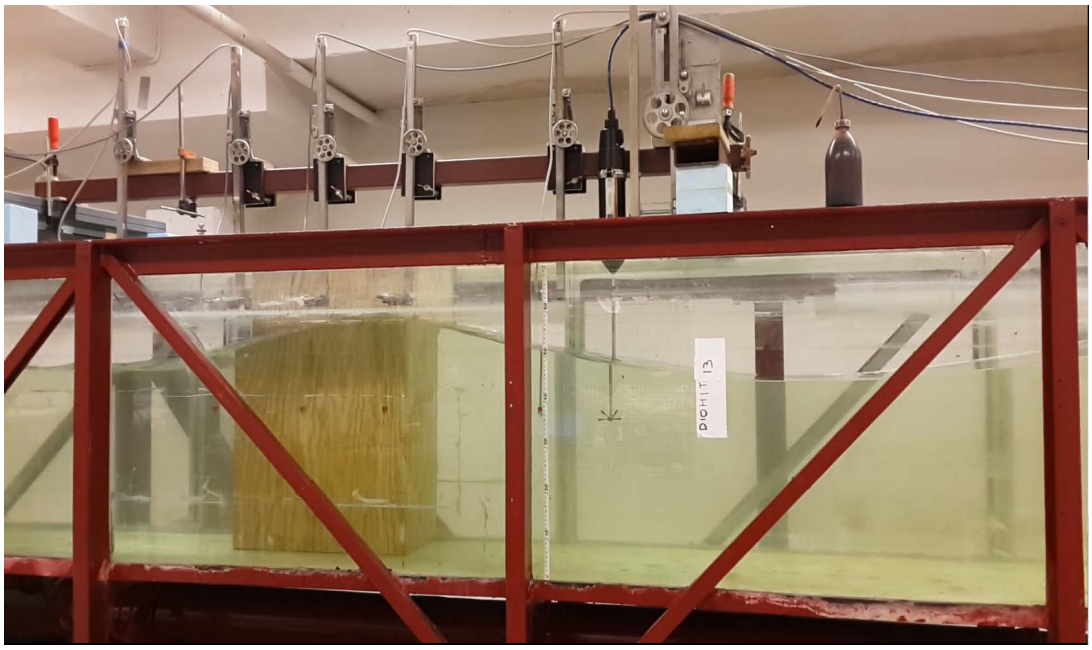

Figure 3.9: Abutment structure in flume

Table 3.5: WG and ADV locations for abutment structure (WM - Wave Maker, FW - Front Wall, WL - Water Level

WG	x (m) From WM	z (m) From FW	ADV	x (m) From WM	y (m) From WL	z (m) From FW
WG1	5	0.285	**ADV 1**	5.775	0.36	0.3
WG2	9.80	0.15	**ADV 2**	9.905	0.345	0.3
WG3	10.20	0.15				
WG4	10.45	0.15				
WG5	10.70	0.15				
WG6	11.10	0.15				
WG7	14.5	0.3				
WG8	15.50	0.3				

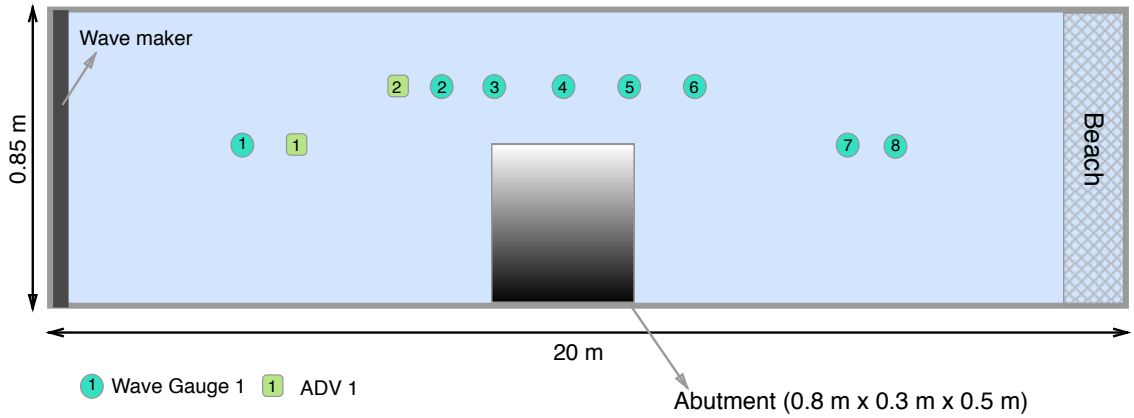

Figure 3.10: Set up for abutment structure test

Before the start of the tests some trial runs were done to know the limit of wave heights that can be generated in this case. Similar to step structure since the abutment covered half of the flume, reflection was expected. So during the trail runs it was clear that wave height above 0.06 m created considerable reflections in the flume and were not viable for validation purpose. The combination of wave heights and wave periods used for the tests are shown in Table 3.6. For tests with H $>$ 0.03, complex wave transformations were witnessed in the space between the abutment and glass walls and also after the structure. For tests with H = 0.06, formation of standing waves was seen in the part between the abutment and the wave maker.

Table 3.6: Test sequence for abutment

Test Number	**Wave Height, H (m)**	**Wave Period, T (s)**
T1	0.01	0.75
T2	0.03	0.75
T3	0.05	0.75
T4	0.06	0.75
T5	0.03	1
T6	0.05	1
T7	0.06	1
T8	0.03	1.25
T9	0.05	1.25
T10	0.06	1.25

3.1.4 Data Processing

Once these tests were completed, the data obtained (surface elevation and velocity) needs to be processed to a usable format. Data processing of surface elevations were done using MIKE0 software by converting the data points into an ASCII format. Processing the ADV data was more complex compared to surface elevation. Output files obtained for these ADVs was converted to readable format using the default Vectrino software. A example for the data obtained from the ADV is shown in Fig. 3.11a. It can be seen that there is a lot of noise in the signal which needs to be removed. So for this the theoretical velocity is calculated for the particular case and the values above it are removed from the time series.This is called Despiking the data where a lot of noise is present. For example if the theoretical velocity is calculated to be 30 cm/s,the velocities above +30 cm/s and velocities less than -30 cm/s are removed from the time series. The resultant time series is shown in Fig. 3.11b.

The resulting time series is then passed through a low pass filtering. A low-pass filter is a filter that passes signals with a frequency lower than a certain cutoff frequency and attenuates signals with frequencies higher than the cutoff frequency. The first, and probably best-known filter approximation is the Butterworth or maximally-flat response which is used in this study. Filters in this class are specified by two parameters, the cutoff frequency and the filter order. The frequency response of these filters is monotonic, and the sharpness of the transition from the passband to the stop band is dictated by the filter order. An despiked time series of velocities passed through a second and twentieth order Butterworth filter with a cut off frequency of 0.4 Hz is shown in Fig. 3.11c and Fig. 3.11d.

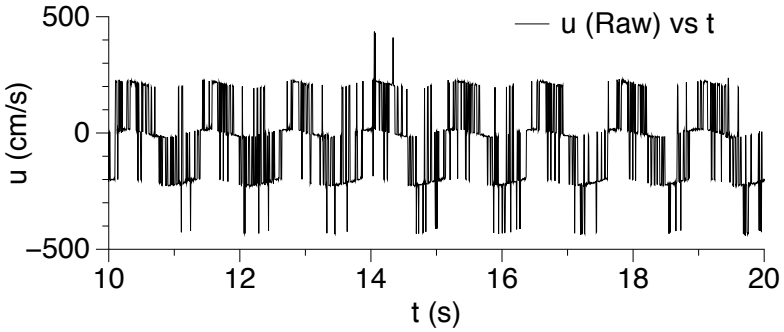

(a) Raw data obtained from ADV

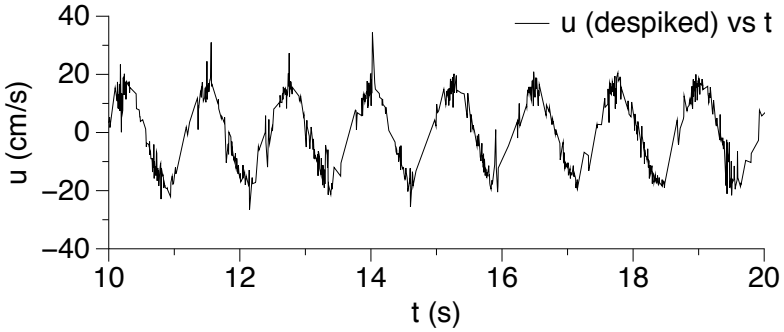

(b) Despiked data from ADV

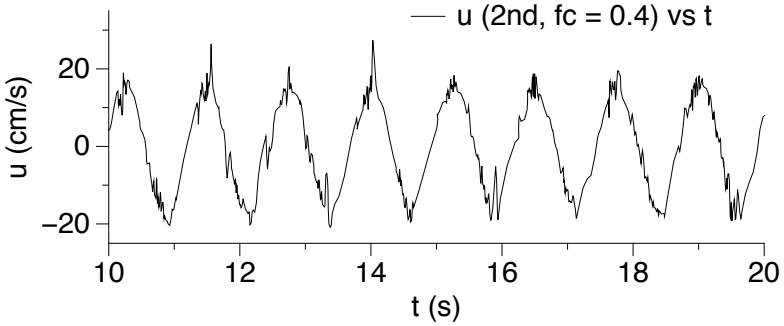

(c) 2nd Order Buttersworth (fc = 1.0)

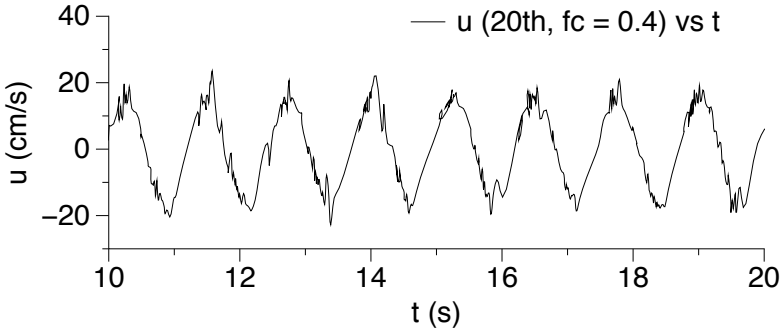

(d) 20th order Buttersworth (fc = 1.0)

Figure 3.11: Data processing of ADV data

3.2 Validation of Regular wave in Numerical wave tank

This section deals with the comparisons between the results obtained from the numerical model and the lab experiments. Both surface elevation and velocities will be compared for different points along the wave flume and numerical wave tank.

3.2.1 Wave tank with no obstacles

Lab experiments described in section 3.1.3.2 was replicated using numerical wave tank feature in the numerical model. The point probes for measuring surface elevation and velocity was placed in locations similar to the lab experiments (Fig. 3.1). Since this was a test with no structures present, 3D wave flume was converted into a 2D numerical wave tank for faster simulations. Simulations were carried out in NWT which is 20 m long and 1 m high and with a water depth of 0.5 m. Locations of wave gauges are exactly the same as used in lab experiments (Fig. 3.6 and Table 3.1).

Three set of results are shown here with the following combinations of H and T. The general idea was to show comparison for small, medium and high wave heights. One of the simulated test for wave tank with no obstacles is shown in Fig. 3.13

- **Test 1**: $H = 0.01$ m and $T = 0.75$ s, $dx = 0.05$ m (Fig. 3.14)
- **Test 2**: $H = 0.05$ m and $T = 1.25$ s, $dx = 0.05$ m (Fig. 3.16)
- **Test 3**: $H = 0.1$ m and $T = 1.25$ s, $dx = 0.05$ m (Fig. 3.18)

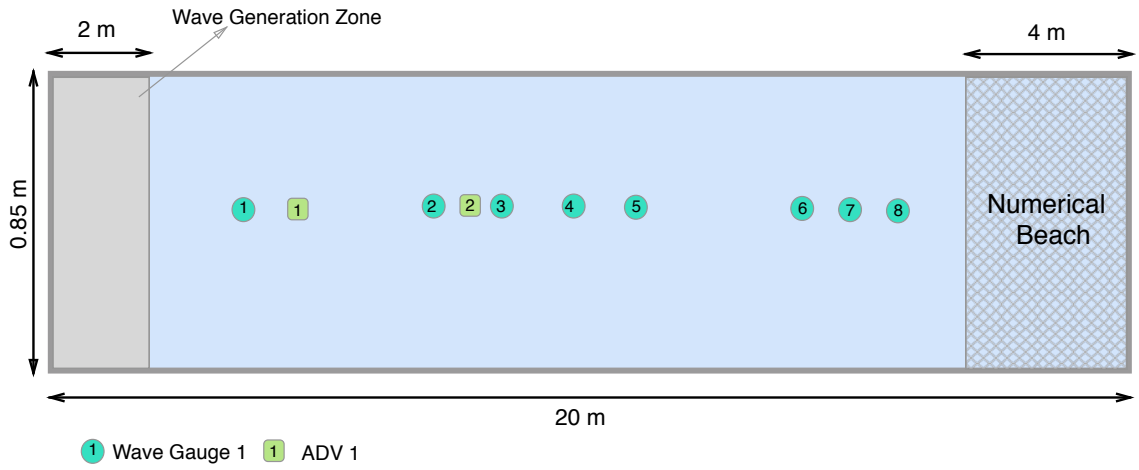

Figure 3.12: Set up for wave tank with no obstacle simulation in NWT

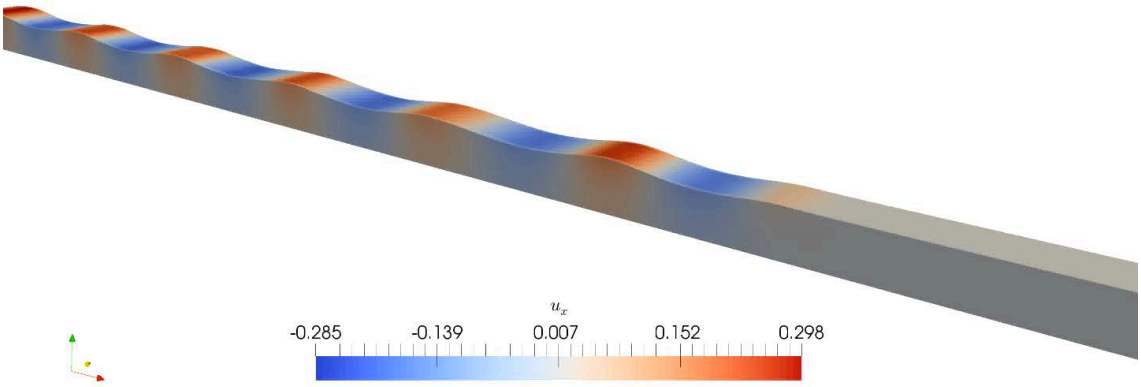

Figure 3.13: Simulated wave tank simulation in NWT

3.2.1.1 $H = 0.01$ m, $T = 0.75$ s $dx = 0.05$ m

The first case simulated in the numerical model was for the case with smallest wave height. The use of finer mesh was not necessary since mesh size of 0.05 m provided good match. The general agreement between the compared results for experimental and numerical results show good match (Fig. 3.14). The results shown are for a period between 20 to 30 s. There was a small phase shift between the numerical and experimental results which is primarily due to the small deviations between the exact and measured distances of the probes in the wave flume. This was manually adjusted while comparing the results. No reflections in the flume are visible from the results shown in Fig. 3.14. A better insight into the possible reflections in the flume can be seen if the results are compared after a longer duration. Comparing for steady state results for this test mentioned above is shown in Fig. 3.15. The results are shown for a period between 50 to 60 s and they also show good match. For test 1 where there is a small mismatch in peaks for WG4 vs P4 and also over prediction of numerical results for WG5 vs P5. Wave gauges 4 and 5 are the closest gauges to the end of the flume and mismatch in peaks is due to reflections. In the numerical model for the wave absorption, relaxation methods are used. The relaxation method dissipate the wave energy by ramping the free surface down to the still water level, the velocity to zero and the pressure to its hydrostatic distribution for still water conditions. In the absorption zone the waves are damped out and all the wave gauges should be placed in the working zone (Fig. 2.3)

From this it is possible to come to a initial conclusion that the artificial beach at the end of the wave flume is absorbing most of the waves and there is less

reflections in the flume.

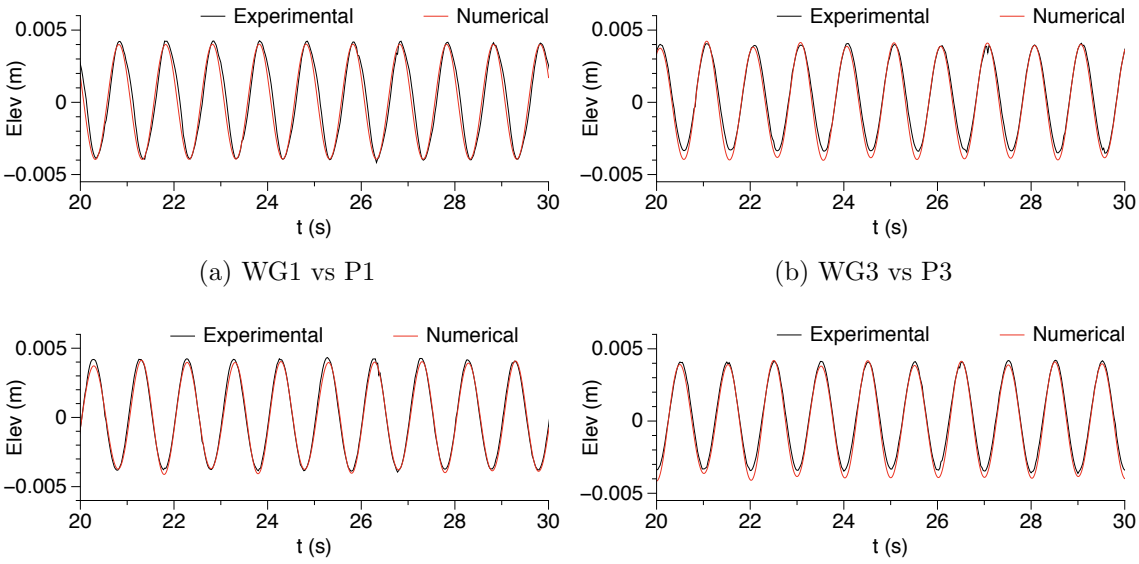

(a) WG1 vs P1

(b) WG3 vs P3

(c) WG4 vs P4

(d) WG5 vs P5

Figure 3.14: Comparison for test 1 - H=0.01 m, T=0.75 s

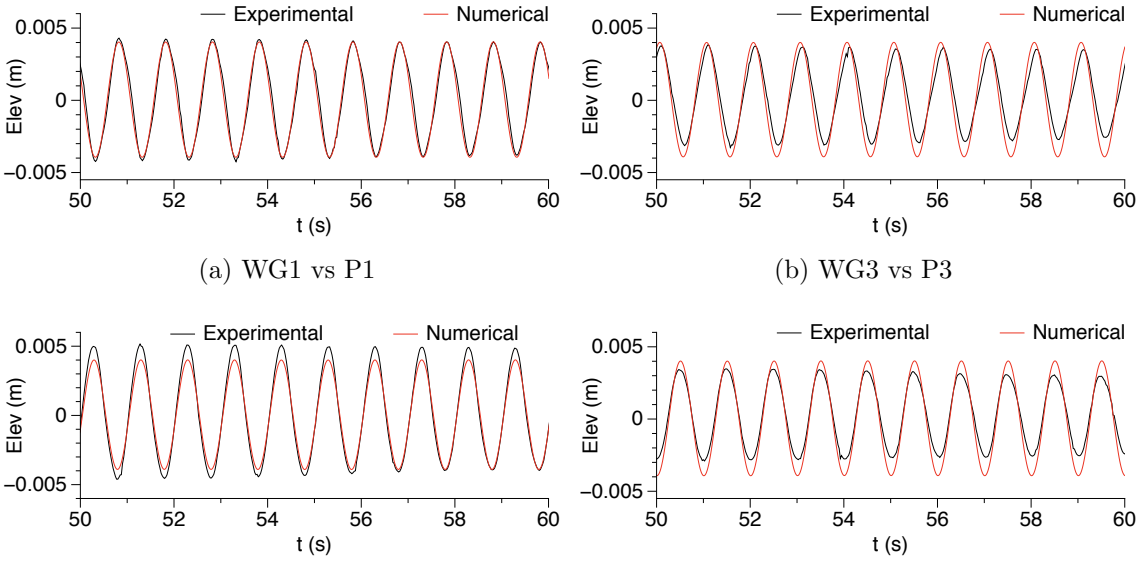

(a) WG1 vs P1

(b) WG3 vs P3

(c) WG4 vs P4

(d) WG5 vs P5

Figure 3.15: Comparison for test 1 - H=0.01 m, T =0.75 s - steady state

3.2.1.2 $H = 0.05$ m, $T = 1.25$ s $dx = 0.05$ m

The second case was done for a wave height of 0.05 m and an increased wave period of 1.25 s. The general agreement between the numerical and experimental results are really good. The firsts set of results are shown for a duration of 20 to 30 s as shown in Fig. 3.16. The peaks and troughs of the waves matches very well for both the set of results. Comparison for 4 set of wave gauges and velocity probes are shown here. The second set of results are shown for a duration between 50 and 60 s (Fig. 3.17) . This, similar to the last test was shown to get a better insight into the possible reflections in flume. Using REEF3D, it is also possible to simulate waves based on different wave theories.

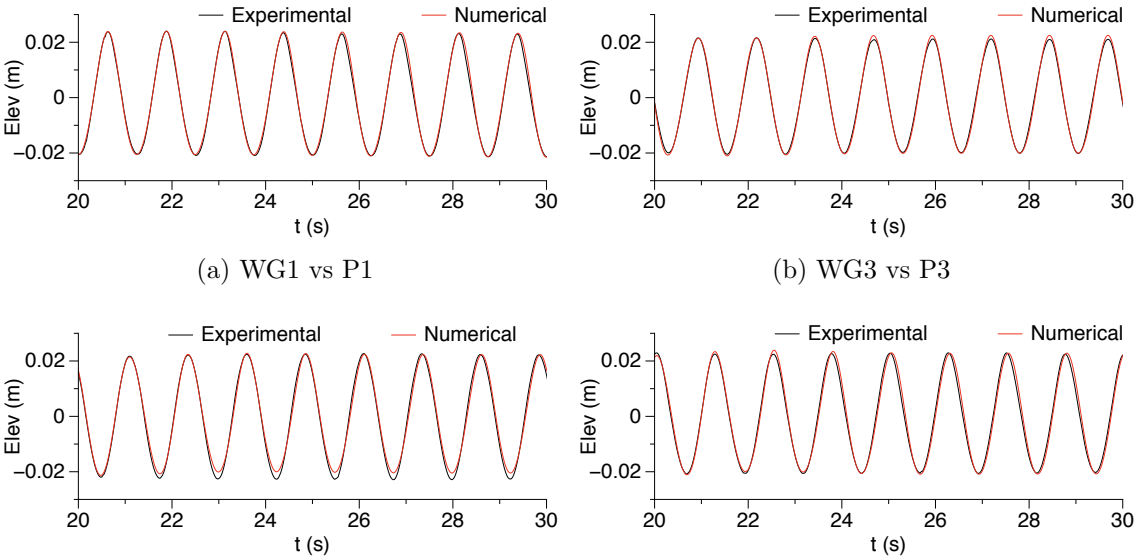

(a) WG1 vs P1

(b) WG3 vs P3

(c) WG4 vs P4

(d) WG5 vs P5

Figure 3.16: Comparison for H=0.05 m, T=1.25 s

Simulation was done for more finer and coarse grid compared to the current grid size and it was seen that for more finer grids the results didn't vary much. Similar relaxation methods was used compared to the previous test which actually works like an active sponge layer to prevent wave reflection at the outlet boundary. The simulation was done for a period of 100 s and the water level was kept at 0.5 m.

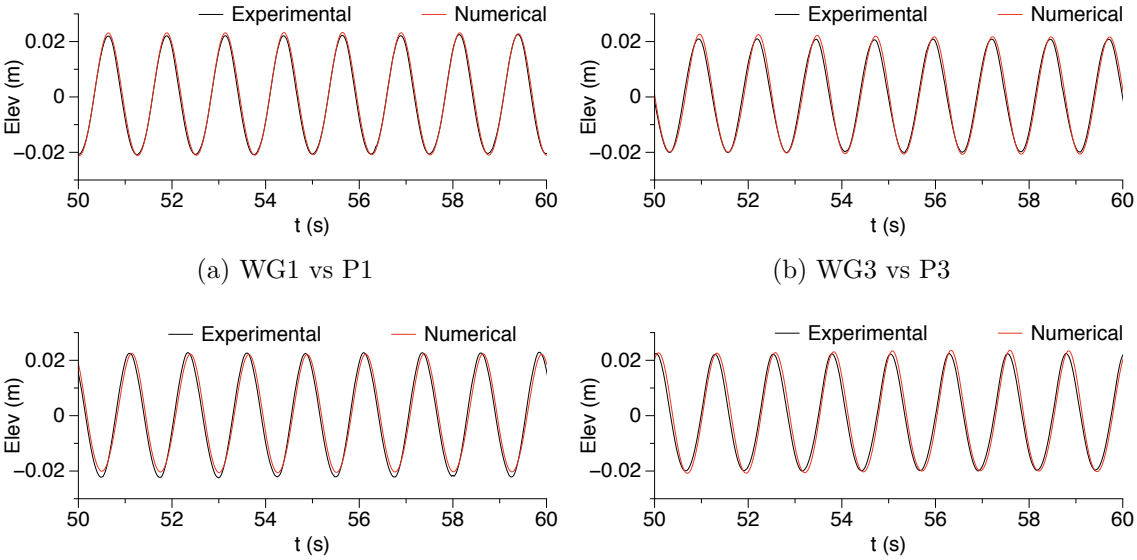

(a) WG1 vs P1

(b) WG3 vs P3

(c) WG4 vs P4

(d) WG5 vs P5

Figure 3.17: Comparison for H =0.05 m, T =1.25 s - steady state

3.2.1.3 $H = 0.1$m, $T = 1.25$s $dx = 0.05$ m

The last test simulated in the numerical model is for the case with highest wave height of 0.1 m and a wave period of 1.25 s. The longer period waves in general will generate less reflection than shorter period waves with same wave height. Almost zero reflections was seen in this case as well. Fig. 3.18 shows comparison for duration between 20 and 30 s. Again the results shows that the artificial beach in the flume are absorbing both shorter and longer period waves in the flume. The next set of results are shown for a period 50 to 60 s, and similar to the previous tests it can be seen that there isn't any mismatches between both set of data.

From these 3 set of simulations the working condition of the flume is observed to be more than satisfactory and give assurance for conducting tests with structures present. The artificial beach which contains multiple perforated sheets dampens out almost all the waves and thereby reducing the reflections in the flume. The waves generated in the numerical model are very close to reality. Next for this same case the velocities are compared.Fig. 3.20 shows the comparison for velocities in both x and y direction for a probe placed 5.75 m from the wave maker. The data from ADV 2 was effected by noise and even after passing through a low pass filter didnt improve the data.

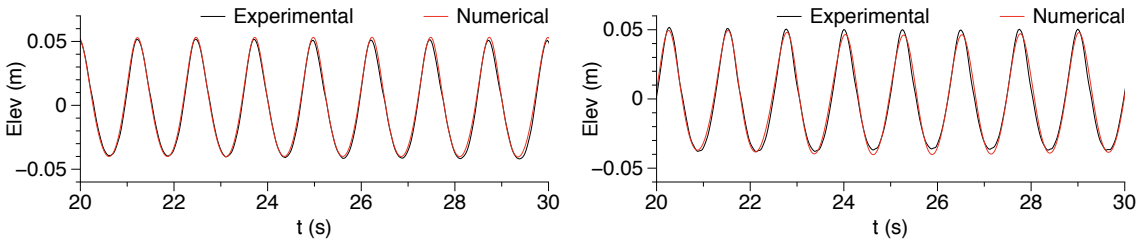

(a) WG1 vs P1

(b) WG3 vs P3

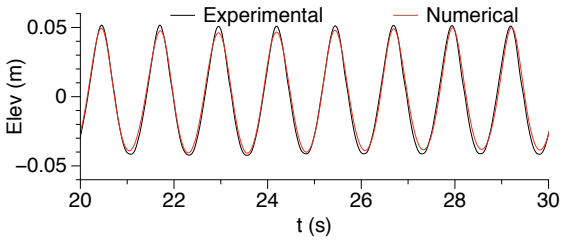

(c) WG4 vs P4

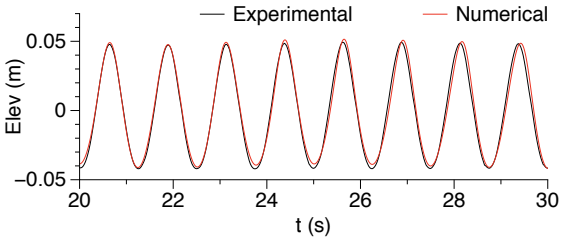

(d) WG5 vs P5

Figure 3.18: Comparison for H=0.10 m, T=1.25 s

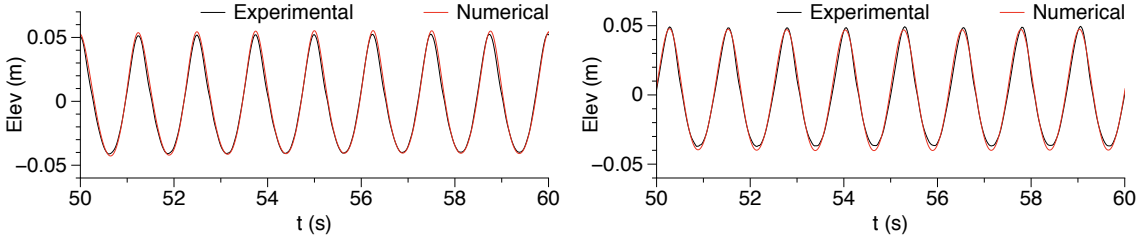

(a) WG1 vs P1

(b) WG3 vs P3

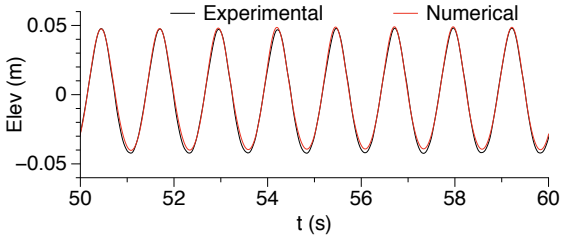

(c) WG4 vs P4

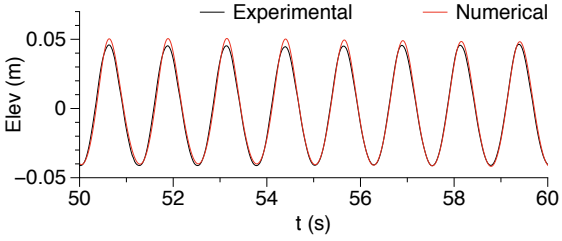

(d) WG5 vs P5

Figure 3.19: Comparison for H=0.10 m, T=1.25 s - steady state

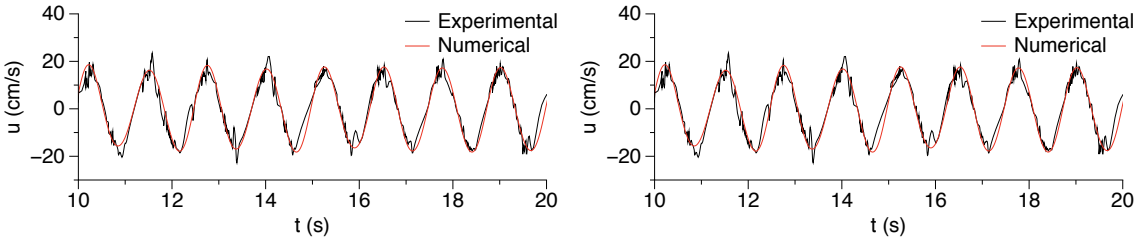

(a) u_x - Probe 1

(b) u_z - Probe 1

Figure 3.20: Comparison for velocity for test 3 - probe 1

3.2.2 Step structure

In this case as described in section 3.1.3.2, a step structure is placed in the NWT of similar dimensions as used in the lab experiments. This case is more complicated compared to the wave tanks tests with no obstacles, since there can be reflections in front of the step as well as some at the end of the flume. So a convergence study is done here to understand the effects of different grid sizes, different wave generation and wave absorption methods. This convergence study was also important to know which combination of methods will have higher accuracy. One of the simulated case for a step structure in the numerical model is shown in Fig. 3.35. The red part under the wave crest is where the velocities are higher when compared to velocities under the trough. As the wave propagates on top of the structure, due to constriction of flow, the velocities increases (acceleration zone) and it reduces after the step. Following are the list of numerical simulations done for the convergence study.

- **Test 1**: $H = 0.034$ m, $T = 1$ s, $dx = 0.01$ m, Relaxation method for wave generation and absorption.
- **Test 2**: $H = 0.034$ m, $T = 1$ s, $dx = 0.01$ m, Dirichlet method for wave generation and active absorption for wave absorption.
- **Test 3**: $H = 0.034$ m, $T = 1$ s, $dx = 0.005$ m, Relaxation method for wave generation and relaxation method 2 for absorption.
- **Test 4**: $H = 0.034$ m, $T = 1$ s, dx= 0.005 m, Dirichlet method for wave generation and active absorption for wave absorption.
- **Test 5**: $H = 0.04$ m, $T = 1$ s, $dx = 0.005$ m, Dirichlet method for wave generation and active absorption for wave absorption.

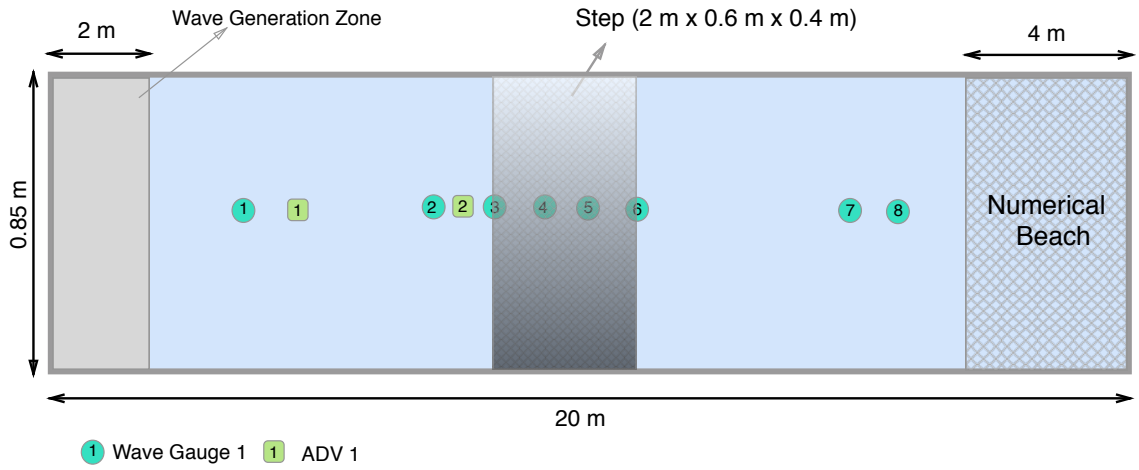

Figure 3.21: Set up for step structure simulation in NWT

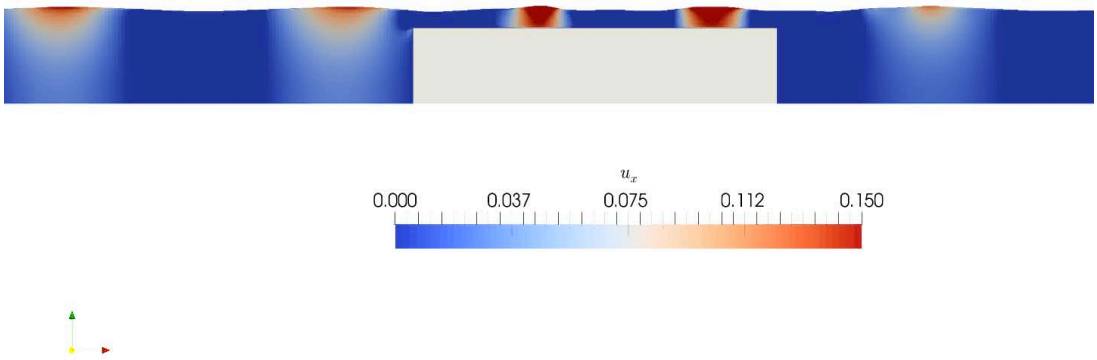

Figure 3.22: Simulated simulation with step structure in NWT

The general arrangement of point probes inside the numerical wave tank is shown in Fig. 3.21. The length of wave generation zone and the numerical beach is an important parameter in the NWT. As mentioned in previous chapters, all the probes should be placed outside of these two zones. For the wave generation zone, a distance of one wave length is chosen and two times the wave length for the wave absorption zone.

3.2.2.1 H = 0.034 m, T = 1 s, dx = 0.01 m, Relaxation method for Wave generation and absorption

To study about the suitable wave generation and wave absorption method for the step structure, wave height of 0.034 m and wave period of 1 s is chosen in this test. This same case is simulated with different grid sizes and different absorption, generation methods in test 3. For this test, relaxation method 2 was used for both generation and absorption. From Fig. 3.23 it can be seen that the peaks of the free surface are not accurately matching. For example WG 4 vs P4 (Fig. 3.23c), the numerical results are off by around 0.45 cm to the experimental results. One of the reason for this mismatch of peaks is due to the grid size chosen. Because for the same combination of absorption and generation methods with a more finer grid (dx = 0.05 m), better results are seen (Fig. 3.27c). The results are shown for a duration of 10 s (from 20 s to 30 s) in Fig. 3.23. Comparisons are also made for steady state situations (50 to 60 s) as shown in Fig. 3.24. It can be seen that general agreement declined when compared to the comparison made in Fig. 3.23. An example for this can

be seen when we compare Fig. 3.23c and Fig. 3.24c. The shape of the wave troughs in Fig. 3.23c are more or less in agreement with the experiment data. But this is not the case when WE consider Fig. 3.24c.

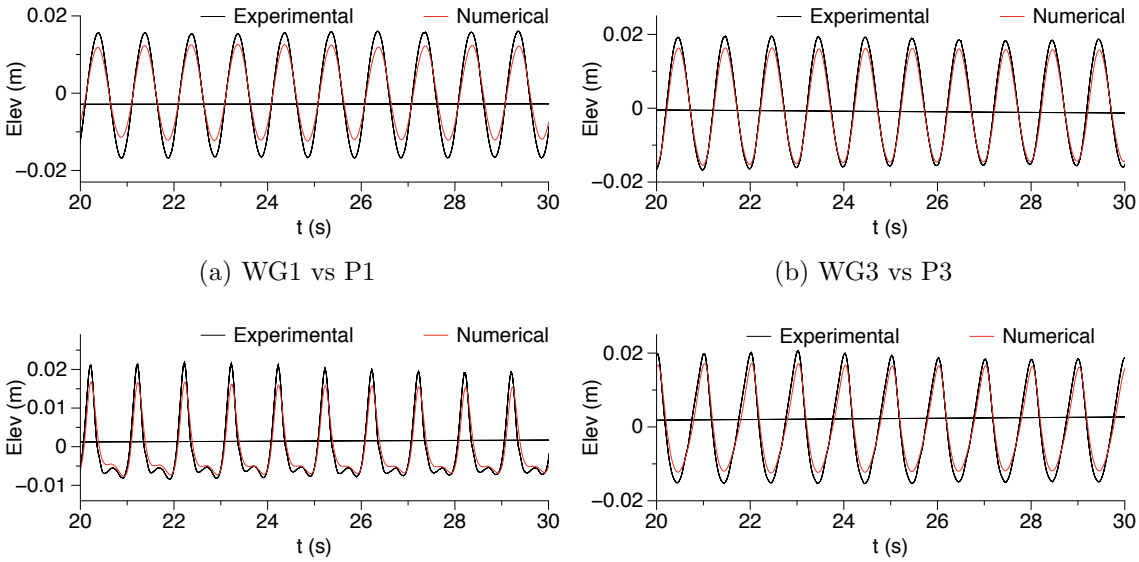

(a) WG1 vs P1

(b) WG3 vs P3

(c) WG4 vs P4

(d) WG5 vs P5

Figure 3.23: Comparison for step structure, test 1

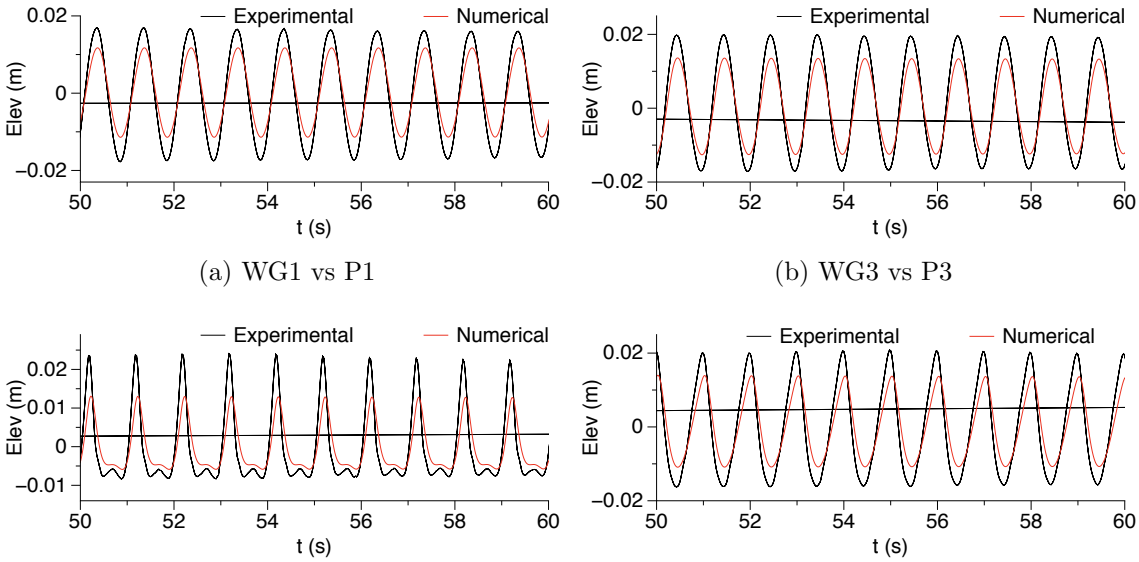

(a) WG1 vs P1

(b) WG3 vs P3

(c) WG4 vs P4

(d) WG5 vs P5

Figure 3.24: Comparison for step structure, test 1 - steady state

3.2.2.2 $H = 0.034$ m, $T = 1$ s, $dx = 0.01$ m,Dirichlet method for Wave generation and Active absorption based on shallow water theory for Numerical beach

In this test, Dirchlet method is used for wave generation and active absorption method for wave absorption. Comparison of experimental and numerical results matches at some points but mismatches in peaks of free surface are seen for a longer simulation period (Fig. 3.25 and Fig. 3.26). This is due to the reflection in front of the step structure and these reflected waves effecting the wave generation. This simulation is done with a grid size of 0.01 m and the general agreement is already better for this set of combination of wave generation and absorption methods.

Comparison of results for test 2 shows that the chosen combination of grid size, absorption and generation method is indeed a good choice as the numerical and experimental data matched accurately. For the remaining tests it was seen that as the wave height increased, the reflection from the step also increased. This was also manually witnessed during the lab experiments as well. Due to this comparison for higher wave heights are not shown in this study as the numerical results didnt match well with the experimental data. These simulations are done as a two dimensional simulation for speeding up the simulation process. Probes are placed in the exact locations as in experiments with the distance for the y direction is taken as the half of the grid size for two dimensional simulations. This means the probes are placed exactly in center of a grid.

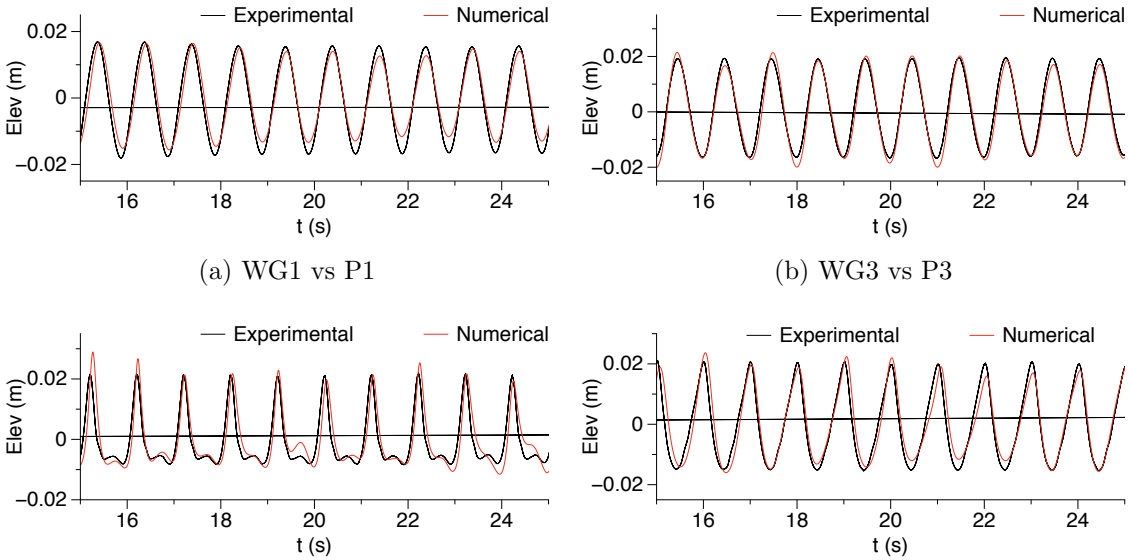

(a) WG1 vs P1

(b) WG3 vs P3

(c) WG4 vs P4

(d) WG5 vs P5

Figure 3.25: Comparison for step structure, test 2

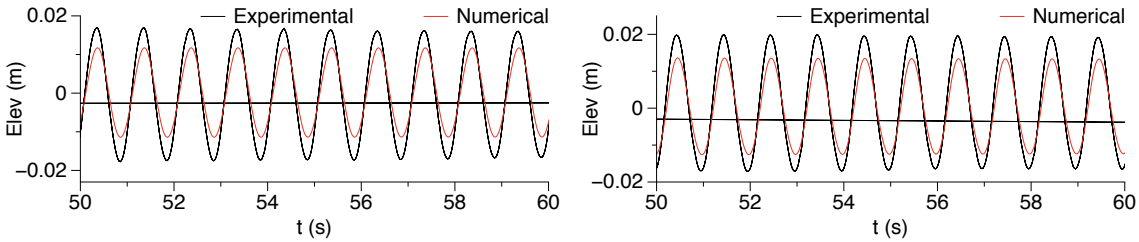

(a) WG1 vs P1

(b) WG3 vs P3

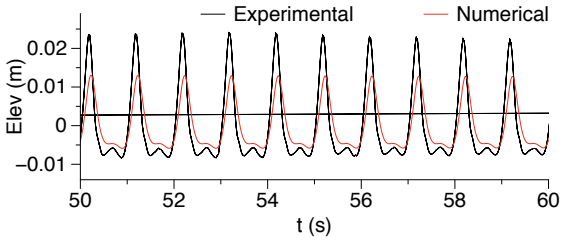

(c) WG4 vs P4

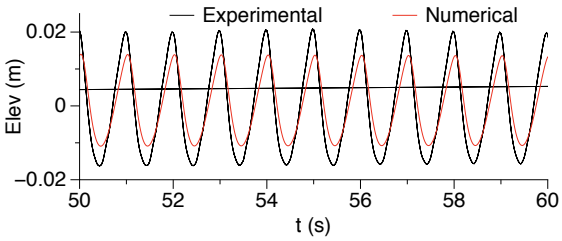

(d) WG5 vs P5

Figure 3.26: Comparison for step structure, test 2 - steady state

3.2.2.3 $H = 0.034$ m, $T = 1$ s, $dx = 0.005$ m, Relaxation method for Wave generation and absorption.

Test 3 was similar to test 1 with same methods for wave absorption and generation but now with a finer grid. Apparently test 3 has good accuracy when compared to the experimental data and also the comparison of steady state surface elevation are not that off to the experimental data compared to the other tests. The results are shown in Fig. 3.27 and comparison for the steady state is shown in Fig. 3.28. So the combination of generation and absorption methods and grid size seems to be good choice considering the results. Test 4 is similar to test 2 where Dirichlet method is used for wave generation and active absorption method for absorption with a grid size of 0.005 m. As expected the general agreement has become better for the comparison of results for a period of 20 to 30 s. This agreement is even better than test 3 and all the peaks and troughs are well captured by the numerical model by using Dirichlet method for wave generation. But the comparison for for a duration of 50 to 60 s (Fig. 3.28) is indeed a concern as it didn't improve much when you consider the improvement in test 3 when compared to test 1.

So from these 4 tests it is concluded that the use of Dirichlet method for wave generation and active absorption for wave absorption is the suitable method after comparing the results from the wave flume and the numerical model. From tests with no obstacles in wave tank, as relaxation zone worked well. The Dirichlet generation provides the best match only because the wavemaker in

the wave flume does not have active absorption. Due to this the wave reflected from the structure travel between the wavemaker and the structure, undergoing multiple reflections and affecting wave generation.

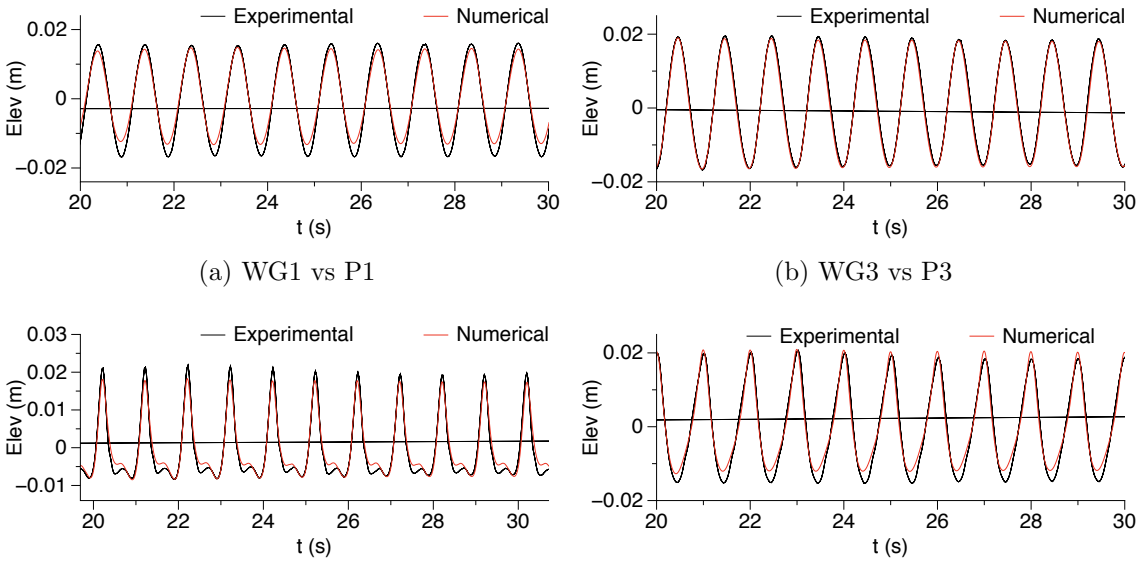

(a) WG1 vs P1

(b) WG3 vs P3

(c) WG4 vs P4

(d) WG5 vs P5

Figure 3.27: Comparison for step structure, test 3

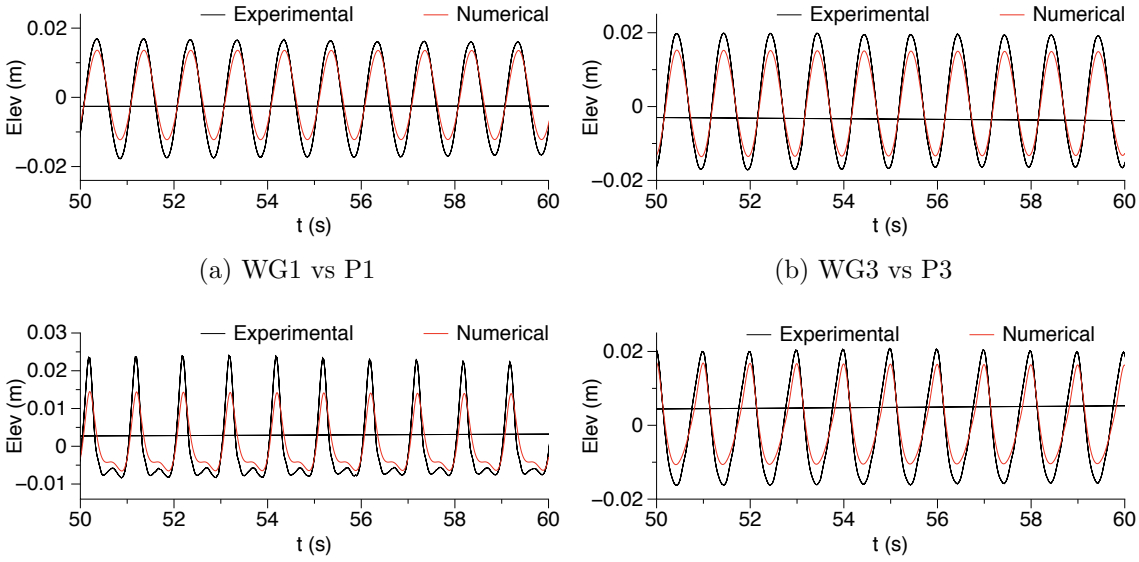

(a) WG1 vs P1

(b) WG3 vs P3

(c) WG4 vs P4

(d) WG5 vs P5

Figure 3.28: Comparison for step structure, test 3 - steady state

Similarly velocities in x and z directions were compared to the data obtained

from ADVs in lab. Comparisons was made and similar to surface elevations, the velocities also matched very well. Probe 1 was 5.75 m from wave maker and probe 2 was 9.9 m from the wave maker which was exactly the same as in the case of lab experiments.

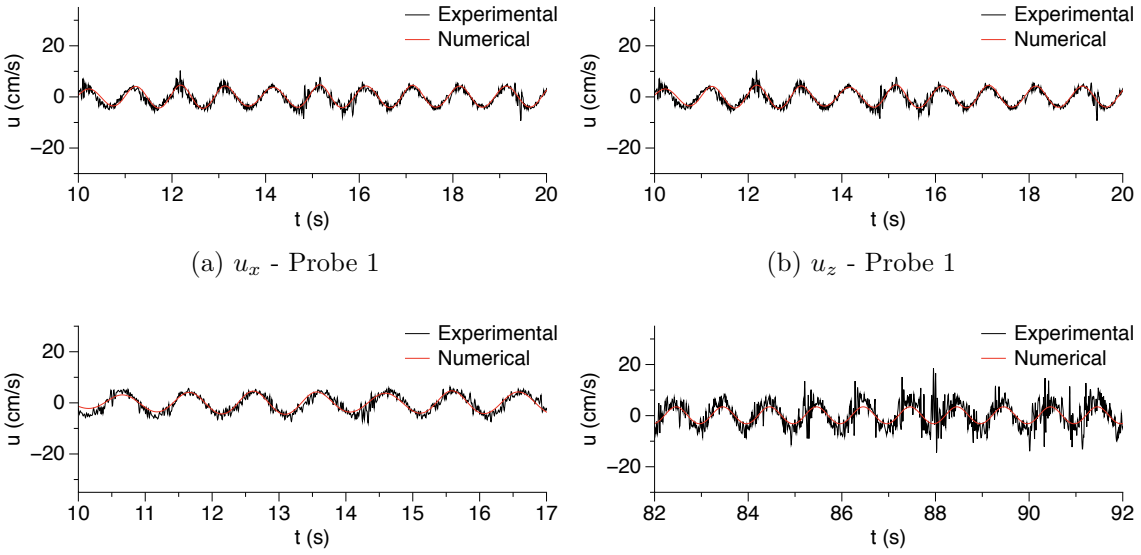

(a) u_x - Probe 1

(b) u_z - Probe 1

(c) u_x - Probe 2

(d) u_z - Probe 2

Figure 3.29: Comparison for velocity - test 3

3.2.2.4 $H = 0.034$ m, $T = 1$ s, $dx = 0.005$ m, Dirichlet method for Wave generation and Active absorption based on shallow water theory for Absorption

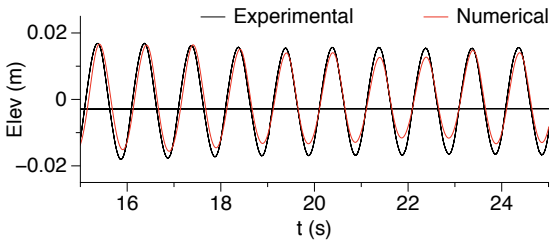

(a) WG1 vs P1

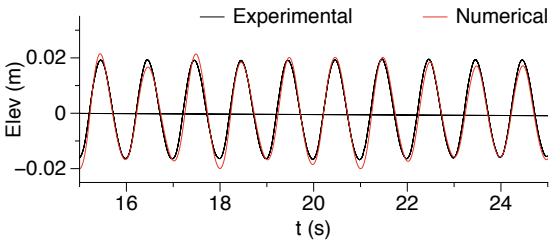

(b) WG3 vs P3

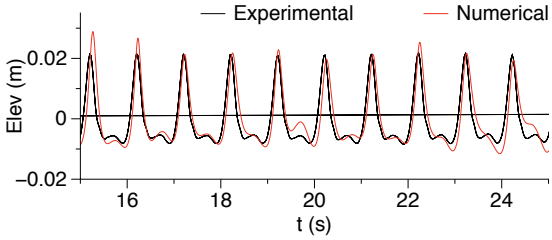

(c) WG4 vs P4

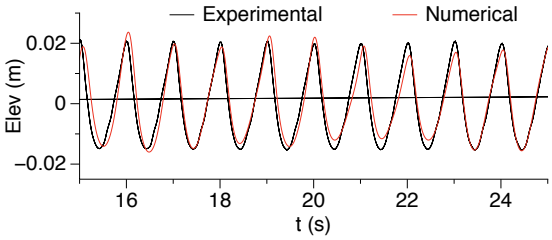

(d) WG5 vs P5

Figure 3.30: Comparison for step structure, test 4

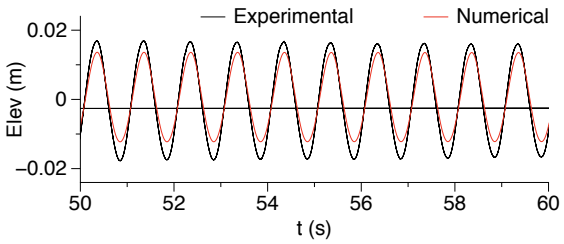

(a) WG1 vs P1

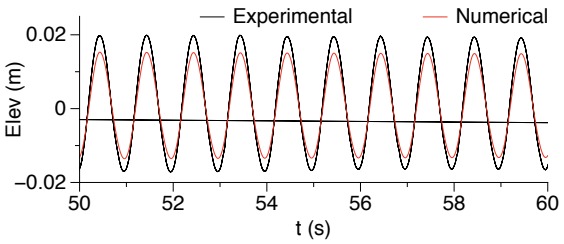

(b) WG3 vs P3

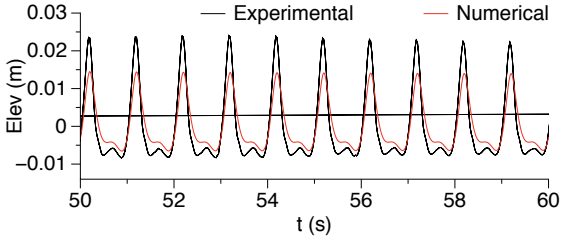

(c) WG4 vs P4

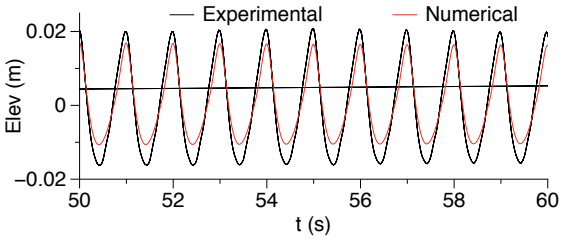

(d) WG5 vs P5

Figure 3.31: Comparison for step structure, test 4 - Steady state

3.2.2.5 $H = 0.04$ m, $T = 1$ s, $dx = 0.005$ m, Dirichlet method for Wave generation and Active absorption based on shallow water theory for absorption

After the Grid convergence study mentioned earlier it was concluded that the use of grid size 0.005 m gave better results and use of Dirichlet method for wave generation and active absorption method based on shallow water theory wave absorption are the preferable methods. Test 5 is done for a wave height of 0.04 m and wave period of 1 s with the above mentioned methods for wave generation and absorption. It was important to check if the preferred methods also produced accurate results for other combination of wave height and wave period as well. Comparisons are shown in Fig. 3.32 and it can be seen that agreement is really good if you consider all the peaks which matches accurately. This suggest that indeed the combinations used are the right ones and can be used for the tests with abutments as well.

For the Dirichlet type of wave generation, waves are generated by assigning values for the free surface and the velocity in the inflow boundary only. The active absorption method based on shallow water theory avoids reflections by generating wave opposite of the reflected wave and thus canceling it out. This method is more efficient in terms of computational efforts as it does not require additional space.

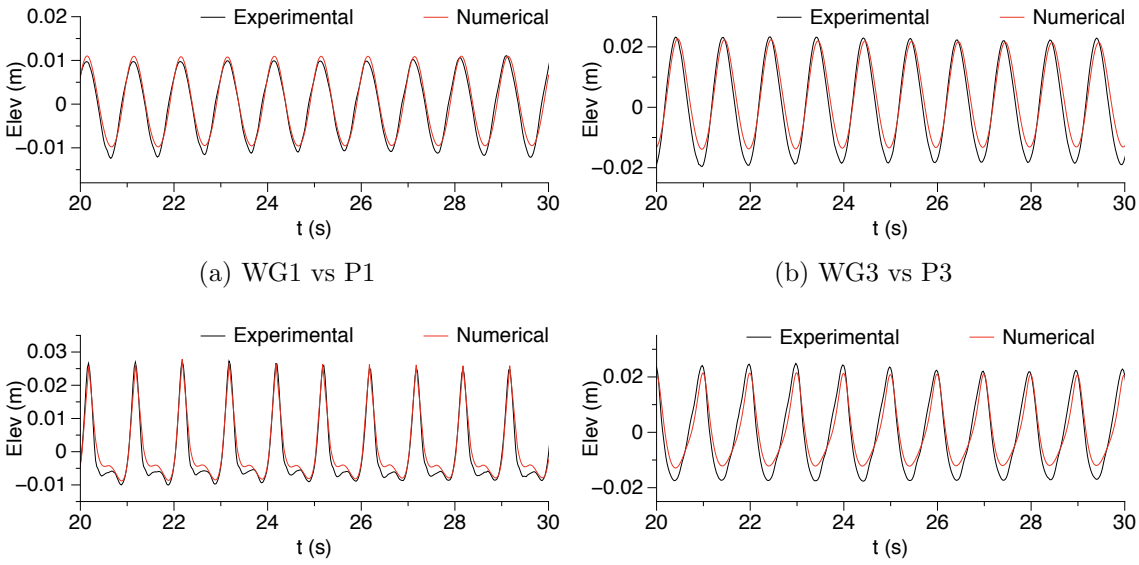

(a) WG1 vs P1

(b) WG3 vs P3

(c) WG4 vs P4

(d) WG5 vs P5

Figure 3.32: Comparison for step structure, test 5

Velocities were also compared for this tests for both probe 1 and probe 2 and are shown in Figure 3.33. The agreement between the velocities obtained from

ADVs in wave flume and from the probes in numerical wave tank shows good match.

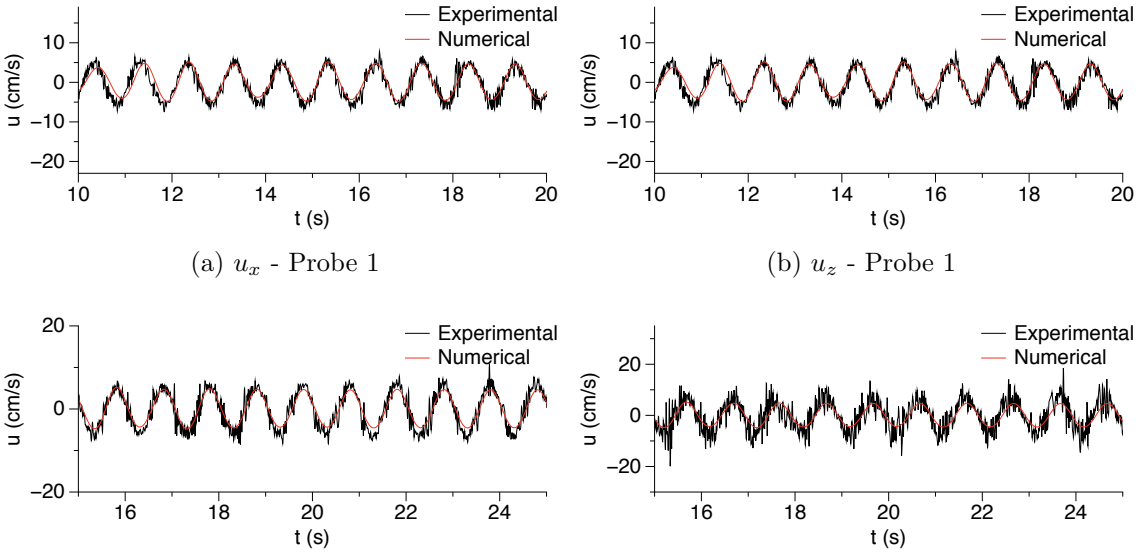

(a) u_x - Probe 1

(b) u_z - Probe 1

(c) u_x - Probe 2

(d) u_z - Probe 2

Figure 3.33: Comparison for velocity - test 5

3.2.3 Abutment

The next set of simulations are done for an abutment structure in the numerical wave tank. This is a 3D investigation unlike the previous 2 simulations which were 2D. The numerical tank is 20 m long, 0.6 m wide and 0.85 m high. The general arrangements for the probes are shown in Fig. 3.34 and the exact distances are mentioned in Table 3.5. Two sets of tests were simulated in the numerical model for this abutment case as mentioned below. The methods which gave the best agreement between numerical and experimental data are used here with a grid size of 0.005 m. Use of a fine grid resulted in more than 70 million cells and required close to 30 hours of simulation time.

- **Test 1**: $H = 0.01$ m, $T = 1$ s, $dx = 0.005$ m, Dirichlet method for Wave generation and Active absorption based on shallow water theory for absorption.
- **Test 2**: $H = 0.05$ m, $T = 1$ s, $dx = 0.005$ m, Dirichlet method for Wave generation and Active absorption based on shallow water theory for absorption.

The length for the wave generation zone is taken as one wavelength and the wave absorption zone as two times the wavelength which was also the distances in previous simulations as well. The water level was kept at 0.5 m and the center of the abutment was kept at 10.45 m away from the wave maker.

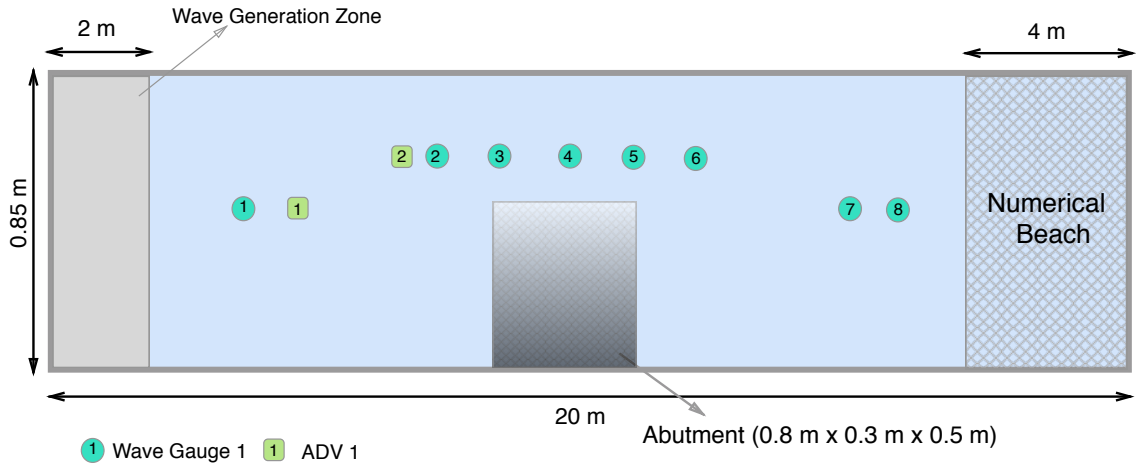

Figure 3.34: Set up for abutment structure simulation in NWT

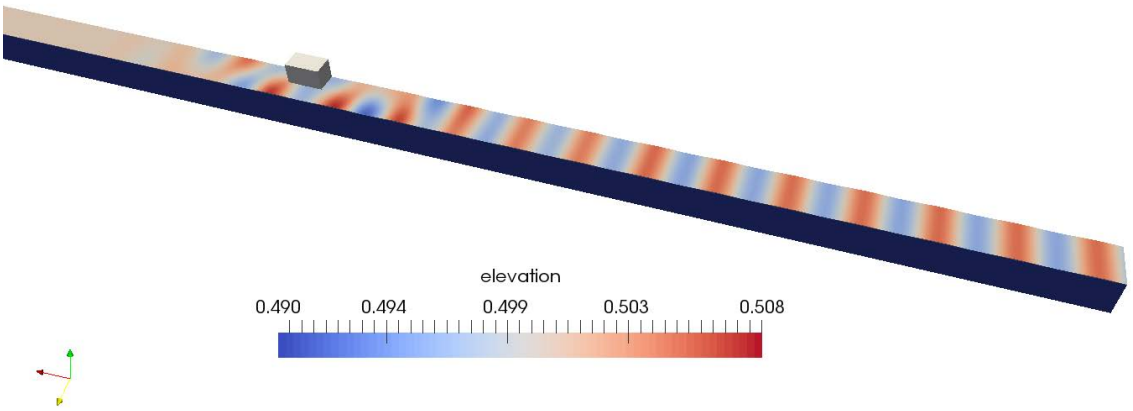

Figure 3.35: Simulated simulation with step structure in NWT

3.2.3.1 $H = 0.01$ m, $T = 1$ s and $dx = 0.005$ m

The first set of test are carried out for a wave height of 0.01 m and a wave period of 1 s. Comparison between the experimental and the numerical simulation is shown in Fig. 3.36. The agreement in general is very good apart from mismatches is peaks which is of very small order. One possible explanation for this is the reflections generated in front of the abutment which might have influenced the data acquisition of wave gauges. More over these reflections were also visually observed during the experiments as mentioned in section 3.1.3.3. This case was for the lowest wave height used in the tests and it is clearly observable that there isn't any changes in the wave kinematics even when the waves are passing through the confined space between the abutment and glass walls. In the comparison shown in Fig. 3.36, WG3 vs P3 and WG4 vs P4 shows the free surface comparison in front of Abutment and it is clearly visible that there is no much change. A possible option to get a better agreement between the peaks of the waves is by using a more finer grid, but will require larger computational effort and space. WG2 vs P2, which means wave gauge used in the lab vs the corresponding probe used in the numerical wave tank shows the best agreement of peaks of the waves. This agreement is actually better than expected since they were in front of the abutment and reflections in front of the abutment should had made the agreement less than what is shown in Fig. 3.37a.

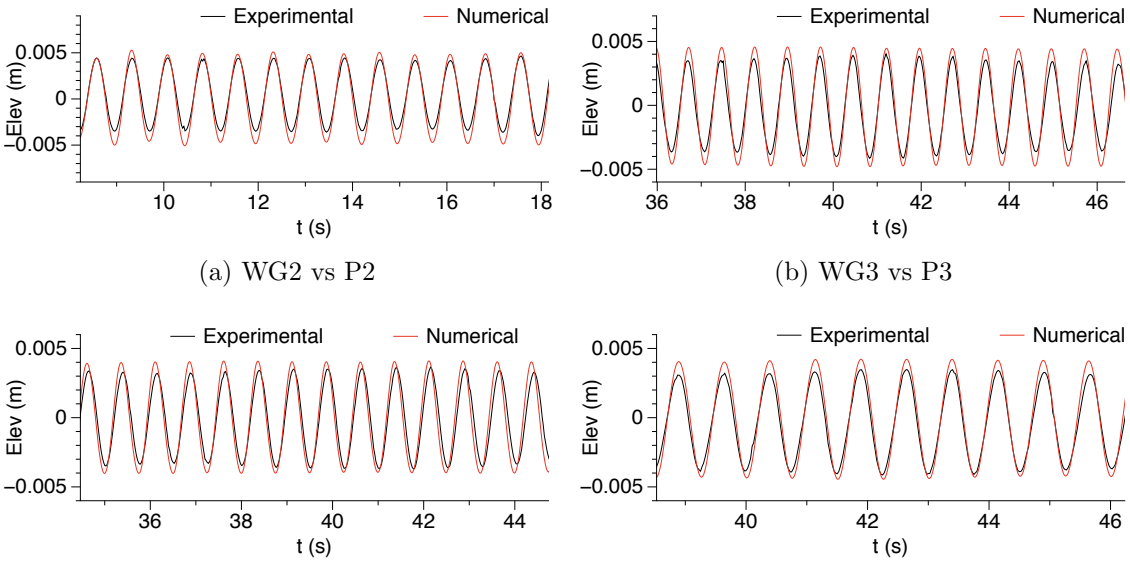

(a) WG2 vs P2

(b) WG3 vs P3

(c) WG4 vs P4

(d) WG6 vs P6

Figure 3.36: Comparison for abutment in flume, test 1

3.2.3.2 $H = 0.05$ m, $T = 1$ s and $dx = 0.005$ m

The second test are conducted for a wave height of 0.05 m and wave period of 1 s. Comparison of the results are shown in Fig. 3.37. This was one of the highest wave height used in the experiments and and the comparison shows the changes in free surface. WG4 vs P4 and WG5 vs P5 (Fig.e 3.37b and Fig. 3.37c) are for the locations in front of the abutment and it can be seen that the peaks have become more steeper and is well captured in the numerical model. For WG2 vs P2, (Figure **??** the duration for the comparison shown is between 18 s to 28 s as after 25 s the reflections from the front of the Abutment was high and the results weren't matching perfectly. For the rest of the comparisons are shown for a duration between 14 to 24 s and shows good agreement between experimental and numerical results. Through these tests the it was noted that the preferred methods for wave generation and absorption concluded after the simulations with the step structure is indeed the correct choice.

Similarly the velocities were also compared for this case. Figure 3.38 shows the comparison of velocities measure through ADVs and the velocity computed in the Numerical model through Probe 2 which is 9.9 m away from the wave maker. The agreement in general is more than satisfactory.

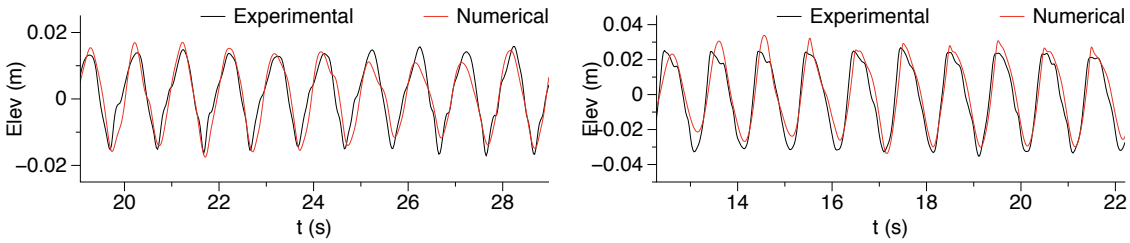

(a) WG2 vs P2

(b) WG4 vs P4

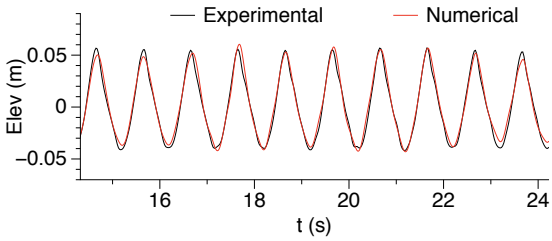

(c) WG5 vs P5

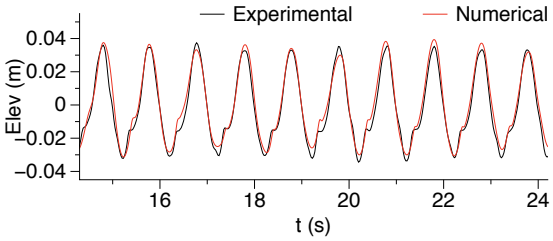

(d) WG6 vs P6

Figure 3.37: Comparison for abutment in flume, test 2

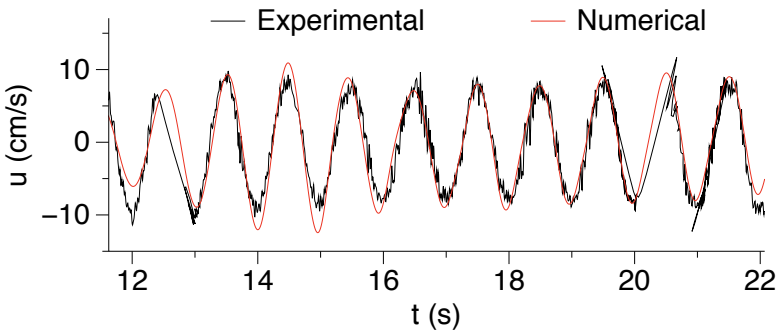

(a) u_x - Probe 2

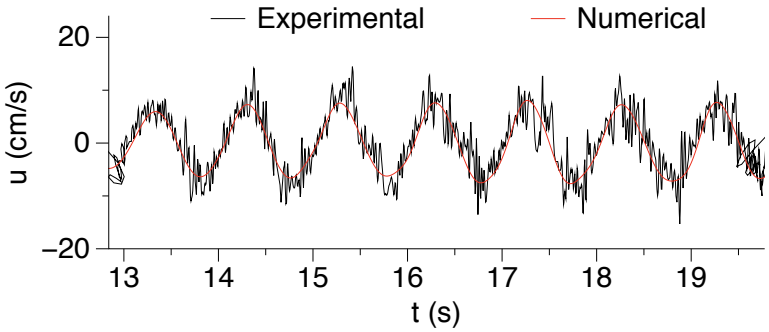

(b) u_z - Probe 2

Figure 3.38: Comparison for velocity - test 2

Chapter 4

Porous Media

4.1 Literature review

4.1.1 Porous media flow

The main difference between free surface flow and the porous flow is the presence of grains and voids. The effect of grains on the flow could be described as a resistance to the flow that dissipates energy. First to find a solution for flow in porous media was Darcy (1856) [6] based on his experimental work in groundwater flow as shown in equation 4.1. He stated that flow velocity in these porous medium is proportional to the hydraulic gradient. This equation is only applicable for laminar flow and for turbulent flow Forchheimer (1901) included friction terms [12] which is influenced by the Reynolds (Re) number. Eq. 4.1 is based on experimental evidence. This equation can also be derived from the Navier-Stokes equations, the basic equations of fluid flow.

$$I = au^f \tag{4.1}$$

$$I = au^f + bu^f \left|u^f\right| \tag{4.2}$$

In Eq. 4.1, a is the inverse of hydraulic conductivity K and u_f is the filter velocity in x direction. Filter velocity is defined as the average velocity which is defined by Eq. 4.3. This is the actual pore velocity averaged over the pores. Here n is the porosity, u the real velocity in the pores. The porosity is usually defined as the pore volume, V_P divided by the total volume, V_T.

$$u_f = \frac{1}{A}\int\int udA = n.u \tag{4.3}$$

Table 4.1: Porous flow regimes

Regime	**Re - range**	**Flow characteristics**
Darcy flow	Re<1-10	Flow dominated by viscous forces, velocity distribution determined by local geometry.
Forchheimer flow	1-10<150	Development of an inertial core flow outside the boundary layers
Unsteady laminar flow	150<300	Transitional flow regime between inertial Forchheimer and fully turbulent flow.
Fully-turbulent flow	300	Highly unsteady and chaotic flow regime

In the Forchheimer equation the pressure gradient has a linear and non-linear term. The linear term relates to laminar flow and turbulent aspect of the flow is included in the non linear term. In the relation, a and b are dimensionless coefficients and are the often refereed to as friction factors. These factors depends on the fluid viscosity, the specific granular composition of the porous medium and the flow regime. Different porous media flow regimes were characterized by Dybbs and Edwards (1984) and are summarized in Table 2.1. They identified 4 main flow regimes based on the Reynolds number $Re_p = u^p D_p/v$ i.e a Reynolds number related to the pore size D_p and pore velocity u^p.

The relation formulated by Forchheimer are based on experimental evidence but, can also be derived from the Navier Stoke's equation. The derivation is given by Burcharth and Anderson (1995) [3] and for a one dimensional stationary closed conduit flow where $u_x = u$, the definition of the hydraulic gradient then becomes Eq. 4.4. Introducing U and D as a characteristic velocity and length scale, Eq. 4.4 reduces to Eq. 4.5

$$I = \frac{1}{g} u \frac{\partial u}{\partial x} - \frac{v}{g} \frac{\partial^2 u}{\partial x^2} \tag{4.4}$$

$$I = \alpha_F \frac{v}{g} \frac{U}{D^2} + \beta_F \frac{1}{g} \frac{U\,|U|}{D} \tag{4.5}$$

Eq. 4.5 is similar to Eq. 4.2. In case of Darcy flow the velocities are small and the inertia term in Eq. 4.4 can be neglected leading to Eq. 4.6 which is similar to Eq. 4.1.

$$I = \alpha_F{}'' \frac{v}{g} \frac{U}{D^2} = a'' U \tag{4.6}$$

When velocities increase turbulence will occur and the viscous term in Eq. 4.4 becomes fully turbulent flow. This viscous term can be neglected compared to the inertia term and reduces to Eq. 4.7 [3]

$$I = \beta_F{}'' \frac{U\,|U|}{gD} = b'U\,|U| \tag{4.7}$$

4.1.2 Unsteady porous media flow

The relation proposed by Forcheimmer is only valid in case of stationary flow. An inertia term for unsteady flow was originally suggested by Polubarinova-Kochina (1962) [34] and is give in Eq. 4.8. Here c is a dimensional coefficient (s^2/m) which will be applied in case of local accelerations. In order to accelerate a certain volume of water in a porous medium, there is extra momentum needed compared to a non-porous medium. Gu and Wang (1991) [13] and van Gent (1992) [40] derived a expression for c and is given in Eq. 4.9 where n is the porosity and γ_F is the virtual mass coefficient.

$$I = au^f + bu^f \left|u^f\right| + c\frac{\partial u^f}{\partial t} \tag{4.8}$$

$$c = \frac{1 + \gamma_F \frac{1-n}{n}}{g} \tag{4.9}$$

Similarly Van Gent (1993) [41] derived a relation for a and b theoretically. In the relation for a and b (Eq. 4.10 and Eq. 4.11), d_{50} is the grain diameter and KC is the Keulegan-Carpenter number which represent the ratio between the turbulence and inertia effects or it basically determines how stationary the flow is. The coefficients α and β have to be determined experimentally which will depend on the Reynolds number, shape of stones, permeability and grade of porous material and are often referred as shape factors. A broad overview of the values of α , β and γ_F is given by Troch (2000) [38]. The review comprises of the work published by various authors on different types of materials in laminar and fully turbulent, steady and unsteady flow conditions. Determining the correct contribution of the a, b and c term for non-stationary situations has been proven to be difficult. Calibrations of these coefficients will be discussed in the upcoming chapter.

$$a = \alpha \frac{(1-n)^2}{n^3} \frac{v}{g d_{n50^2}} \tag{4.10}$$

$$b = \beta(1 + \frac{7.5}{KC}) \frac{(1-n)}{n^3} \frac{1}{g d_{n50}} \tag{4.11}$$

4.1.3 Porous media flow modeling

There are a lot of issues in practice to directly resolve the fluid flow in highly complex and irregular porous medium. Sollit and Cross (1976) [37] proposed the concept of seepage velocity where the real flow velocity inside the porous voids is replaced by a velocity over a continuous body. This replacement cancels out the need for detailed representation of the voids. The presence of these voids are included through the porosity and permeability in the flow description. Loss of flow detail and the porous medium properties being assumed time invariant are few issues with this method. This seepage velocity is indeed similar to the filter velocity mentioned in Eq. 4.3. Seepage velocity is defined as the average velocity of the fluid contained in the averaging volume while in filter velocity it is averaged in specific volume containing both fluids and solids. Different approaches have been followed to implement the seepage velocity concept. Volume-Averaged Reynolds-Averaged Navier Stokes (VARANS) equations [21], [36] and time averaging of volume-averaged approaches

The main difference between both approaches can be related to the treatment of turbulence in porous media flow. By using the concept of seepage velocity and the Forchheimer relation (Eq. 4.2 and Eq. 4.8) helps to represent the flow losses in the model. Few authors have worked on the modelling of macroscopic turbulence in the porous media flow using the seepage velocity concept of Nakayma and Kuwahara (1999) [30]. Applying a volume-averaging to the Reynolds Averaged Navier Stoke (RANS) equations is done by splitting instantaneous velocity or pressure into a volume averaged component, a turbulent and a spatial fluctuations as shown in Eq. 4.12.

$$u = \langle \bar{u} \rangle^f + u' + u'' \tag{4.12}$$

In this method the RANS equations are retrieved with additional terms due to volume-averaging. According to del Jesus (2011) [7], one advantage of the VARANS approach is that the shear stress term can be explicitly modeled inside the porous media. He applied volume averaging to two different turbulence models: the $k - \omega$ model and the SST model ([29]). Experiments have also shown ([15]) that air entrainment can result in a reduction of the hydraulic conductivity, which can be explained with the help of noticeable changes in the physical processes involved in two-phase turbulent porous media flow, e.g. the transport of air bubbles and possible blockage of pore holes by these bubbles.

4.1.4 VARANS (Volume Averaged Reynolds Averaged Navier-Stokes)

To average the Navier Stoke equation inorder to solve flow in a porous medium can be done many ways. In this study the numerical model uses the Volume-Averaged Reynolds-Averaged Navier Stoke equations (VARANS) and is implemented based on the work done by Jensen et al. (2014) [23] . This work includes discussion about the different equations found in literature with details regarding the underlying assumptions and ranges of applications. The starting point is the incompressible Navier Stokes equations formulated with the continuity equation (Eq. 4.13) and momentum equation (Eq. 4.14).

$$\frac{\partial u_i}{\partial x_i} \tag{4.13}$$

$$\frac{\partial \rho u_i}{\partial t} + \frac{\partial \rho u_i u_j}{\partial x_j} = -\frac{\partial p}{x_i} + g_j x_j \frac{\partial p}{x_i} + \frac{\partial}{\partial x_i}\mu\left(\frac{\partial u_i}{\partial x_j} + \frac{\partial u_j}{\partial x_i}\right) \tag{4.14}$$

In order to solve the above equation in the porous medium, the Navier Stokes equation will be averaged over a volume that is assumed to be larger than the length scales of the pores. This will result in velocities which is averaged over the volume and is called as a filter velocity. The continuity equation mentioned in Eq. 4.13 is to represent the volume density of the outward flux of a vector field from an extremely small volume around a pore and this outward flux of the filter velocity being zero is a physically correct representation according to del Jesus et al. (2012) [8]. This means that the filter velocity will be constant in the flow direction and when volume averaged over the entire volume will have 0 flux for the velocity field. The continuity equation can be then expressed as shown in Eq. 4.15. Here $\bar{u_i}$ is the volume averaged velocity over the total control volume.

$$\frac{\partial \left\langle \bar{u_i} \right\rangle}{\partial x_i} = 0 \tag{4.15}$$

Similarly for the momentum equation the formulations are based on filter velocities which are divided by the porosity to get the correct momentum contributions because of the use of filter velocities instead of actual pore velocity. Momentum equation after using filter velocity then becomes as shown below.

$$(1 + C_m)\frac{\partial}{\partial t}\frac{\rho \left\langle \bar{u_i} \right\rangle}{n} + \frac{1}{n}\frac{\partial}{\partial x_j}\frac{\rho \bar{u_i}\bar{u_j}}{n} = -\frac{\partial \left\langle \bar{p} \right\rangle^f}{\partial x_j} + g_j x_j \frac{\partial \rho}{\partial x_i} + \frac{1}{n}\frac{\partial}{\partial x_j}\mu\left(\frac{\partial \bar{u_i}}{\partial x_j} + \frac{\partial \bar{u_j}}{\partial x_i}\right) + F_i \tag{4.16}$$

In Eq. 4.16, C_m is the added mass coefficient which takes into account for the grain-water interaction. F_i on the right side of the equation 4.16 take account of the resistance offered by the porous medium. The use of a filter velocity in the momentum equation will result in providing different values for pressure gradients both inside and outside the porous media. So the pressure needs to be defined as pore pressure in momentum equation so that the hydrostatic pressure distribution both inside and outside will be linear and identical.
Averaging of the momentum equation inside the porous medium will give rise to two new terms, one representing the frictional forces from the porous media and pressure forces from the individual grains.

4.1.5 Calibration of Resistance Coefficient

As shown in the previous section, the formulation of Darcy-Forchheimer equation includes 2 resistance coefficients, α and β which must be determined empirically. These coefficients comes into the equation due to the volume averaging of the RANS equation. When the momentum equation is volume averaged, terms arises which represents the frictional forces and pressure forces from individual grains. The derivation of these terms is not shown here. The precise description of α and β coefficients are still not fully understood. These coefficients depend on several parameters such as the Reynolds number, the shape of the stones, the grade of the porous material, the permeability and the flow characteristics.

The existing knowledge on the variation of resistance coefficients originates from theoretical considerations, physical experiments and numerical calibrations. Engelund (1953) [10] presented formulation for resistance terms in the Darcy-Forchheimer equation with recommendations for the resistance coefficients for irregular sand grains. The values were proposed up to $\alpha = 1500$ and $\beta = 3.6$. These values were based on the work with sand grains and is hardly applicable to porous coastal structures. Van Gent (1995) [42] and Burcharth and Anderson (1995) [3] have suggested different values for these coefficients based on experiments which incorporated the effect of an oscillating flow via KC number. The resistance coefficients were proposed to take the values $\alpha = 1000$ and $\beta = 1.1$. Del jesus et al (2012) [8] performed a dam break experiments similar to the one done in Lin (1999) [28].Here the resistance coefficients were calibrated by testing a range of both α and β . Three values of α were selected as $\alpha = [5000, 10000, 20000]$, while β remained constant at $\beta = 3.0$. The best comparison for the results were found for $\alpha = 10000$ and $\beta = 3.0$. These values were then reformulated into the formulations given by Van Gent (Eq. 4.10 and Eq. 4.11) and the coefficients take up a value of $\alpha = 2500$ and $\beta = 3.6$, and assuming a porosity of n=0.49.

It has been generally experienced over the years that under oscillatory flow and waves propagating over slopes or breaking, values existing the literature may

not be valid anymore. Since there are no predictive methodology to determine the α and β coefficients in advance, calibration has to be performed.

4.2 2D Dam break

The equations presented in the previous section requires calibration of numerical parameters defined in the porous medium. The first case is done for 2D dam break case based on the experiments carried out by Lin (1999) [28].

4.2.1 Experimental Setup

These experiments have a simple set up comprising of wide range of conditions which are very suitable for this study. Also another reason for choosing these experimental data is because they also provide free surface evolution in both inside and outside the porous medium. Lin (1999) tested a dam break flow in a fish tank (89 cm horizontally and 58 cm vertically) for 2 types of materials,

- Crushed Rock with $D50$ of 15.9 mm and porosity (n) of 0.49
- Glass beads with $D50$ of 3.0 mm and porosity (n) of 0.39

These experiments were conducted in combination with video recording techniques to obtain the free surface along the domain. General setup of the dam break experiment is given in Fig. 4.1. This includes the clear flow region and also the inside of the porous medium. The porous dam was kept in the middle of the tank which was 29 cm long and 58 cm high. The water was set to flow from the left side of the tank and is separated from the porous medium using a moving gate. This gate was placed 2 cm away from the porous medium and thereby creating a reservoir with a certain depth. At the beginning of the experiments the gate is opened manually within about 0.1 s. These experiments were conducted for 3 set of water level 35 cm, 25 cm, and 14 cm. This above mentioned physical set up was always the same regardless of the porous medium of water level tested. The flow through the glass beads was found to be laminar, and closer to a Darcy flow and flow through the crushed rock being fully turbulent since velocities and pore sizes are larger. Further details about the experiments can be found in Lin (1999) [28].

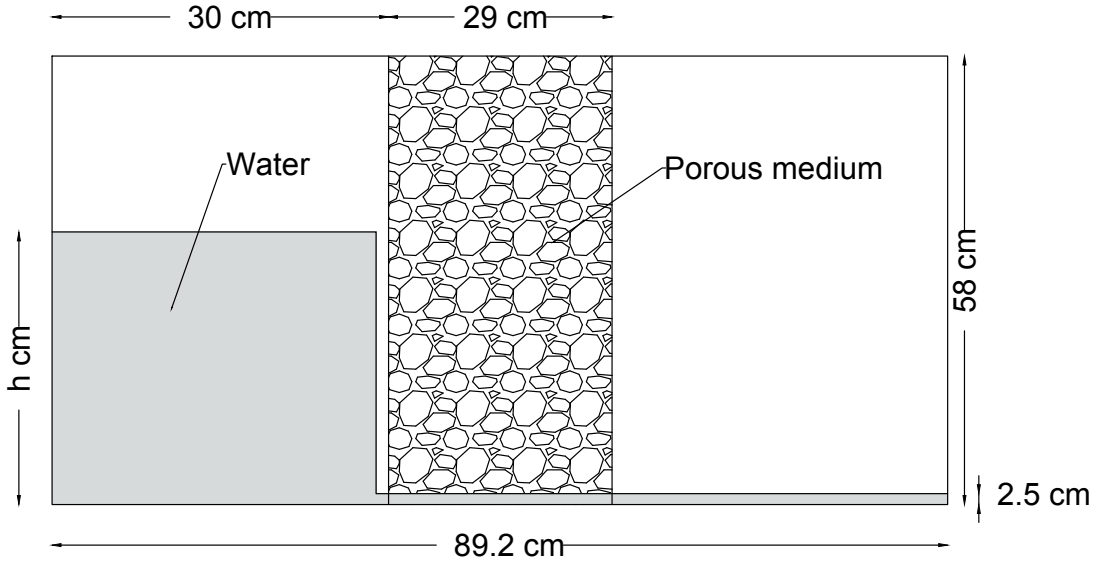

Figure 4.1: Dam break-setup for physical experiments

4.2.2 Numerical Validation using REEF3D

4.2.2.1 Porous medium with crushed rock

The whole tank used for experiments is reproduced numerically in 2D in the numerical wave tank with the exact dimensions as the physical experiment. This gave a length of 0.89 m and a height of 0.3 m and also the water level is set at 25 cm. The porous dam is placed at the center of the domain. Uniform grid resolution is applied throughout the domain with a grid size of 0.5 cm in all directions. This resulted in a total of 10,680 grid cells. The total simulation time is done for 3 s for comparison with the experimental data. The flow in this situation corresponds to a transition between the Forchheimer and turbulent flow regime. The system starts from a state of rest with the water and porous medium set at their initial location. Turbulence is modeled using the $k-\epsilon$ model. The calibration of resistance coefficients is done by completing a simulation matrix, where the 2 coefficients are varied as $\alpha = [500, 650, 750, 1000, 2500]$ and $\beta = [1, 1.5, 2, 2.2, 3]$.

The same case is also done with a grid size of 1 cm and it was noted that the both free surface evolution obtained for both the grids is almost identical, except for very small scale details. No significant differences are observed in the seeping process inside the porous medium.

The results for the best case (h= 25 cm, α= 650 and β= 2.2) will be discussed here and is shown in figure 4.2 . Figures a-l shows the comparison between

the numerical results and laboratory data for free surface profiles during the period when the flow is passing through the porous dam. In general, the overall agreement is very good particularly for t>0.6 s. The flow at the end which is also influenced by the return flow is very well represented by the model. For t=0.4 s and t = 0.6 s there is a small disagreement between the experimental and numerical results especially inside the porous medium. One possible reasoning for this is due to the difference in initial flow in experiments and in numerical model. In the experiments, at the initial stage the water is blocked with a gate and opening of the gate results in water being rushed to the porous medium. As a result of this impact on the porous medium, water piles up to form a small upward jet on the surface of the porous medium [28]. Also the gate is opened manually in the experiments within a finite duration (0.1s). This results in the water close to the bottom to move earlier than the water at free surface.

In addition to above reasoning, the uncertainties of the empirical coefficients in the numerical model can also be reason for the disagreement, mainly in the early stage when the flow in strongly transient. In figures c-f where the flow through the porous medium is mainly due to the pressure difference and the agreement gets better as the time progresses. Figures g-j represents the situation where the water have reached the right wall and is reflected back. This reflected wave breaks again on the porous medium and this is well captured in the numerical model. Figure k-l represents the period after breaking where water on the right side oscillates a little while water from the left side is still seeping through the porous medium.

Since the flow regime corresponds to a transition between Forchheimer and turbulent flow regime which is based on the pore based reynolds number, a strong dependency on the non linear coefficient,β was expected. This large dependency of β was also reported by Lin (1999) [28]. It was important to carry out simulations for different values of α and β to check their influence on the flow. This will give a better knowledge about the absolute error of the numerical solution with respect to the laboratory data. The best suitable time interval to study about the differences in the numerical results with laboratory data is a time interval between the initial and final state. This is because at the very beginning of the simulation this error will be high due to the issue with the gate separation mentioned earlier. Also at the end of the simulation the error will be close to zero. So a time of 1.2 seconds which is between these 2 bounds is selected. The difference between the numerical results and laboratory results for different values of α and β were compared and it was concluded that the best match were found for α= 650 and β= 2.2. These values are lower than the values used by Liu (1999) [28], where he used α= 1000 and β= 1.1. Comparison for these values are shown in figure 4.2 and evolution of free surface and variation in pressure is shown in figure 4.3.

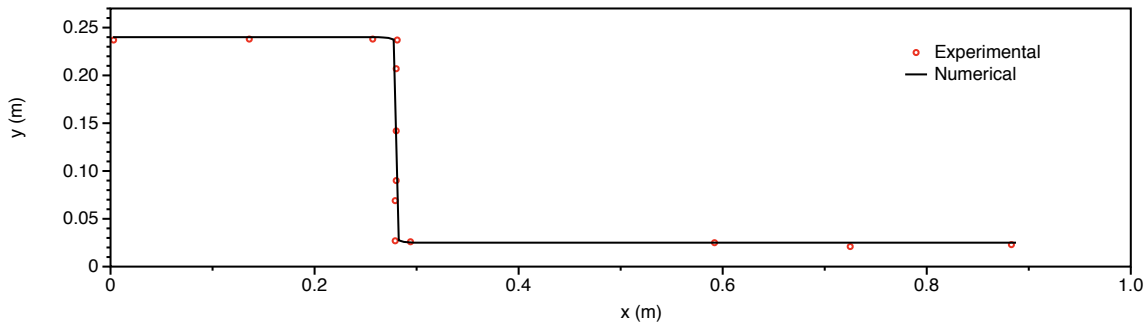

(a) 0.0 s

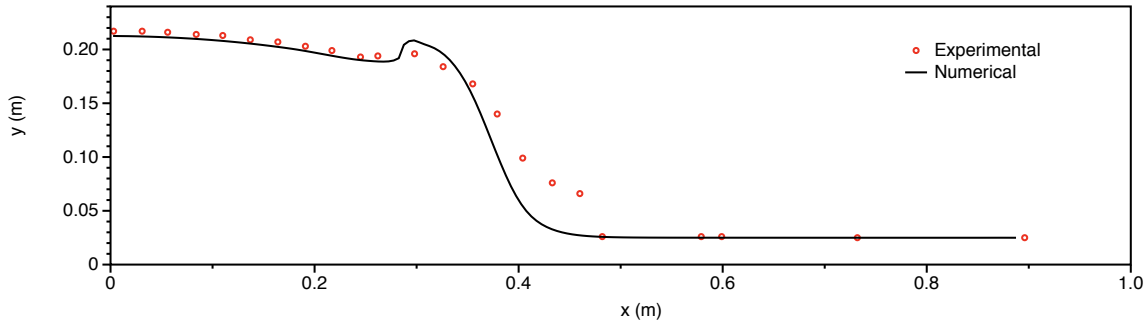

(b) 0.2 s

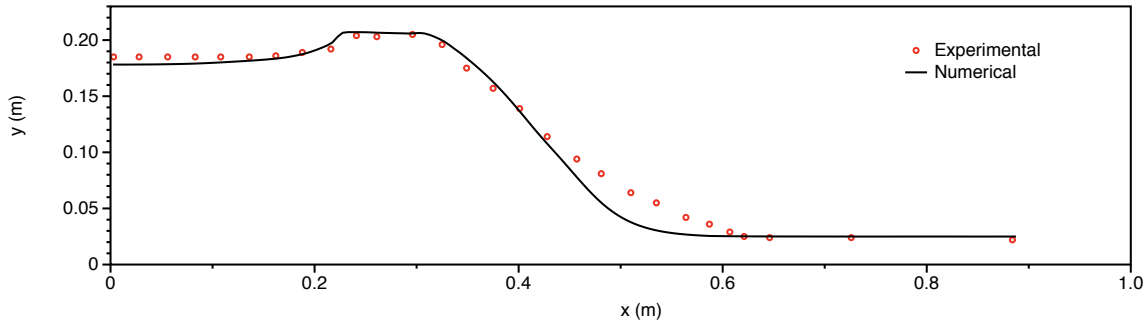

(c) 0.4 s

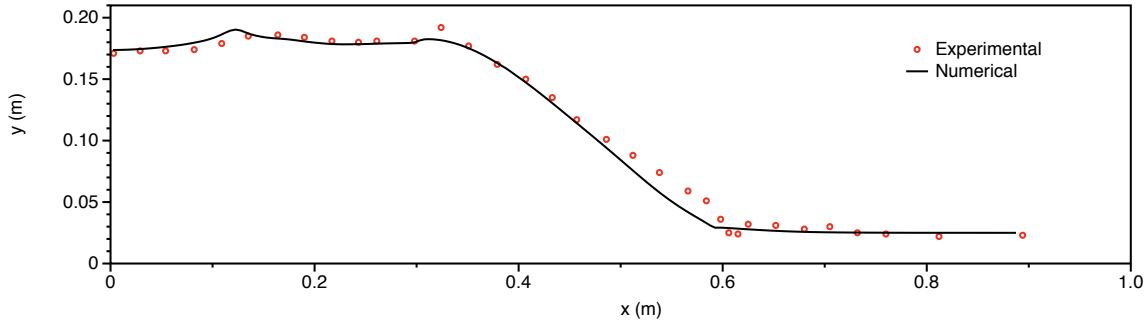

(d) 0.6 s

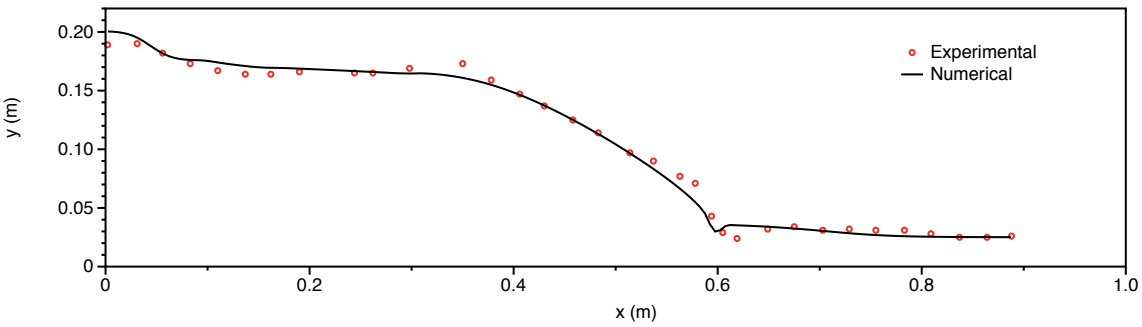

(e) 0.8 s

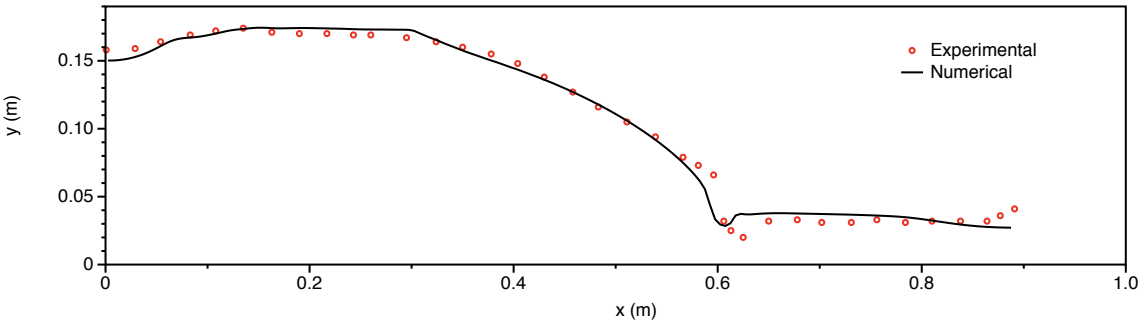

(f) 1.0 s

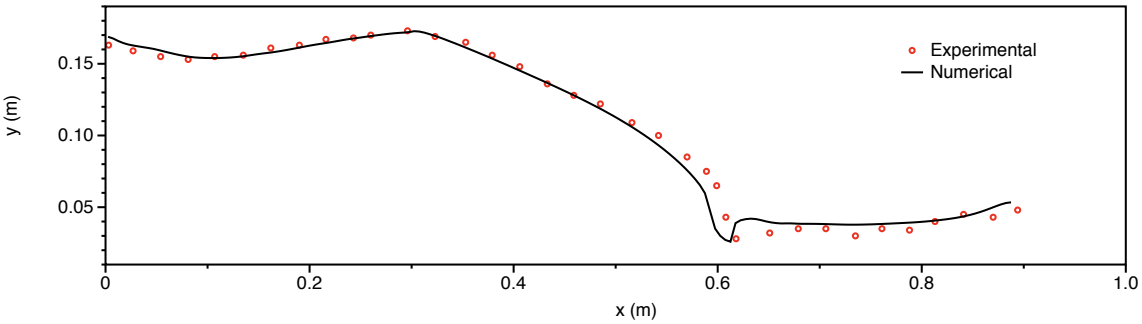

(g) 1.2 s

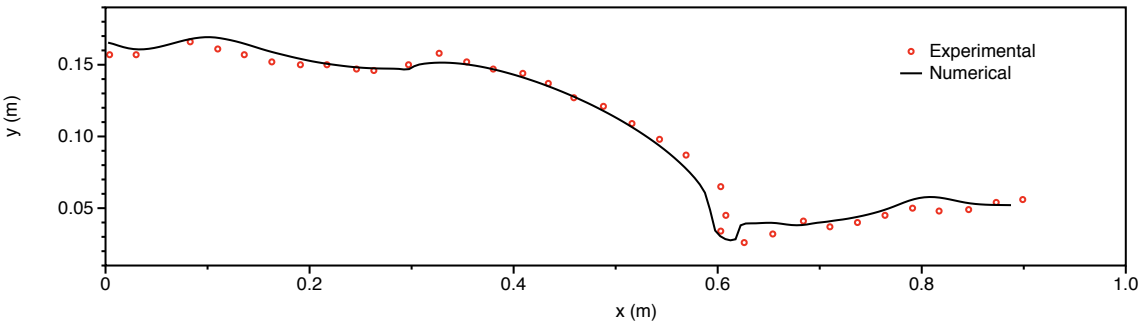

(h) 1.4 s

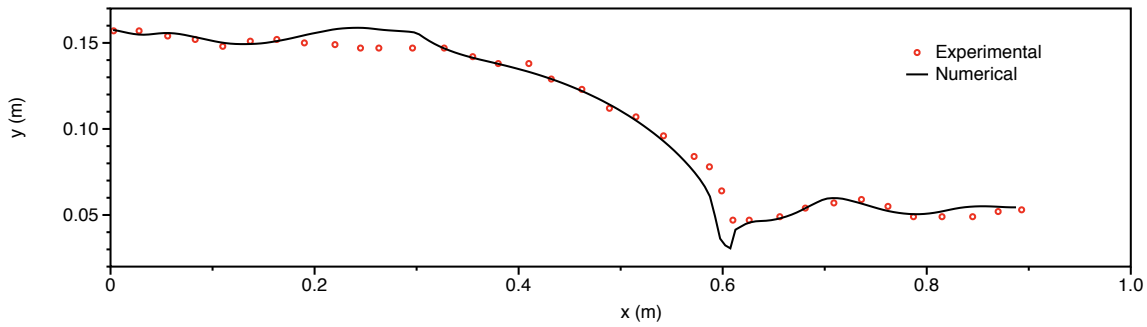

(i) 1.6 s

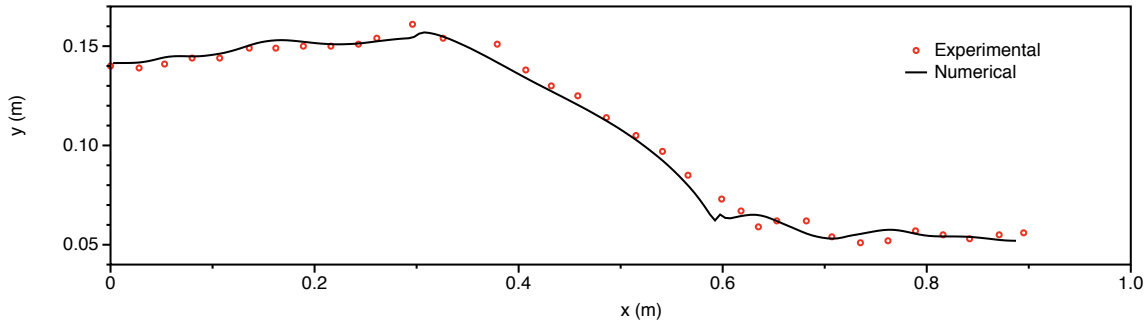

(j) 1.8 s

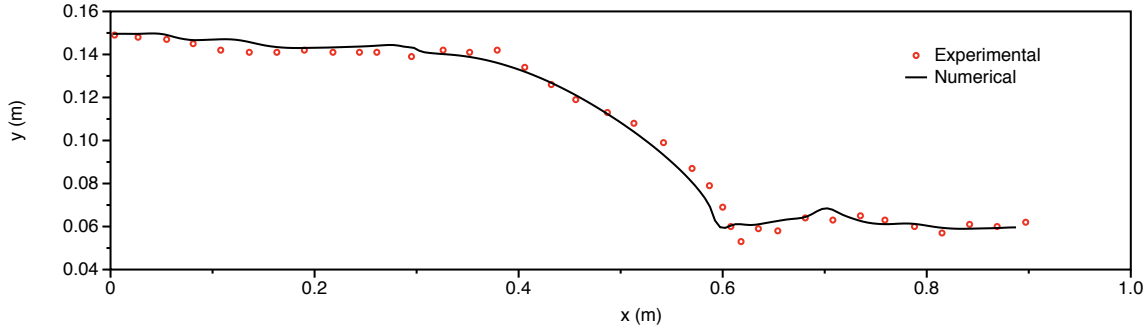

(k) 2.0 s

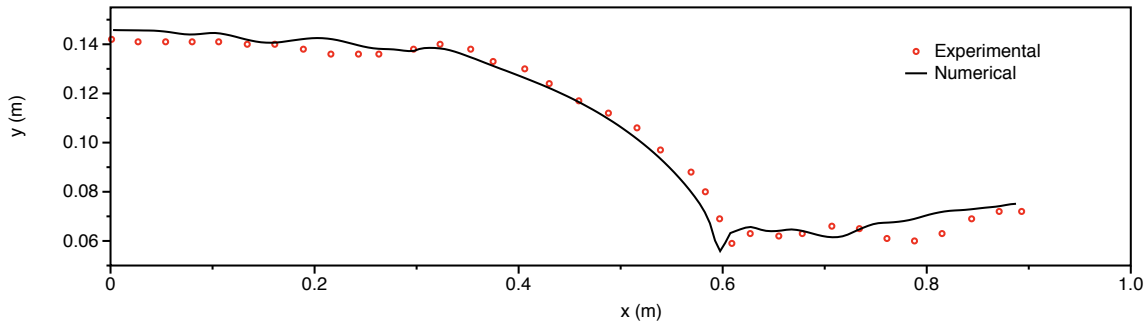

(l) 2.2 s

Figure 4.2: Comparison of free surface profiles for flow passing through porous medium - crushed rock with water level of 25 cm.

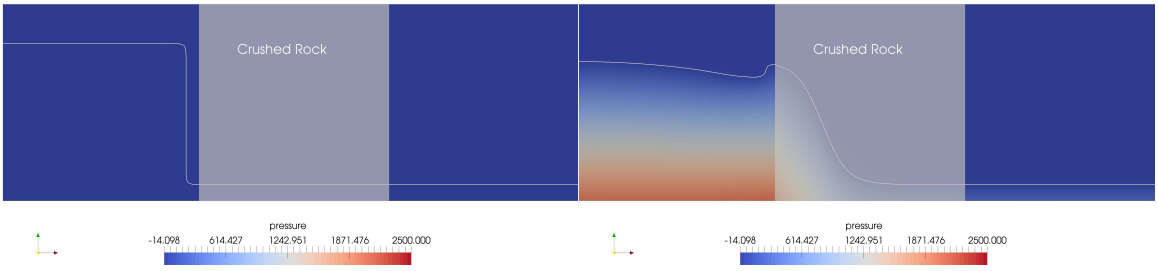

(a) 0 s

(b) 0.2 s

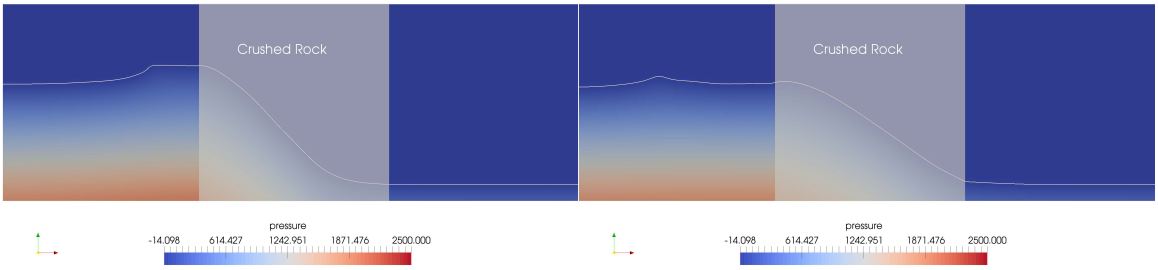

(c) 0.4 s

(d) 0.6 s

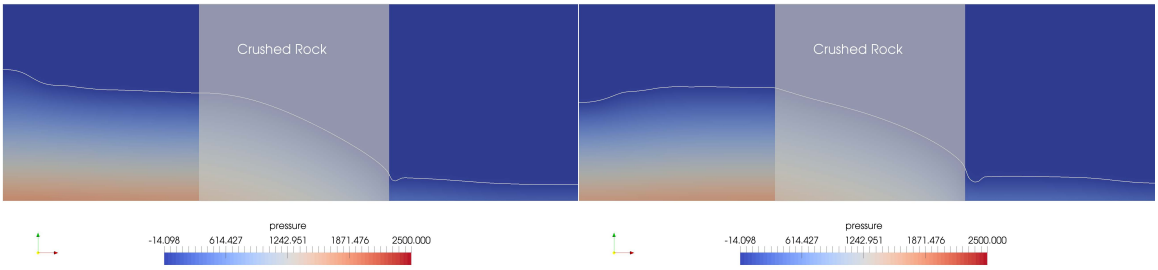

(e) 0.8 s

(f) 1.0 s

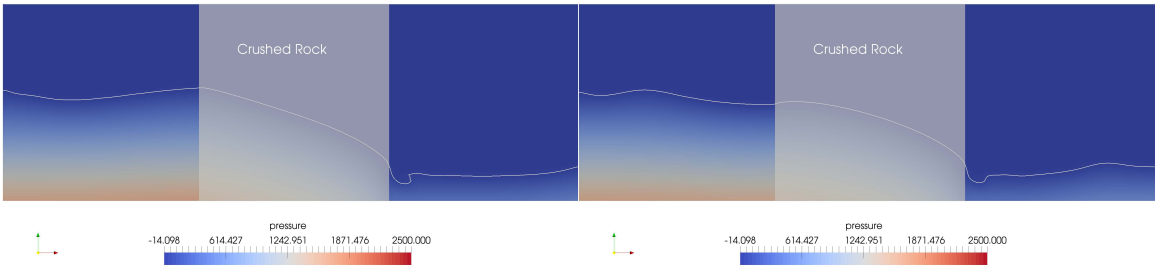

(g) 1.2 s

(h) 1.4 s

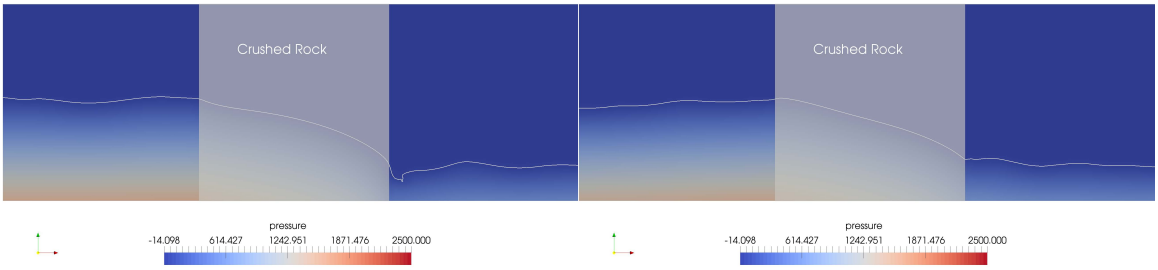

(i) 1.6 s

(j) 1.8 s

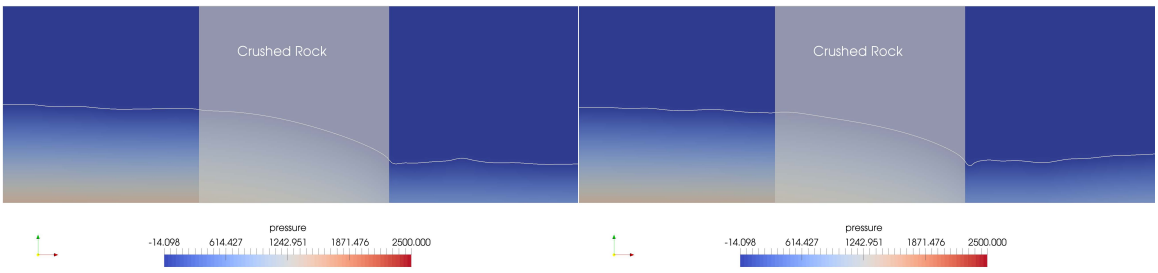

(k) 2.0 s (l) 2.2 s

Figure 4.3: Pressure variation and free surface in 2D Dam break - crushed rock

4.2.2.2 Porous medium with Glass beads

Similar experimental set up as used for the crushed rock experiments were employed for this experiments as well. The numerical wave tank was setup as a two-dimensional domain with a length of 0.89 m and width of 0.3m. The water level was kept at 14 cm and the pore Reynolds number corresponds to a Forchheimer flow regime. The porous dam was kept at the center of the tank and a uniform grid size of 0.5 cm is applied which resulted in a total of 10680 grid cells. The total simulation is done for 4 secs and is then compared to the experimental data obtained from Lin (1999). The porous dam is made out of spherical glass beads in the experiments with a diameter of 3 mm and porosity of 0.34. As a start, the first simulation is done using the same calibrated values crushed rock which is α= 650 and β= 2.2. Very poor agreement is found between the numerical and experimental data especially for the evolution of free surface inside the porous medium. This just proves that these empirical coefficients indeed depend on the the Reynolds number, the shape of the stones,the grade of the porous material, the permeability and the flow characteristics.

Due to this poor agreement a simulation is done with the suggested empirical coefficients by van Gent (1995), α= 1000 and β= 1.1. The results are show in figure 4.6. The agreement is now better than those with α= 650 and β= 2.2, mainly for the free surface inside the porous medium. Based on the comparison of the numerically simulated free surface and experimentally obtained free surface, an important observed feature is that the seepage process is slower in glass beads compared to the seepage in crushed rock. This influence is also noticeable at later time instants where water takes longer duration to percolate through the dam. As mentioned earlier the agreement of the results has improved and the water surface levels show no significant differences at both the sides of the porous dam. The free surface on the right side of the tank i.e. after the porous dam shows good agreement except for t = 4 secs. This indicates that the return flow near the back side of the dam is well captured in the numerical model. Im-

provement of this overall agreement between the numerical and experimental results will be discussed next.

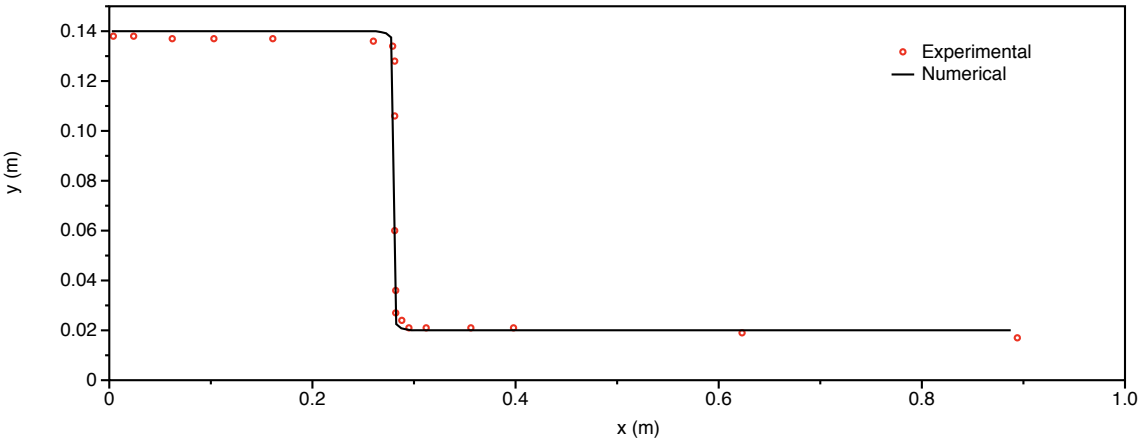

(a) 0.0 s

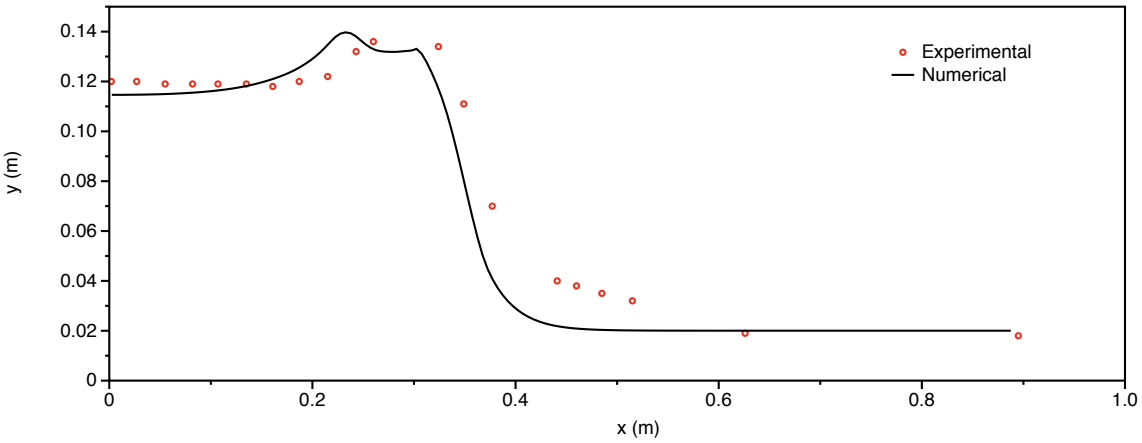

(b) 0.4 s

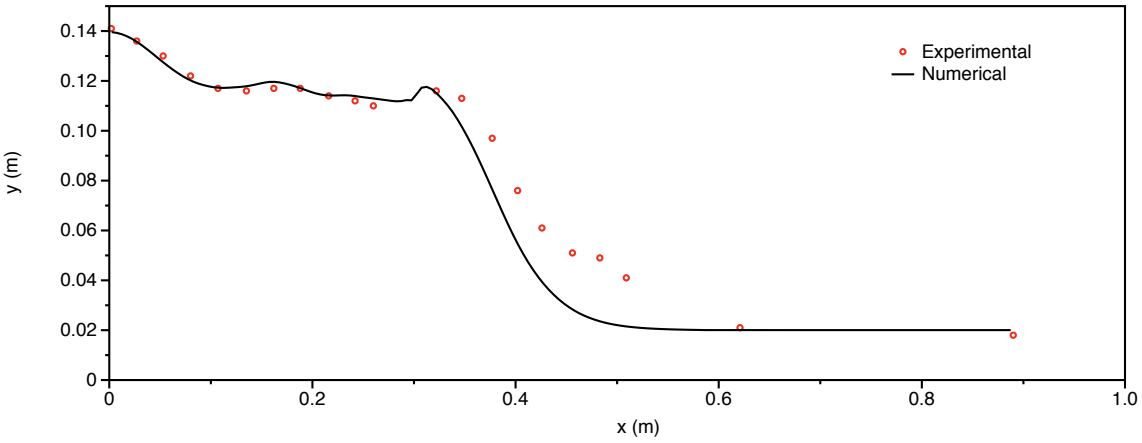

(c) 0.8 s

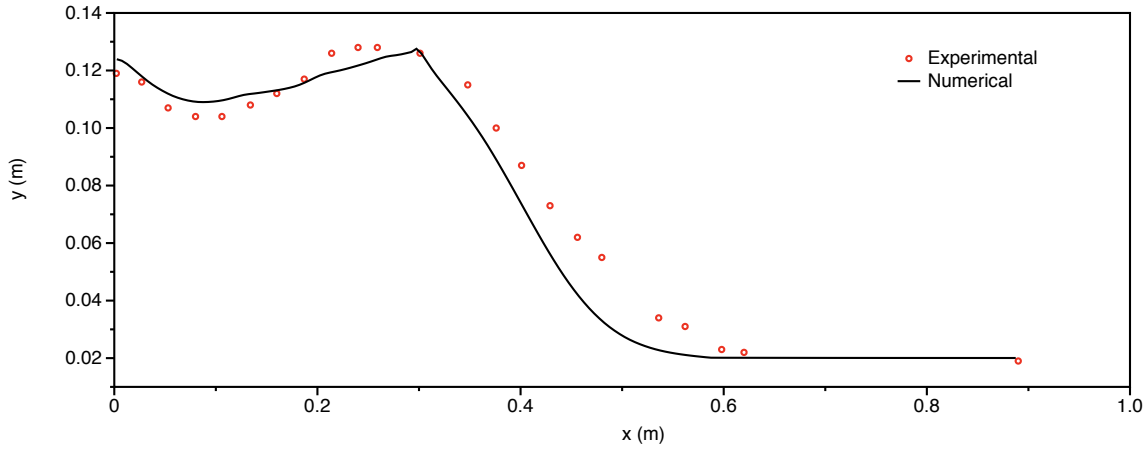

(d) 1.2 s

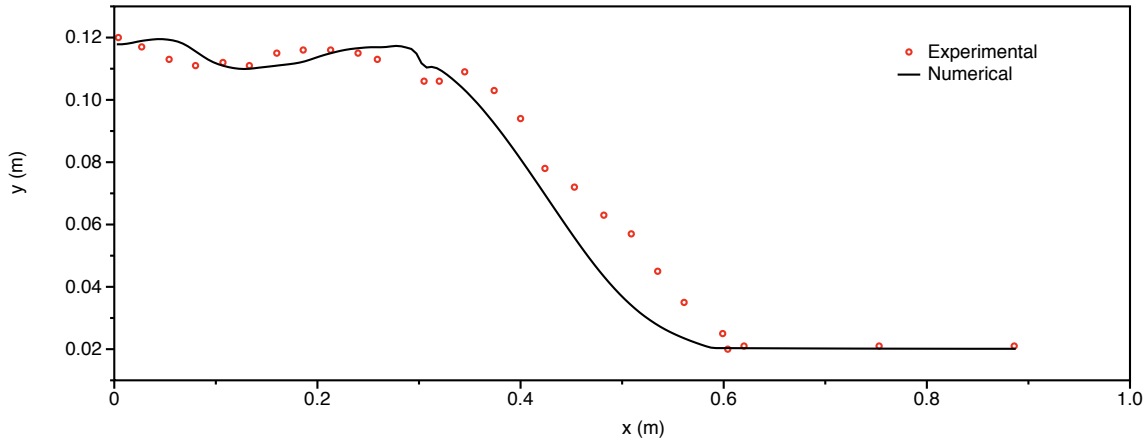

(e) 1.6 s

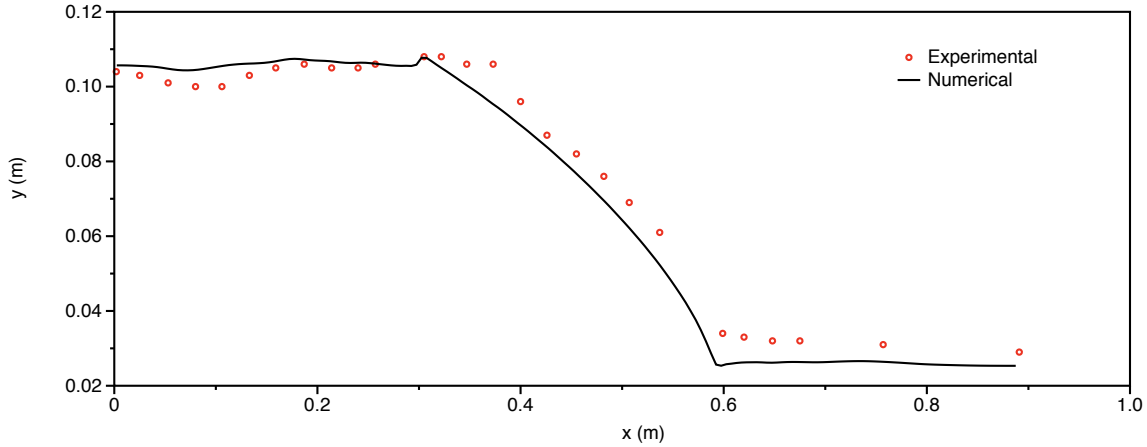

(f) 4.0 s

Figure 4.4: Comparison of free surface profiles for flow passing through porous medium - Glass beads with water level of 14 cm and with α= 1000 and β= 1.1.

In order to obtain a better agreement the α and β needs to be modified. Since the flow regime corresponds to a Forchheimer regime, a strong dependency on the α parameter is expected. From the simulation done using the α= 1000 and β= 1.1 which is suggested van gent(1995), the value for β is retained since it generates good results and the α needs to be modified. It should be also noted that the the size of glass beads are out of the test range of Van Gent (1995).

The calibration is again done by completing a simulation matrix, where the α coefficients is varied as $\alpha = [25, 50, 75, 100, 200, 300, 500, 650]$ and β is kept as 1.1. After the simulation of flow for all the possible combination selected through the simulation matrix, α= 100 and β= 1.1 gave the best agreement. Free surface levels shows decent match with no significant differences at both sides of porous dam and within the porous obstacle as shown in figure 4.5.

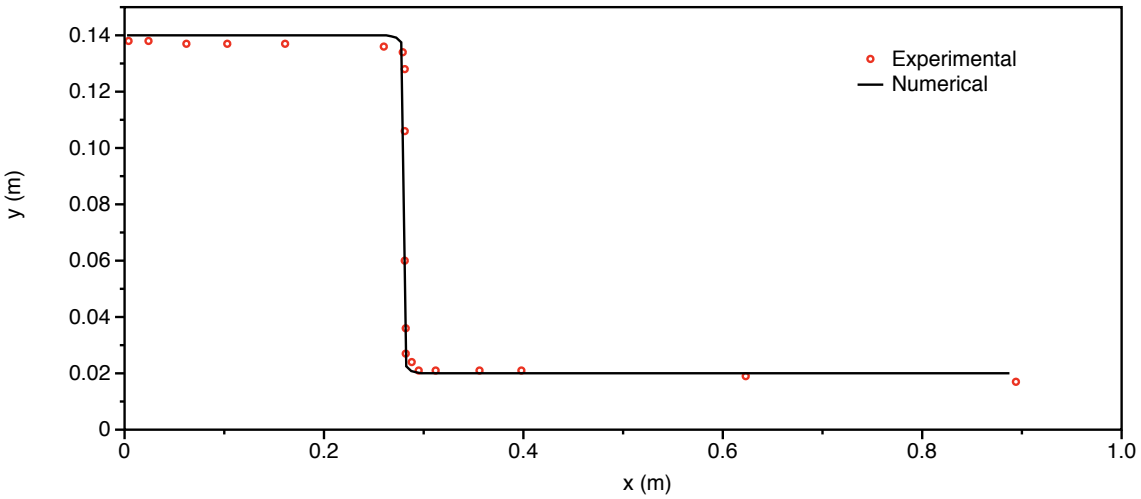

(a) 0.0 s

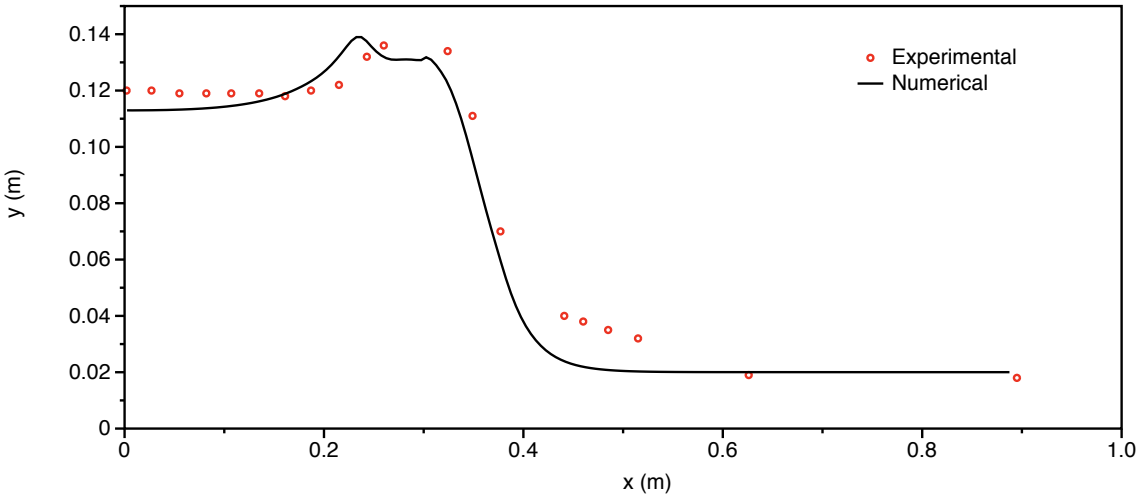

(b) 0.4 s

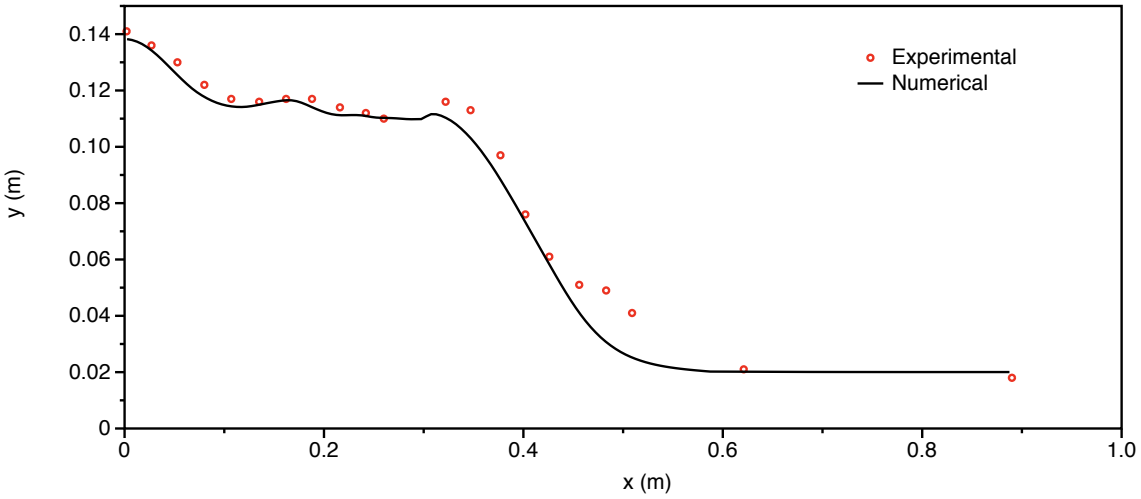

(c) 0.8 s

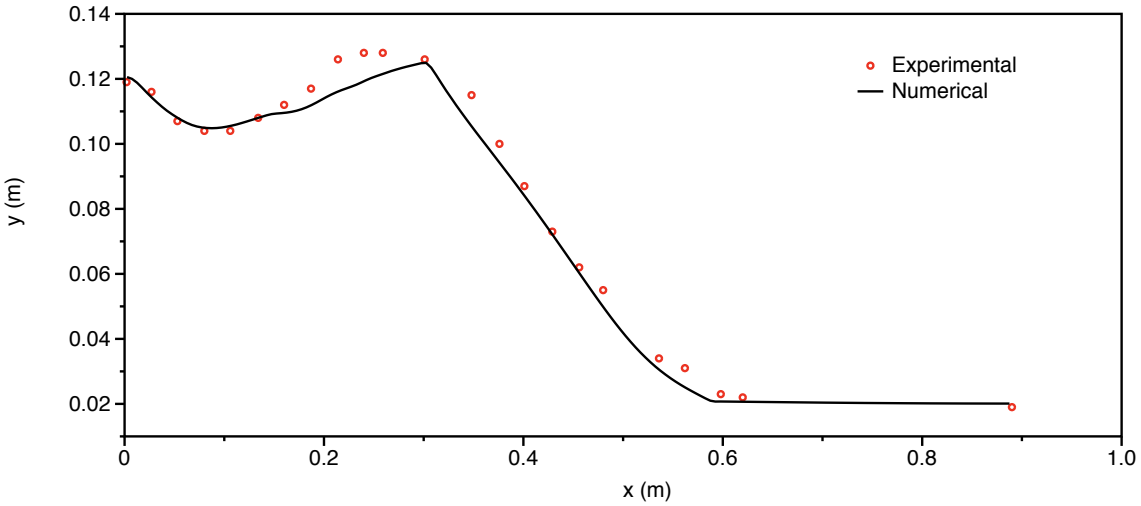

(d) 1.2 s

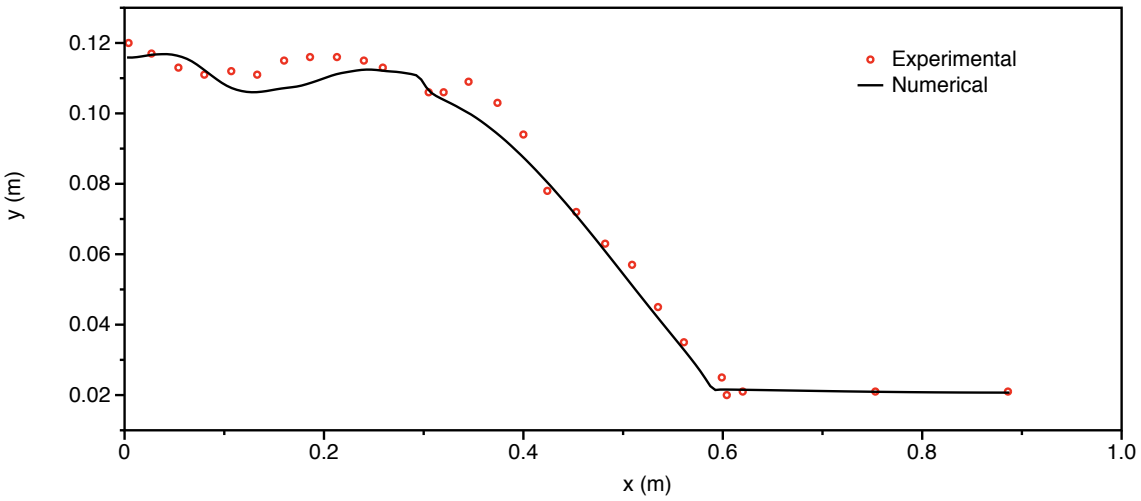

(e) 1.6 s

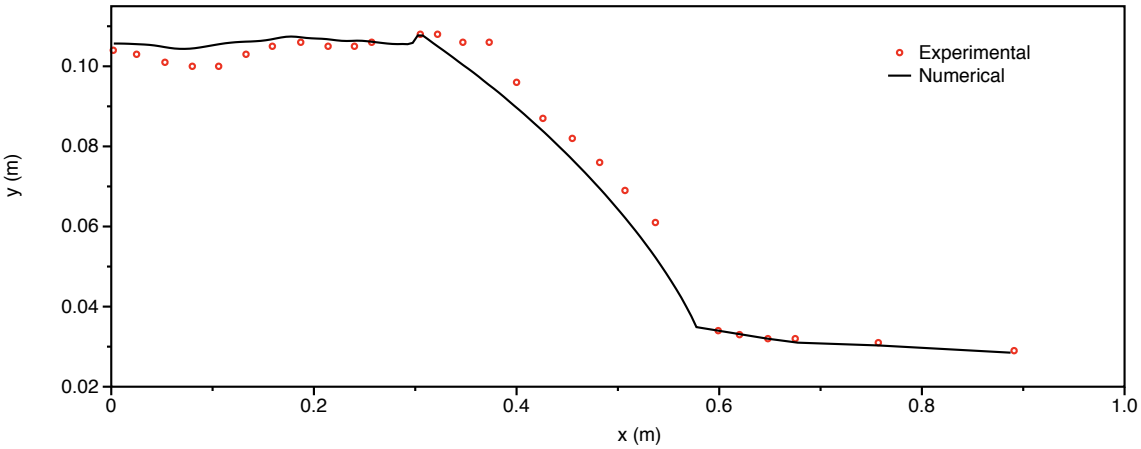

(f) 4.0 s

Figure 4.5: Comparison of free surface profiles for flow passing through porous medium - Glass beads with water level of 14 cm and with α= 100 and β= 1.1.

It is to be noted that the coefficient α is reduced by a factor of 10 , i.e. α= 100 from the originally proposed value bu van Gent (1995). This reduction is justifiable as the original coefficient (α= 1000) has been obtained from tests where viscous effects were almost negligible and can contain errors. From figure 4.5 the agreement in general is very good, but still there are some discrepancies in the agreement. So this suggests that a better method of calibration of the α is necessary when we are dealing with flow situations with low Re_p where linear frictional forces are negligible. One explanation for disagreements between the experimental and numerical results are because during the lab experiments the free surfaces in the porous dam have been found to stick on the glass wall at some locations ([28]). This is probably caused because of the surface tension and capillary effect and which may result in overestimating the free surface inside the porous dam. The simulated case in the numerical model is shown in Fig.

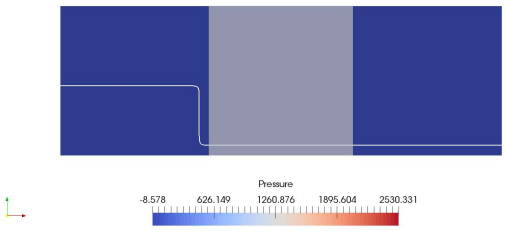

(a) 0 s

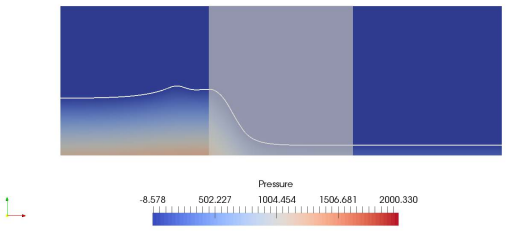

(b) 0.4 s

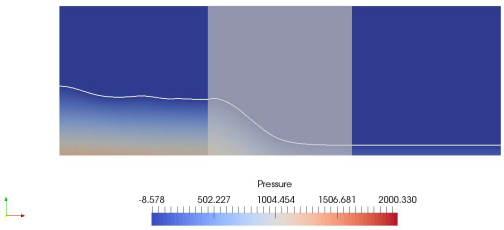

(c) 0.8 s

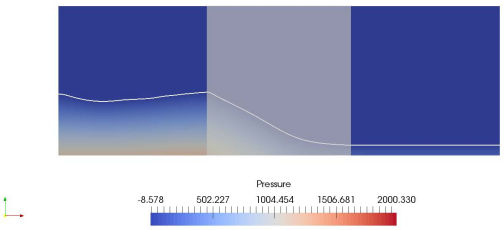

(d) 1.2 s

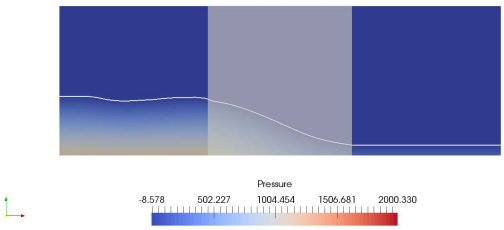

(e) 1.6 s

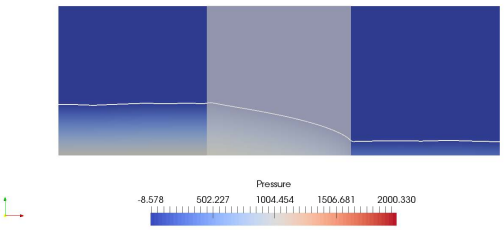

(f) 4.0 s

Figure 4.6: Pressure variation and free surface in 2D Dam break - glass beads

4.3 Three-dimensional interaction of waves with a porous structure

In the last section, the capabilities of the model have been proven to work in two-dimensional cases. In this section, the simulations are extended to full three-dimensional domain. The interaction of a solitary wave with a vertical porous structure is simulated here.

4.3.1 Experimental Setup

The experiments carried out by Lara et al. (2012) [25] in the wave basin at University of Cantabria is used for validating the numerical model REEF3D. The basin was 17.8 m long, 8.6 m wide and 1.0 m high. A porous structure is built with a metallic mesh and is filled with granular material to allows water to flow across. The porous structure is positioned at right angles to the wave propagation direction. This porous structure is 4.0 m long, 0.5 m wide and 0.6 m high. The mean stone diameter is 15 mm and have a porosity of 0.51. This porous structure is attached to one of the lateral walls with it's seaward face being 10 m away from the wave maker. The waves are created by a piston-type wave-maker which is used in the experiments. The plan view of the set up used in the experiments in shown in Fig. 4.7.

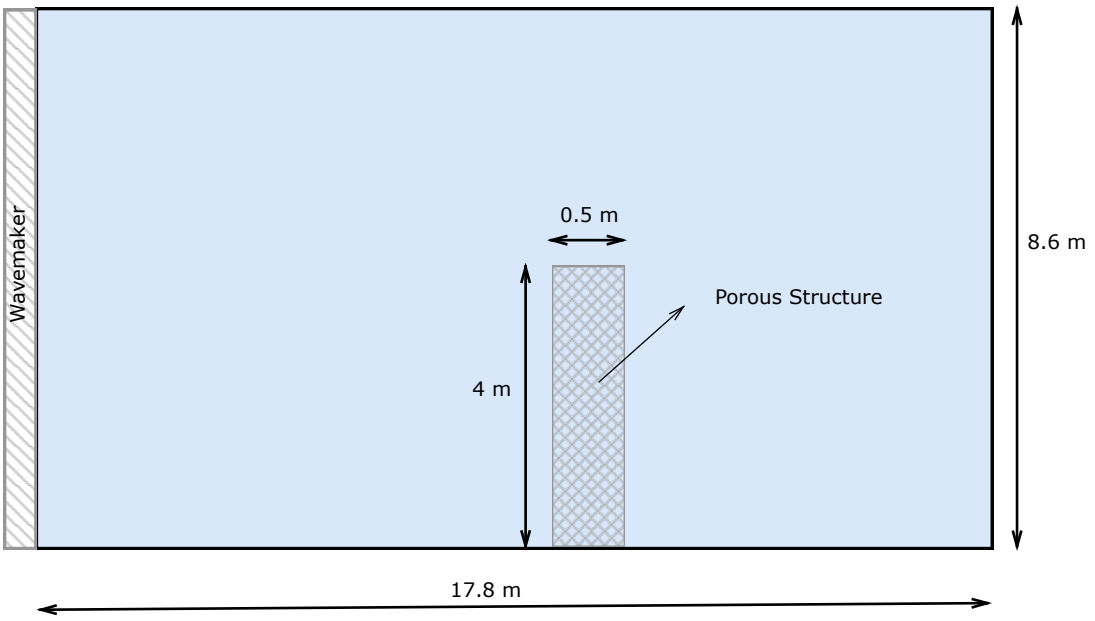

Figure 4.7: Setup for porous abutment in wave basin

All the experiments carried out in the basin is composed of three completely

reflective vertical walls. The water depth is kept constant and equal to 0.4 m. Both solitary waves and regular waves are tested in the experiments.

4.3.2 Numerical validation using REEF3D

In order to replicate such a wave tank of these dimensions numerically, it requires very high computational power and space. The use of a grid size of 0.01 m would result in more than 90 million cells. So the dimensions of the tank are reduced in order to make it computationally feasible. The total length of the tank was reduced to 11 m, width to 6.0 m and height to 0.6 m. The porous abutment retained its original dimensions. The seaward face of the porous structure was 6 m away from the wave maker. The location of wave gauges needed to adjusted according to the new dimensions of the wave tank. The new arrangement of wave tank used in numerical model with the location of wave gauges is shown in Fig. 4.8.

Two wave gauges (wave gauge 1 2) are kept in front of the porous structure (seaward face) and two wave gauges (wave gauge 4 5) after the porous structure (leeward face). In addition 1 wave gauge is also kept in between the tip of the porous structure and glass walls. Experiments are done for a duration of 20 sec and it was reported in Lara et al. (2012) [25] that the solitary waves get reflected at several locations on the basin. The solitary wave gets reflected from the end wall, the lateral walls and also from the wave maker. Since in the numerical model the wave tank was scaled down to 11 m, the accuracy of the results for a longer duration will be less due to all the possible reflections. So for this case, the total simulation is done for 10 sec.

Location of wave gauges are given in Table 4.2. The simulated case is for a 5th order solitary wave with a wave height of 0.09 m. The size of the stones and porosity of the the porous structure was similar to the values used in the dam break case with crushed rock. So the starting point for resistance parameters for this case was α= 650 and β= 2.2 which are calibrated values for the dam break case. The general agreement using these values were satisfactory but, more accurate results are found for α= 750 and β= 2.2 and is shown in Fig. 4.9.

Table 4.2: Location of wave gauges

Wave Gauge	**x dist. (m)**	**z dist (m)**
1	5.0	1.0
2	5.0	3.0
3	6.25	5.0
4	7.5	3.0
5	7.5	1.0

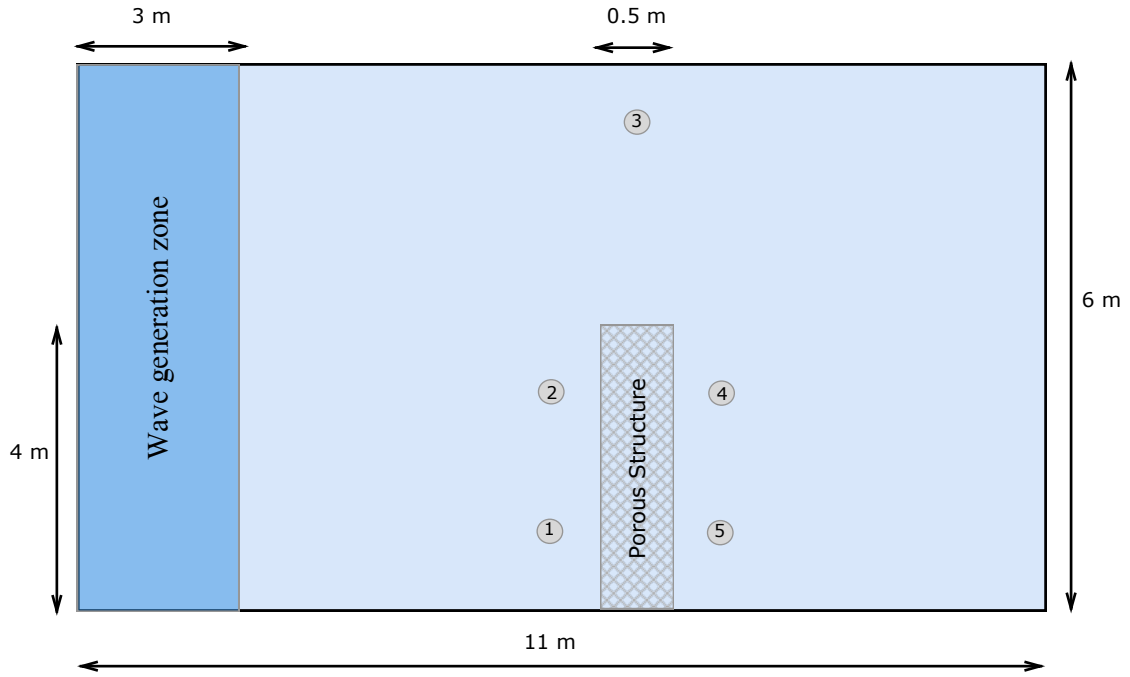

Figure 4.8: Setup for porous abutment in numerical wave tank

4.3.3 Results

The VARANS method implemented in REEF3D is proven to reproduce the relevant hydraulic process in wave-structure interaction in a three-dimensional domain. The solitary wave validation shown in Fig. 4.9 shows good agreement between the experimental and numerical results. The numerical results are simulated for a grid size of 0.025 m which resulted over 4 million cells in the domain. The model simulates the energy reflected at the porous structure quite well which can be seen for wave gauge 1 and 2 (Fig.4.9a and Fig.4.9b), which is located seawards and close to the porous structure. The transmitted wave heights at the leeward side of the porous structure is also reproduced numerically. There was a phase lag between the experimental and numerical results due to rescaling of wave tank in the numerical model.

The only major disagreement is between the free surface trough of the reflected wave in wave gauge 2 (Fig.4.9b). It is reported by Lara et al. (2012) [25] that during the experiments it was revealed that at least half of the water column was affected by trapped air. Wave gauge 4 in this simulations is not only affected by diffraction but also by wave transmission across the porous medium. The degree of accuracy of the model reproducing the combination of both processes is observed to be good.

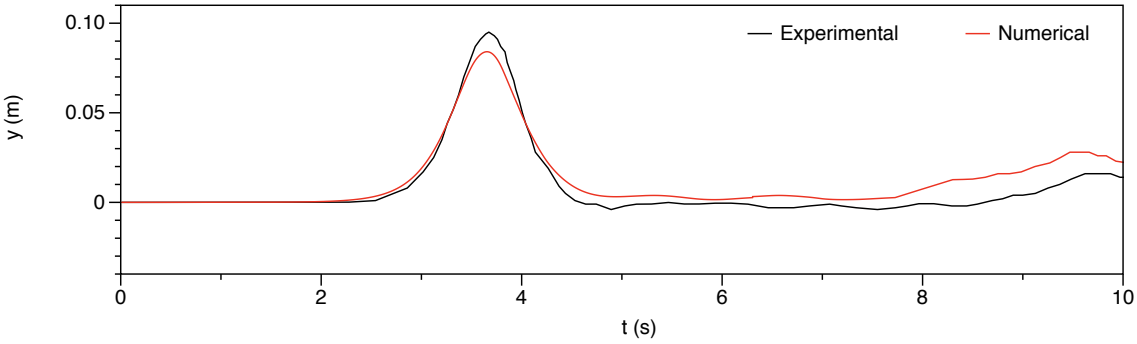

(a) WG1

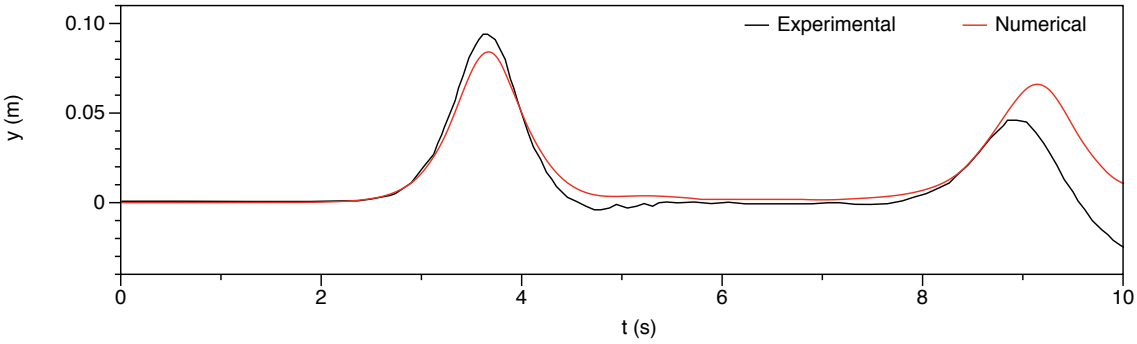

(b) WG2

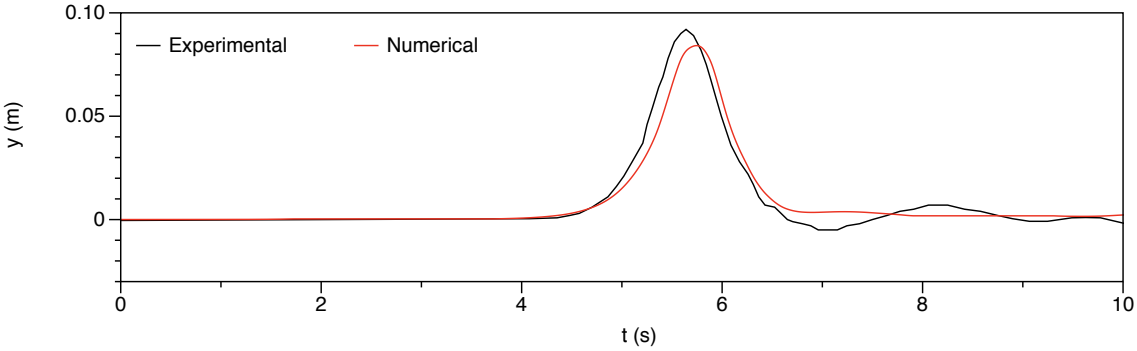

(c) WG3

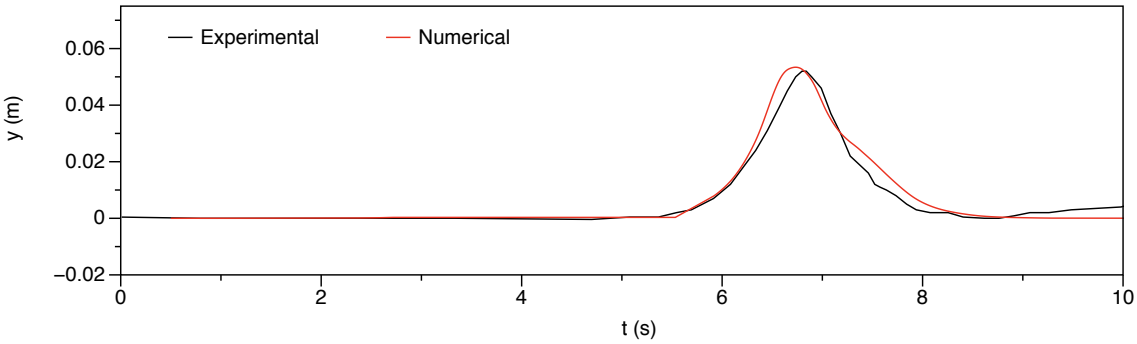

(d) WG4

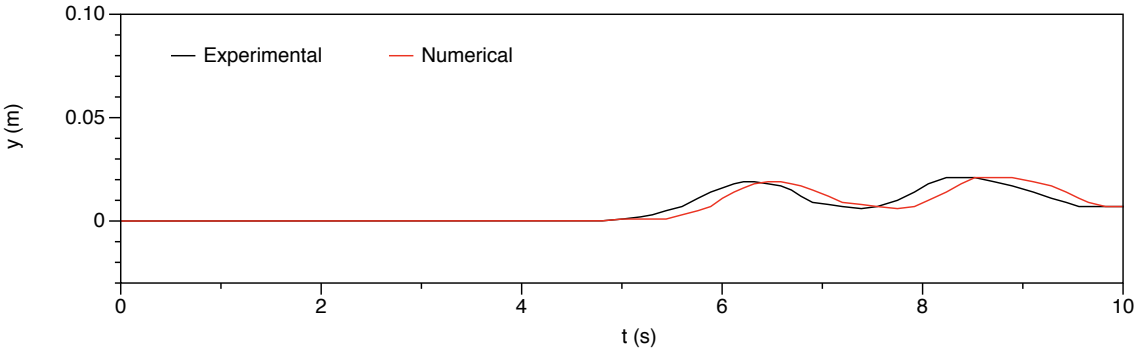

(e) WG5

Figure 4.9: Comparison of free surface profiles for porous abutment with α= 750 and β= 2.2.

4.4 Regular wave interaction with porous breakwater

From the good agreement between the experimental and numerical results for porous structures using the VARANS method, a porous breakwater case is simulated in REEF3D. This tests was done as a starting point for further improvement and added applications in the CFD model REEF3D. One of the challenges in simulating wave interaction with porous breakwater is that it needs multiple $\alpha$and β values based on the type of porous material. As of now REEF3D doesn't have that function to call multiple $\alpha$and β values, which means implementing multiple porous layers is not possible. So a simple breakwater geometry is considered here. A breakwater with non porous inner core with one single porous layer on top of it. Changes in free surface through the porous medium and the damping out of waves as it reaches the lee side of the breakwater is discussed here.

The main factor in simulating wave interaction with a porous breakwater is to manage the wave transformation processes that encompass with the interaction with the structure. These wave transformations includes reflection in front of the structure and also wave damping inside the porous medium. The simulated results are shown in Fig. 4.10 where t = 5 to 9 sec shows one wave breaking on the breakwater slope and t = 11 to 15 sec shows the breaking of second wave. Fig. 4.10b and Fig. 4.10c shows the damping of free surface inside the porous medium which results in a more or less calm condition on the lee side of the breakwater. In case of breakwaters with multiple porous layers, the damping effects will large. But this needs correct and accurate representation of the resistance parameters, α and β which is still under research.

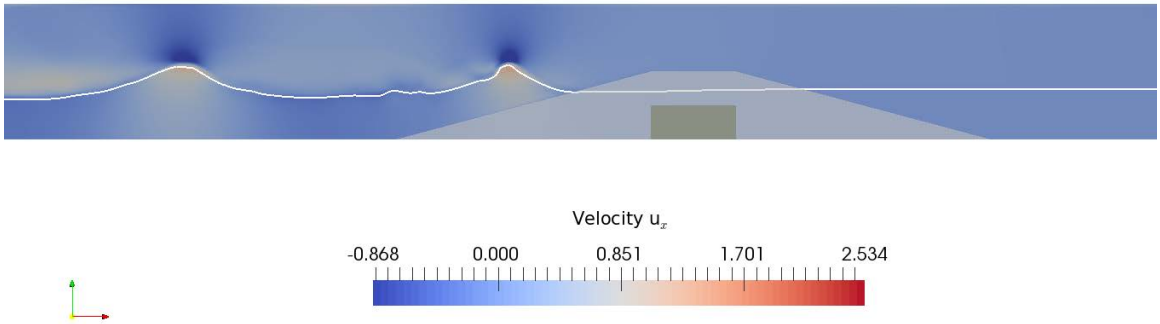

(a) t=5 sec

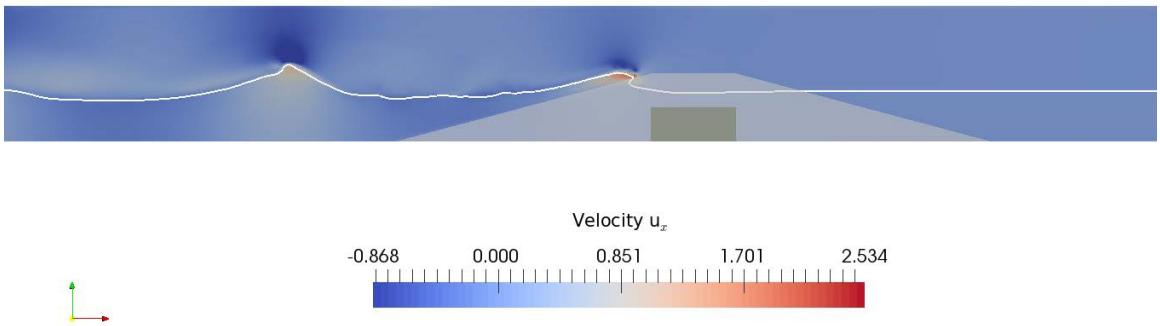

(b) t=7 sec

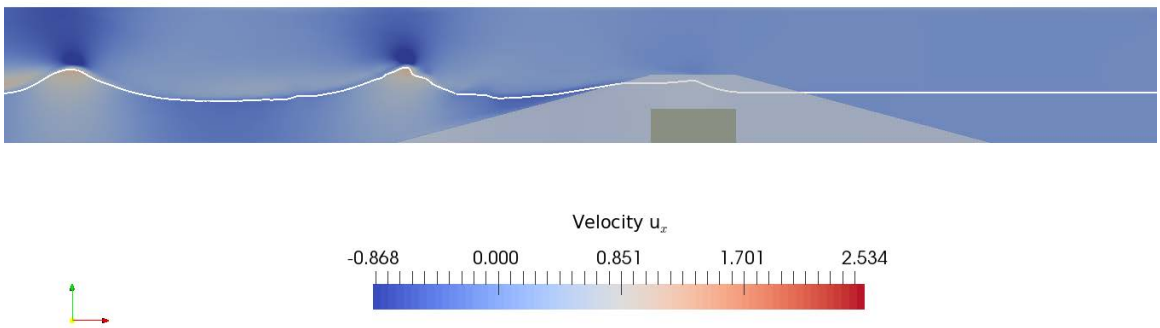

(c) t=9 sec

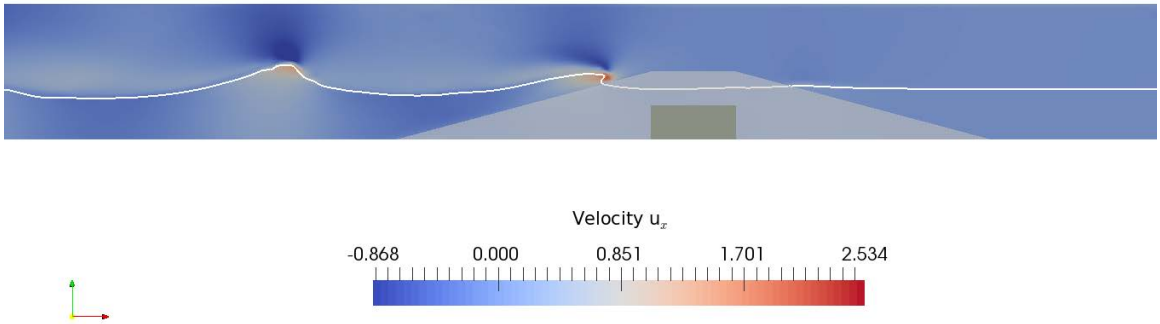

(d) t=11 sec

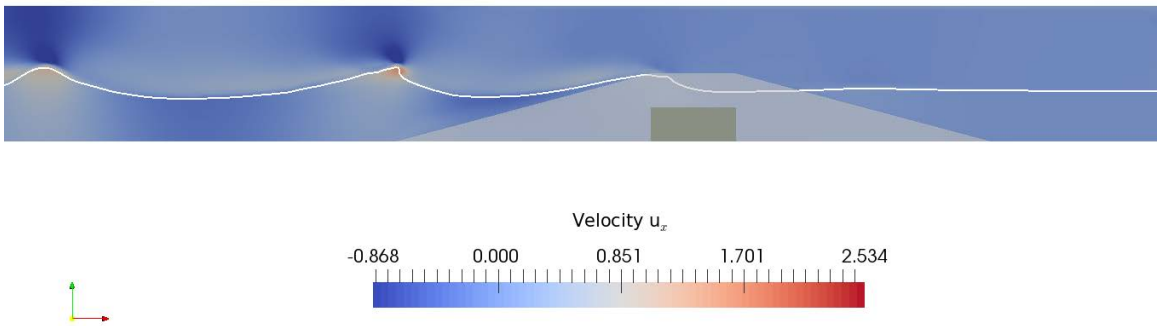

(e) t=13 sec

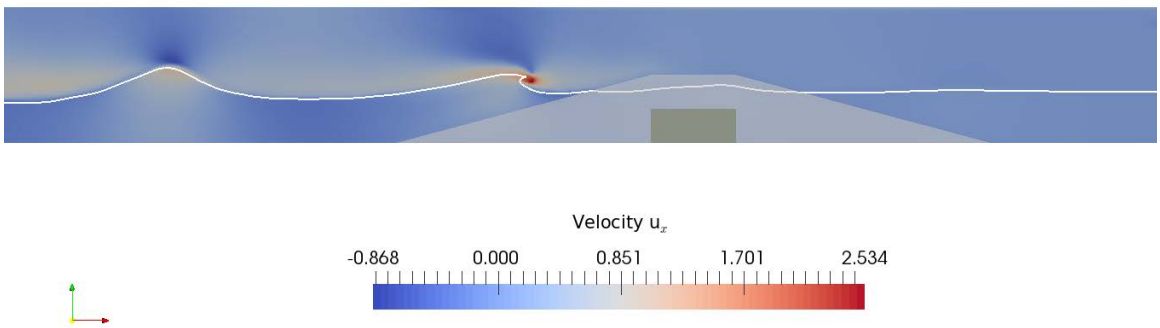

(f) t=15 sec

Figure 4.10: Change in free surface in presence of porous breakwater

Chapter 5

Conclusions and outlook

5.1 Conclusions

The main focus of this thesis was to validate the implemented VARANS method in REEF3D for solving the porous flow. A brief overview of the basic concepts of CFD and the methods employed in the CFD model REEF3D has been discussed in Chapter 2. It was important to validate the numerical model before simulating porous medium cases to check the wave generation, change in wave kinematics in presence of structures, water particle velocities and absorption capabilities.

The numerical wave tank in REEF3D is validated by conducting lab experiments in the wave flume. Three set of experiments were done in the lab. Tests with no obstacles, with a step structure and an abutment structure was performed in the wave flume. Results from validation and performance testing of the wave tank are very promising. This study used the wave tank to simulate unidirectional regular waves. Different grid sizes were used in the study to know about the accuracy variation in results. A brief overview about the tests and the predictive capabilities of the model is presented below.

In the first scenario, a basic flat-bottom 2D wave tank with no structures was simulated to know the working conditions of the flume and also to show the quality of the generated waves when compared to the reality. Both free surface and velocities were compared for this case and an extremely satisfactory agreement was seen between both the sets of results. In the second scenario, test were done with the presence of a step structure in the flume to assess the capability of REEF3D in generating and absorbing the wave and also the changes in wave kinematics are accurately presented in the numerical model. This case was as a two-dimensional simulation to ease up the computational efforts. The effect of wave generation and absorption methods available in the numerical model REEF3D is studied for a same case. Wave generation methods like Relaxation methods and Dirichlet method based on shallow water theory and intermediate

water theory was tested. Similarly wave absorption methods like relaxation method and active wave absorption methods were also tested since the absorption capabilities of the wave flume was uncertain. From the simulated cases with the step structure it was concluded that the best agreement between the experimental and numerical results were found by using the Dirichlet method for wave generation and active absorption for wave absorption. From tests with no obstacles in wave tank, as relaxation zone worked did work well. The Dirichlet generation provides the best match only because the wavemaker in the wave flume does not have active absorption. Due to this the wave reflected from the structure travel between the wavemaker and the structure, undergoing multiple reflections and affecting wave generation. The recommended grid size is of 0.005 m. These combinations were again tested for a case with step structure but now with a higher wave height and the results showed good accuracy.

The 3rd and final simulations was done with an abutment structure in the numerical wave tank with the use of methods and grid sizes mentioned above. Comparisons for surface elevation and velocities was good and some mismatches in the peaks were solely due to the reflections generated in front of the abutment which have influenced the generated waves approaching the structure. The choice of wave heights and wave periods used for the tests were limited due to reflections, size of the flume and data acquisition of wave gauges. Through this validation cases, it shows that REEF3D has the capability of correctly modeling of regular wave propagation both in generation and absorption of the waves as well as simulating the wave behavior interacting with structures.

Chapter 4 deals with the investigation of porous media flow based on a volume-averaging approach of the RANS equation. First the equations representing the porous media flow is presented and the VARANS method is introduced. In the first validation case, the flow in porous media is simulated for two dimensional dam break case. The experimental data was taken from the tests conducted by Lin (1999) [28]. Two types of porous materials was used in the porous medium. First simulation was done for a porous medium consisting of crushed rock with D50 of 15.9 mm and porosity (n) of 0.49. In this section, emphasis was put on calibrating the resistance coefficients α and β. A simulation matrix was completed in order to calibrate the α and β values. The best match of results was found for α= 650 and β= 2.2. For the second case, porous media was represented by glass beads with D50 of 3.0 mm and porosity (n) of 0.39. Calibrated α and β for the tests with crushed rock was used as a starting point for this case. Due to less agreement between the results, coefficients proposed by van Gent (1995) which was α= 1000 and β= 1.1 was used and the results showed decent agreement. There were still mismatches between the experimental and numerical results and again a simulation matrix had to be completed for better agreement. The resistance parameters was calibrated as α= 100 and β= 2.2.

In the situation with a crushed rock due to a larger nominal diameter a larger Reynolds number has been observed. The non linear drag coefficient appears to

be the most important parameter. For the case with glass beads the linear drag parameter has the largest influence because the Reynolds number decreases. The seconds validation case was done for a porous abutment in a wave tank. This was modeled as a three-dimensional simulation with wave gauges to measure the free surface both in front and back of the porous abutment. The type of the porous material and porosity used in this case and for crushed rock in dam break case was similar. So the resistance coefficients used for crushed rock was used as a start and was tweaked to get a better agreement. Results for solitary waves interacting with the porous medium show a high degree of accordance with the laboratory data.

In the final part of this study, porous breakwaters are tested in the numerical model. This tests was done as a starting point for further improvement and added applications in the CFD model REEF3D. The model already shows good promise in case of breakwaters with single porous layer. Implementing multiple α and β values for different breakwater layers should be next priority.

Different flow regimes of porous media flow have been correctly modeled, demonstrating the model capabilities. In general the numerical and measured free surface agree well for both the porous media which was tested. Porous flow parameters have been found to be different because of the type of flow in both the cases. The model was found to correctly predict interactions with both two and three dimensional structures.

5.2 Outlook

The study presented in this thesis shows that REEF3D has promising results for wave interaction with porous structures. This study dealt with validation of two porous structures, in both two-dimensional and three-dimensional domain. It is recommended to validate more cases with porous structures in case of solitary and regular waves. The potential of the model can thus be further enhanced to study a more complex wave- porous structure interaction, for ex. breakwaters. Based on the observations for the breakwater simulations, it is recommended to include functions to represent breakwaters with multiple porous layers of different stone diameters and porosity. This should be validated by comparing the numerical results to the experimental results. Since it is much less time consuming changing geometry and material properties in a numerical model than in a physical model (certainly at large scale), it would make sense to firstly perform a numerical study on such problems. And, in future with these added features, REEF3D can prove to be a efficient tool to deal with such complex coastal engineering problems.

Bibliography

[1] Andersson. *Computational Fluid Dynamics for Engineers*. Cambridge University Press, 2012.

[2] P. A. Berthelsen and O. M. Faltinsen. A local directional ghost cell approach for incompressible viscous flow problems with irregular boundaries. *Journal of Computational Physics*, 227:4354–4397, 2008.

[3] H. Burcharth and C. Christensen. On stationary and non-stationary porous flow in coarse granular materials. *MAST G6-S,Aalborg University*, 89(3):327–333, 1995.

[4] M. Chella. *Breaking Wave Charecteristics and Breaking Wave Forces on Slender Cylinders*. PhD thesis, Norwegian University of Science and Technology, 2016.

[5] A. Chorin. Numerical solution of the Navier-Stokes equations. *Mathematics of Computation*, 22:745–762, 1968.

[6] H. Darcy. Les fontaines publiques de la ville de dijon. *Dalmont*, 1:1–14, 1856.

[7] M. del Jesus. Three-dimensional interaction of water waves with coastal structures. *Ph.D. thesis. Universidad de Cantabria, Santander (Spain)*, (1):57–72, 2011.

[8] M. del Jesus. Three-dimensional interaction of waves and porous structures. *Coast. Eng.*, (64):57–72, 2012.

[9] J. F. Douglas Enright, Ronald Fedkiw and I. Mitchell. A hybrid particle level set method for improved interface capturing. *Journal of Computational Physics*, (183(1))::83116.

[10] F. Engelund. On the laminar and turbulent flow of ground water through homogeneous sand. *Transactions of the Danish Academy of Technical Sciences 3l.*, 7(5):293–306, 1953.

[11] R. D. Falgout, J. E. Jones, and U. M. Yangr. The design and implementation of hypre, library of parallel high performance preconditioners. Technical report, 2006.

[12] P. Forchheimer. Ing. 48. *Wasserbewegung durch bodem. Z. Ver. Deutsch.*, page 17821788, 1901.

[13] Z. Gu and H. Wang. Gravity waves over porous bottom. *J. Waterw. Port Coast. Ocean Eng.*, 24:209–215, 1991.

[14] E. Hairer. Solving ordinary differential equations. *Springer-Verlag, Berlin New York*, 1993.

[15] A. Hannoura and J. McCorquodale. Rubble mounds: hydraulic conductivity equation. *Waterway, Port, Coastal and Ocean Engineering*, 111, 1985.

[16] A. Harten. High resolution schemes for hyperbolic conservation laws. *Journal of Computational Physics*, 49:357–393, 1983.

[17] A. Harten, B. Engquist, S. Osher, and S. Chakravarthy. Uniformly high order accurate essentially non-oscillatory schemes, iii. *Journal of Computational Physics*, 71:231–303, 1987.

[18] P. Higuera, L. J. Lara, and I. J. Losada. Realistic wave generation and active wave absorption for NavierStokes models application to OpenFOAM. *Coastal Engineering*, 71:102–118, 2013.

[19] C. Hirt and B. Nichols. Volume of fluid (vof) method for the dynamics of free boundaries. *Journal of Computational Physics*, 39:201–225, 1981.

[20] M. S. Hossain and W. Rodi. Mathematical modeling of vertical mixing in stratified channel flow. *Second Symposium on Stratified Flows, Trondheim, Norway*, 1980.

[21] T. Hsu, T. Sakakiyama, and P. Liu. A numerical model for wave motions and turbulence flows in front of a composite breakwaterr. *Coastal Engineering*, 46:25–50, 2002.

[22] N. G. Jacobsen, D. R. Fuhrman, and J. Fredsøe. A wave generation toolbox for the open-source CFD library: OpenFOAM. *International Journal for Numerical Methods in Fluids*, 70(9):1073–1088, 2011.

[23] B. Jensen, N. Jacobsen, and E. Christensen. Investigations on the porous media equations and resistance coefficients for coastal structures. . *Coastal Engineering*, 84:56–72, 2014.

[24] G. S. Jiang and D. Peng. Weighted ENO schemes for Hamilton-Jacobi equations. *SIAM Journal on Scientific Computing*, 21:2126–2143, 2000.

[25] M. Lara, J.L.and del Jesus and I. Losada. Three-dimensional interaction of waves and porous structures. *Coastal Engineering*, 64:24–46, 2012.

[26] J. Larsen and H. Dancy. Open boundaries in short wave simulations - a new approach. *Coastal Engineering*, 7:285–297, 1983.

[27] B. E. Launder and D. B. Spalding. The numerical computation of turbulent flows. *Comput. Methods Appl. Mech. Eng.*, 3:269–289, 1974.

[28] P. Liu, P. Lin, K. Chang, and T. Sakakiyama. Numerical modeling of wave interaction with porous structures. *J. Waterw. Port Coast. Ocean Eng.*, 125:322–330, 1999.

[29] F. R. Menter. Two-equation eddy-viscosity turbulence models for engineering applications. *The American Institute of Aeronautics and Astronautics Journal*, 32:1598–1605, 1992.

[30] K. F. Nakayama, A. A macroscopic turbulence model for flow in a porous medium. *Journal of Fluids Engineering*, 121:1–43.

[31] Nortek. *Vectrino velocimeter Users Guide*. NORTEK.

[32] S. Osher and J. A. Sethian. Fronts propagating with curvature- dependent speed: algorithms based on Hamilton-Jacobi formulations. *Journal of Computational Physics*, 79:12–49, 1988.

[33] M. Peric and J. Ferziger. *Computational Methods for Fluid Dynamics*. Springer, 2001.

[34] P. Y. Polubarinova-Kochina. Theory of ground water movement. *Princeton University Press, Princeton, N.J.*, 10:252–271, 1962.

[35] C. W. Shu and S. Osher. Efficient implementation of essentially non-oscillatory shock capturing schemes. *Journal of Computational Physics*, 77:439–471, 1988.

[36] J. Slattery. Advanced transport phenomena. *Cambridge University Press, Cambridge (UK)*, 1(6), 1999.

[37] H. Song, L. Tao, and S. Chakrabarti. Wave reflection and transmission at permeable breakwaters. *Technical Report. Defense Technical Information Center, U.S. Army Corps of Engineers (USA)*, 229(5):1498–1513, 1976.

[38] P. Troch. Experimentele studie en numerieke modellering van golfinteractie met stortsteengolfbrekers. *Ph.D. thesis. Faculty of Engineering and Architecture, Ghent University, Ghent (Belgium)*, 0:131–160, 2000.

[39] H. Van der Vorst. Bi-gstab: A fast and smoothly converging variant of bi-cg for the solution of nonsymmetric linear systems. *SIAM J. Sci. Stat. Comput.*, 13:631–644, 1992.

[40] M. van Gent. Formulae to describe porous flow. *Communications on hydraulic and geotechnical engineering,Delft University of Technology, Delft (The Netherlands)*, 92-2:42–46, 1992.

[41] M. van Gent. Stationary and oscillatory flow through coarse porous media. *Communications on hydraulic and geotechnical engineering,Delft University of Technology, Delft (The Netherlands)*, 93-9:42–46, 1992.

[42] M. van Gent. Wave interaction with permeable coastal structures. *Communications on hydraulic and geotechnical engineering,Delft University of Technology, Delft (The Netherlands)*, 93-9:42–46, 1995.

[43] S. Wallin and A. V. Johansson. An explicit algebraic reynolds stress model for incompressible and compressible turbulent flows. *Journal of Fluid Mechanics*, 403:89–132, 2000.

[44] D. C. Wilcox. *Turbulence modeling for CFD.* DCW Industries Inc., La Canada, California., 1994.

[45] M. Zijlema. On the construction of a third-order accurate monotone convection scheme with application to turbulent flows in general domains. *Int. J. Numer. Meth. Fluids,*, 190(22):619–641, 1996.